HELSINKI UNIVERSITY OF TECHNOLOGY
Faculty of Electronics, Communications and Automation
Department of Radio Science and Engineering

Pekka Halla

Specific absorption rate design of 3rd generation handsets

Thesis submitted in partial fulfillment of the requirements for the degree of Master of Science in Engineering in Espoo, Finland, February 1, 2008.

Supervisor

Professor (pro tem) Clemens Icheln

Instructor

Petteri Yrjälä, M.Sc.

Abstract

HELSINKI UNIVERSITY OF TECHNOLOGY Abstract of the Master's Thesis

Author:	Pekka Halla
Name of thesis:	Specific absorption rate design of 3rd generation handsets
Date:	01.02.2008 **Number of Pages:** 107
Faculty:	Faculty of Electronics, Communications and Automation
Department:	Department of Radio Science and Engineering
Supervisor:	Professor (pro tem) Clemens Icheln
Instructor:	Petteri Yrjälä, M.Sc.

Within wireless communications systems antennas hold a special meaning, as they enable the transmission and reception of signals in free space. A matter of public concern is the amount of radiation the users of wireless devices are exposed to and the health effects the exposure may have. Regarding handsets the level of user exposure can be controlled and, most importantly, lowered with good antenna design.

This thesis covers the fields of handset antenna design and electromagnetic exposure of the user. The motivation for this work arose from the needs of a realistic handset platform project and its antenna design. After an introductory literature study a specific method involving an additional parasitic radiator is investigated as a solution in the handset project for lowering the amount of power absorbed by the handset user. The implementation of the method within the project required special optimization steps.

First, background theory of antennas is presented, along with the electromagnetic principles and mechanisms needed to understand the power absorption inside tissues. Then as a further motivation, the subject of human exposure to electromagnetic fields is elaborated on. Next, specific issues concerning handset antenna design are covered. Finally the research on lowering the power absorption in the handset user is reported.

As a result of this work, an informative package on the studied fields was gathered. In addition, new understanding on the practical feasibility of the promising method for lowering the power coupling into handset users was gained. The research on the method shows that with a combination of preparatory simulations and verifying measurements the method is applicable when designing mobile handsets.

Keywords: Mobile terminal antenna, specific absorption rate, SAR reduction

Tiivistelmä

TEKNILLINEN KORKEAKOULU **Diplomityön tiivistelmä**

Tekijä:	Pekka Halla	
Työn nimi:	Kolmannen sukupolven matkaviestinlaitteiden suunnittelu ominaisabsorptionopeuden osalta	
Päivämäärä:	01.02.2008	**Sivumäärä:** 107
Tiedekunta:	Elektroniikan, tietoliikenteen ja automaation tiedekunta	
Laitos:	Radiotieteen ja -tekniikan laitos	
Työn valvoja:	Professori (ma.) Clemens Icheln	
Työn ohjaaja:	DI Petteri Yrjälä	

Langattomassa tietoliikenteessä vapaassa tilassa kulkevien signaalien lähettämiseen ja vastaanottamiseen käytetyillä antenneilla on tärkeä rooli. Langattoman viestinnän yhteydessä huolta aiheuttava tekijä on laitteiden käyttäjien kokeman säteilyaltistuksen määrä sekä altistuksen aiheuttamat mahdolliset terveysvaikutukset. Säteilyaltistuksen määrään voidaan vaikuttaa matkaviestinten antennisuunnittelulla.

Tämä diplomityö käsittelee matkaviestinten antennisuunnittelua ja käyttäjän säteilyaltistuksen vähentämistä. Perehdyttävän kirjallisuuskatsauksen jälkeen tutkitaan käytännön sovelluksena menetelmää, jossa hyödynnetään loissäteilijää matkaviestimen käyttäjään imeytyvän sähkömagneettisen energian määrän pienentämiseksi. Tavoitteena oli optimoida menetelmä erään matkapuhelinalustan tarpeisiin.

Aluksi työssä esitellään olennaiset osat antennien ja sähkömagnetiikan taustateoriasta, jonka jälkeen syvennytään ihmisen ja sähkömagneettisten kenttien vuorovaikutukseen. Seuraavaksi keskitytään matkaviestinantennien erityispiirteisiin. Lopuksi raportoidaan työn tutkimusosa ja siinä saadut tulokset.

Työn tuloksena syntyi informatiivinen katsaus läpikäytyihin aiheisiin. Lisäksi matkaviestinten käyttäjiin kohdistuvan säteilyaltistuksen vähentämiseen tähtäävää menetelmää tutkittaessa opittiin uusia menetelmän käytännön soveltuvuuteen vaikuttavia asioita. Tutkimuksen perusteella voidaan päätellä, että menetelmää voidaan käyttää hyväksi matkaviestinten suunnittelussa sopivalla yhdistelmällä alustavia simulointeja ja varmistavia mittauksia.

Avainsanat: Matkaviestinantenni, ominaisabsorptionopeus, SAR:n pienentäminen

Acknowledgements

This thesis was written at Elcoteq Design Center in Salo. I want to thank the company along with my managers and co-workers for giving me the resources to work on this interesting topic.

This work was supervised by Professor Clemens Icheln, whom I want to thank for all his professional and patient help. Professor Pertti Vainikainen also deserves acknowledgement for setting this project in motion.

Petteri Yrjälä aided me with his professional experience and critical approach. Without his contribution this work would be of less quality. Thank you.

During my studies my parents have given me all the mental and material support I have asked for, and more. For this I want to express my gratitude towards them. Also, a thank you is due to my brothers for setting a great example in life for me to learn from.

Saija, thank you for your love and encouragement during the past five years. You make the troubled days easier for me.

Salo, February 1, 2008

Pekka Halla

Table of contents

Abbreviations

3G	Third generation mobile technology
ABC	Absorbing boundary condition
ANSI	American National Standards Institute
BEM	Boundary element method
BER	Bit error rate
BT	Bluetooth
BVR	Bandwidth-to-volume ratio
BW	Bandwidth
CENELEC	European Committee for Electrotechnical Standardization
DECT	Digital Enhanced Cordless Telecommunications
DUT	Device under test
EIRP	Effective isotropically radiated power
EMC	Electromagnetic compatibility
ERP	Effective radiated power
FDTD	Finite-difference time-domain
FEM	Finite element method
GO	Geometrical optics
GSM	Groupe Spécial Mobile or Global System for Mobile Communications
GTD	Geometrical theory of diffraction
ICNIRP	International Committee for Non-Ionizing Radiation Protection
IEC	International Electrotechnical Commission
IEEE	Institute of Electrical and Electronics Engineers
MEG	Mean effective gain
MoM	Method of moments
PIFA	Planar inverted-F antenna

PML	Perfectly matched layer
PO	Physical optics
PTD	Physical theory of diffraction
PWB	Printed wiring board
RF	Radio frequency
SA	Specific absorption
SAR	Specific absorption rate
STUK	Säteilyturvakeskus, Radiation and Nuclear Safety Authority of Finland
TETRA	Terrestrial Trunked Radio
TIS	Total isotropic sensitivity
TRP	Total radiated power
UMTS	Universal Mobile Telecommunications System
VSWR	Voltage standing wave ratio
WHO	World Health Organization
WLAN	Wireless Local Area Network

Symbols

∇	Nabla (vector differential operator)	
Δ	Difference operator	
A, a	Notation for vector	
A, a	Notation for scalar	
$\overline{\overline{A}}$	Notation for dyadic	
$\mathbf{B}(\mathbf{r},t)$	Magnetic flux density	[T, Vs/m^2]
B_r	Relative bandwidth	
BW	Bandwidth	[Hz]
b	Normalized susceptance	[S]
C	Conductance	[F]
c	Speed of light	[m/s]
c_p	Specific heat capacity	[J/(kg K)]
$\mathbf{D}(\mathbf{r},t)$	Electric flux density	[As/m^2]
D	Directivity at pattern maximum	
$D(\theta,\varphi)$	Directivity	
d	Longest dimension of an antenna	[m]
$\mathbf{E}(\mathbf{r},t)$	Electric field	[V/m]
$\mathbf{E}_{\theta,\varphi,x,y,z}$	Electric field component	[V/m]
$\mathbf{E}_n$	Electric field component normal to medium boundary	[V/m]
$\mathbf{E}_t$	Electric field component tangential to medium boundary	[V/m]
E_{rms}	Electric field, root-mean-square value	[V/m]
E_y	Scalar electric field component	[V/m]
f	Frequency	[Hz]
f_0	Center frequency	[Hz]
f_r	Resonance frequency	[Hz]

f_{r1}, f_{r2}	First and second resonance frequencies of a patch antenna	[Hz]
f_{3dB}	Half-power frequency	[Hz]
G	Gain at pattern maximum	
$G(\theta,\varphi)$	Gain	
$\overline{\overline{G}}(\mathbf{r}-\mathbf{r}')$	Green's dyadic	[1/m]
$G(\mathbf{r}-\mathbf{r}')$	Scalar Green's function	[1/m]
g	Normalized conductance	
g_r	Normalized conductance, radiation losses	
g_c	Normalized conductance, conductive losses	
g_d	Normalized conductance, dielectric losses	
$\mathbf{H}(\mathbf{r},t)$	Magnetic field	[A/m]
$\mathbf{H}_{x,y,z}$	Magnetic field component	[A/m]
H_x	Scalar magnetic field component	[A/m]
h	Height of a parasitic radiator	[m]
$\overline{\overline{I}}$	Unit dyadic	
$\mathbf{J}(\mathbf{r},t)$	Electric current density	[A/m^2]
J_{rms}	Current density, root-mean-square value	[A/m^2]
$\mathbf{J}_m(\mathbf{r},t)$	Magnetic current density	[V/m^2]
k	Wave number	[rad/m]
L	Inductance	[H]
L_{ret}	Return loss	[dB]
L_1, L_2	Primary and secondary lengths of a patch antenna	[m]
l	Length of a parasitic radiator	[m]
dm	Infinitesimal mass	[kg]
$P_n(\theta,\varphi)$	Normalized power density of an antenna	
P_A	Power available at feed line	[W]
P_S	Sensitivity threshold of a receiver	[W]

P_{rec}	Received power	[W]
P_V	Incident power, vertical polarization	[W]
P_H	Incident power, horizontal polarization	[W]
P_{in}	Power accepted by antenna	[W]
P_r	Radiated power	[W]
P_l	Loss power	[W]
dP_l	Loss power in an infinitesimal mass	[W]
Q	Quality factor	
Q_l	Loaded quality factor	
Q_0	Unloaded quality factor	
Q_e	External quality factor	
Q_r	Quality factor of radiation losses	
Q_c	Quality factor of conductive losses	
Q_d	Quality factor of dielectric losses	
$\mathbf{r}$	Field vector point	
$\mathbf{r}'$	Source vector point	
R	Distance from antenna	[m]
R_1	Outer boundary distance of reactive near-field	[m]
R_2	Outer boundary distance of radiating near-field	[m]
R_a	Antenna input resistance	[Ω]
R_r	Antenna radiation resistance	[Ω]
R_l	Antenna loss resistance	[Ω]
r_a	Radius of smallest sphere enclosing an antenna	[m]
$\mathbf{S}$	Poynting vector (power density)	[W/m^2]
SAR	Specific absorption rate	[W/kg]
SAR_i	SAR at frequency i	[W/kg]
SAR_L	SAR limit	[W/kg]

t	Time	[s]
Δt	Time step	[s]
ΔT	Temperature change	[K]
$\tan \delta$	Dielectric loss tangent	
TRP	Total radiated power	[W]
$\mathbf{u}_\theta$	Elevation unit vector	
$\mathbf{u}_\varphi$	Azimuth unit vector	
V	Volume	[m^3]
V_a	Antenna volume	[m^3]
v	Speed of light in a medium	[m/s]
W	Energy stored in a resonator	[J]
W_1, W_2	Primary and secondary widths of a patch antenna	[m]
X_a	Antenna input reactance	[Ω]
x, y, z	Cartesian coordinate axes	
Δx, Δy, Δz	Cartesian coordinate grid steps	
Z_a	Antenna input impedance	[Ω]
Z_0	Feed line impedance	[Ω]
Γ	Reflection coefficient	
δ_S	Skin depth	[m]
ε	Permittivity	[As/Vm]
ε_0	Permittivity in vacuum, $8{,}8542 \cdot 10^{-12}$	[As/Vm]
ε_r	Relative permittivity	
ε_r'	Real part of relative permittivity	
ε_r''	Imaginary part of relative permittivity	
ε''_{rd}	Imaginary part of relative permittivity, dielectric losses	
η	Wave impedance	[Ω]
η_p	Polarization efficiency	

η_r	Radiation efficiency	
η_{refl}	Reflection efficiency	
η_{tot}	Total antenna efficiency	
η_u	User absorption coefficient	
θ, φ, z	Spherical coordinate axes	
θ	Elevation angle, spherical coordinates	[rad]
λ	Wavelength	[m]
μ	Permeability	[Vs/Am]
μ_0	Permeability in vacuum, $4\pi \cdot 10^{-7}$	[Vs/Am]
μ_r	Relative permeability	
$\rho_e(\mathbf{r},t)$	Electric charge density	[C/m^3]
ρ	Density	[kg/m^3]
σ	Conductivity	[S/m]
σ_{eff}	Effective conductivity	[S/m]
τ	Thermal time constant	[s]
φ	Azimuth angle, spherical coordinates	[rad]
χ_e	Electric susceptibility	
Ω	Solid angle	
ω	Angular frequency	[rad/s]

1 Introduction

1.1 Background

The possibility to send electromagnetic signals through the air was first discovered in the late 19th century, but only during the last two decades mobile wireless communication has become accessible to the general public, most remarkably through mobile handsets. Over that period of time, the mobile communications industry has become economically significant, especially in Finland, and a vast amount of research has been conducted to further improve the quality of wireless systems.

In wireless communications systems antennas hold special significance, as they are the interface to the free space. Although many of the parameters describing the performance of antennas can be used universally, the targets and priority of the parameters vary significantly depending on the purpose of each antenna. Thus specific challenges can also be found when designing handset antennas.

Antenna design often relies heavily on reported commonly known antenna models, experience and analysis. The design process typically starts with a ballpark model known to produce approximately the desired performance. Then, based on the analyzed resulting antenna performance, corrective design is executed until the targets are reached. The examination of antenna properties with analytical calculations is a gruelling and time-consuming task. Thus analysis is usually performed with simulations and practical measurements.

A critical issue regarding the usage of handsets is the amount of electromagnetic radiation the user is exposed to and what, if any, effects the radiation has on humans. A central concept related to the exposure is specific absorption rate (SAR), which describes the level of radio frequency power absorption in tissues. SAR is also the measure, in which the regulative limits on exposure from mobile terminals are set, and it is one of the central parameters the antenna designer has to take into account. With good antenna design it is possible to control the level of power absorption into the user, but only to a degree.

The research on the biological and health effects of mobile handsets has been extensive. The current exposure limits are based on the knowledge gained from the research and the limits provide a substantial safety margin to the exposure levels known to produce adverse effects. However, the research is still ongoing, most notably concerning the epidemiological effects of mobile terminals.

1.2 Objectives and scope

This thesis was written during the development process of a 3rd generation handset and its antenna. The motivation was to learn about the theoretical background of antenna design and see how these guidelines could be applied in the process, more specifically regarding the SAR design of the handset. The actual research part of the work dealt with a specific method used to decrease the electromagnetic exposure of the handset user. The method utilizes an additional parasitic radiator attached to the handset chassis. The target was to apply the method in the given handset project, which required special optimization procedures. The research was conducted with simulations and experimental measurements.

A secondary purpose of this work was to provide the author's employer with a kind of beginner's guide to handset antennas. The theoretical background of antennas and radiation exposure is presented in a way suitable for initiation.

The field of antenna design is an extensive one and cannot be covered comprehensively within one master's thesis. This work offers a look on the subject from the author's point of view. At first, issues relating to antennas in general are discussed, but later the focus is turned to handset antennas. The research part also partly deals with the method under investigation on a general level, but the boundary conditions of the handset project were kept in mind throughout the research. The research essentially aimed at the application and optimization of the method in the specific handset case.

1.3 Thesis structure

This thesis is divided into six chapters. Basic issues regarding electromagnetics and antennas are first introduced in Chapter 2. The approach of Chapter 2 is rather fundamental, and it can be considered as theoretical initiation material to antenna design. Chapter 3 then elaborates on the subject of SAR. The chapter includes a brief introduction to the research on the effects electromagnetic fields have on humans and

the means with which the radiation exposure from mobile handsets is regulated. In Chapter 4 design topics concerning specifically handset antennas are presented. Chapter 5 includes the research part of this thesis. In the chapter, the research conducted to investigate the method for reducing SAR in the specific handset design case is reported. Finally, in Chapter 6 a summary is provided along with conclusions based on this work.

2 Antennas and radiation

2.1 Introduction

In telecommunications, signals are usually transmitted with waveguides or wireless radio links. The inconvenience and cost of constructing a cable link speaks in favor of the use of wireless links. In addition, the exponential attenuation of waveguides makes them lossier over long distances [1], [2]. In any case, and perhaps most importantly, mobile communication systems cannot be realized without wireless links.

All electronic devices transmit and receive electromagnetic radiation to some extent. As a distinction for antennas this action is desirable and planned. By definition [3], an antenna is ”that part of a transmitting or receiving system which is designed to radiate or to receive electromagnetic waves”. In other words, an antenna is the interface between a guided wave and a free-space wave.

Today, antennas are used in a wide range of applications with varying requirements. As a consequence a vast selection of antenna types have been developed over the history of telecommunications. Antennas can be divided into many categories, e.g. current element, aperture and traveling-wave antennas, plus antenna arrays.

This chapter gives an introduction to the background theory and basic parameters concerning antennas and their performance. In addition, methods for electromagnetic field simulation are discussed. The bulk of this chapter is basic theory that can be found in introductory antenna and radio engineering textbooks, e.g. [1], [4], [5].

2.2 Electromagnetic radiation

Electromagnetic radiation is transversal wave motion propagating at the speed of light. It is created by an accelerating or decelerating electrical charge. The radiation is characterized by its frequency f and wavelength λ, which are connected by

$$f = \frac{c}{\lambda}, \tag{2-1}$$

where c is the speed of light in vacuum. In a general case the speed of the wave v is determined by the properties of the medium and it can be calculated by

$$v = \frac{1}{\sqrt{\mu\varepsilon}}, \tag{2-2}$$

where ε and μ are the permittivity and permeability of the medium, respectively.

The spectrum of electromagnetic radiation is subdivided into groups depending on frequency and wavelength [5]. Radio waves are located at the lower end of the frequency scale, ranging up to about 3 THz. Radiation types with higher frequency include infrared, visible light, ultraviolet, X-ray and gamma radiation. Radio waves are divided further into RF-waves (radio frequency, below 300 MHz), microwaves (300 MHz – 30 GHz) and millimeter waves (30 GHz – 300 GHz). This thesis work deals mainly with microwaves from 300 MHz to 3 GHz.

2.2.1 Maxwell's equations

James Clerk Maxwell (1831 – 1879) was a Scottish mathematician and physicist best known for the eponymous set of equations expressing the laws of electricity and magnetism. Maxwell himself did not discover all the physical laws behind the equations, but he was responsible for grouping together for the first time all the necessary equations for describing the relationships between electric and magnetic fields, electric current and electric charge. All analysis of electromagnetic radiation is based on Maxwell's equations. Hence they are also the starting point for the analysis of antenna radiation. Below, Equations (2-3) – (2-6) represent Maxwell's equations as modified into differential vector form by Heaviside and Gibbs [6]:

$$\nabla \cdot \mathbf{D}(\mathbf{r},t) = \rho_e(\mathbf{r},t) \qquad \text{(Gauss's law)} \tag{2-3}$$

$$\nabla \cdot \mathbf{B}(\mathbf{r},t) = 0 \tag{2-4}$$

$$\nabla \times \mathbf{E}(\mathbf{r},t) = -\frac{\partial \mathbf{B}(\mathbf{r},t)}{\partial t} \qquad \text{(Faraday's law)} \tag{2-5}$$

$$\nabla \times \mathbf{H}(\mathbf{r},t) = \mathbf{J}(\mathbf{r},t) + \frac{\partial \mathbf{D}(\mathbf{r},t)}{\partial t} \qquad \text{(Ampère's law and Maxwell's extension)} \tag{2-6}$$

The different variables in the equations above are electric field strength and flux density (**E**, **D**), magnetic field strength and flux density (**H**, **B**), electric current density (**J**) and electric charge density (ρ_e). In linear materials the field strengths and densities are connected by the electric and magnetic properties of the medium as $\mathbf{D}(\mathbf{r},t) = \varepsilon\mathbf{E}(\mathbf{r},t)$ and $\mathbf{B}(\mathbf{r},t) = \mu\mathbf{H}(\mathbf{r},\mathrm{t})$.

Maxwell's equations contain the divergence operator $\nabla\cdot$ and the curl operator $\nabla\times$. The former describes the tendency of the vector field to diverge or converge from a point, and the latter shows the vector field's rate of rotation [7]. For convenience, the equations can be deciphered and explained in a practical form.

Equations (2-3) and (2-4) describe the starting point for electromagnetic activity. Equation (2-3) states that the divergence of the electric flux through a closed surface equals the electric charge density within, while Equation (2-4) claims that the total divergence of the magnetic flux is always zero. This highlights the fact that electric monopoles, i.e. ions, do indeed exist, but despite extensive research magnetic monopoles have not been found. Equations (2-5) and (2-6) play a major role in understanding the creation of an electromagnetic wave, which is depicted in Figure 2-1.

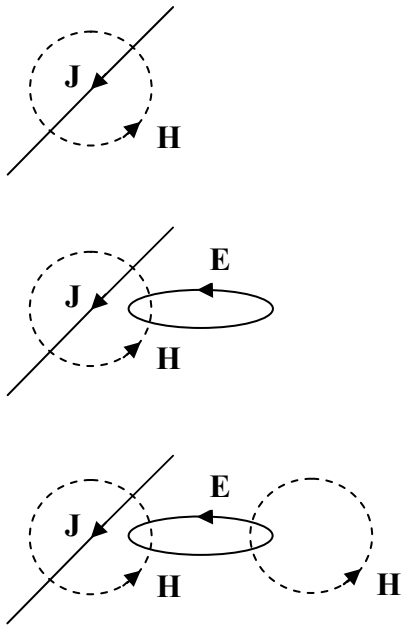

Figure 2-1. The creation of an electromagnetic wave, caused by alternating current.

As illustrated in the first part of Figure 2-1, and as stated by Equation (2-6), a current density produces a magnetic field around it. If the current changes over time, the alternating magnetic field causes an alternating electric field following Equation (2-5). The E-field, in turn, causes another H-field, as in Equation (2-6), etc. Thus a propagating wave is created. The mechanism can be thought of as a transformation of the energy of the moving electrons into photons. The power density a wave carries is calculated with the help of Poynting vector

$$\mathbf{S} = \frac{1}{2}\mathbf{E} \times \mathbf{H}^{*}. \tag{2-7}$$

Most of the electromagnetic phenomena can be regarded as time-harmonic or as superposition of time-harmonic components having the angular frequency $\omega = 2\pi f$ [5]. Time-harmonic fields can be presented as

$$\mathbf{A}(\mathbf{r},t) = \Re\left[\mathbf{A}(\mathbf{r})e^{j\omega t}\right], \tag{2-8}$$

which means that the field at a given point can be considered as a complex vector with constant amplitude. The real part of that vector represents the actual field strength as a function of time. This interpretation leads to a simpler notation of the Maxwell's equations, since $\partial e^{j\omega t}/\partial t = j\omega e^{j\omega t}$. Equations (2-5) and (2-6) now read

$$\nabla \times \mathbf{E}(\mathbf{r}) = -j\omega\mathbf{B}(\mathbf{r}) \tag{2-9}$$

$$\nabla \times \mathbf{H}(\mathbf{r}) = \mathbf{J}(\mathbf{r}) + j\omega\mathbf{D}(\mathbf{r}). \tag{2-10}$$

2.2.2 Wave losses

When traveling through a medium, the electromagnetic wave experiences attenuation. The losses are caused by two mechanisms, conductivity and polarization, which are described next. These principles are also put to use when determining the radio frequency power absorbed by the human body, which gives rise to the notion of specific absorption rate (SAR). SAR is discussed more thoroughly in Chapter 3.

As mentioned earlier, the electromagnetic properties of a medium are represented by permittivity ε and permeability μ, which are usually given relative to those of vacuum, i.e. $\varepsilon_r = \varepsilon/\varepsilon_0$ and $\mu_r = \mu/\mu_0$. For example, for air the relative values are approximately $\varepsilon_r = \mu_r = 1$. For a lossy medium ε_r and μ_r are complex numbers.

The first loss mechanism considered here is the conductivity σ of media with free electric charge carriers. In such a medium an electric field produces current according to Ohm's law $\mathbf{J} = \sigma\mathbf{E}$, and the dissipated power can be calculated by $\mathbf{J}\cdot\mathbf{E}$ [6]. Now, the conductivity losses can be taken into account in the expression for permittivity. Remembering the connection between the electric field and the electric flux density, $\mathbf{D} = \varepsilon\mathbf{E}$, Equation (2-10) can now be written as

$$\nabla \times \mathbf{H} = \sigma\mathbf{E} + j\omega\varepsilon\mathbf{E} = j\omega\varepsilon_0\left(\varepsilon_r' - j\frac{\sigma}{\omega\varepsilon_0}\right)\mathbf{E}, \tag{2-11}$$

where ε_r' is the real part of permittivity and the conductivity losses are included as the imaginary part of permittivity.

Let us now consider the polarizing effect of an electric field. Figure 2-2(a) shows the situation in vacuum. The polar molecules of a medium have an electric dipole moment, which causes them to turn parallel to the external field, as seen in Figure 2-2(b). Single atoms are also polarized by the field, because it disturbs the movement of electrons [5]. The polarization weakens the electric field and now the relation of electric field **E** and electric flux **D** becomes

$$\mathbf{D} = \varepsilon_0(1 + \chi_e)\mathbf{E} = \varepsilon\mathbf{E}, \tag{2-12}$$

where χ_e is the electric susceptibility and

$$\varepsilon = \varepsilon_0(1+\chi_e) = \varepsilon_0\varepsilon_r = \varepsilon_0(\varepsilon_r' - j\varepsilon_{rd}''). \tag{2-13}$$

Here the imaginary part of permittivity ε_{rd}'' represents the losses in the polarized medium. The losses are caused by the frictional forces acting upon the polarized particles trying to turn in synchronism with the electric field. The lost energy is transformed into heat.

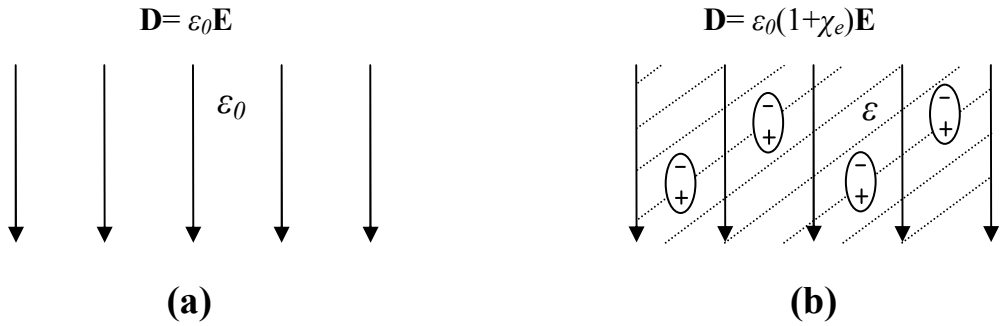

Figure 2-2. The polarizing effect of an electric field.

The two different imaginary parts of permittivity in Equations (2-11) and (2-13), caused by the two loss mechanisms, can be combined in the imaginary part of relative permittivity ε_r'' as

$$\varepsilon_r = \varepsilon_r' - j\varepsilon_r'' = \varepsilon_r' - j\left(\varepsilon_{rd}'' + \frac{\sigma}{\omega\varepsilon_0}\right). \tag{2-14}$$

All of the losses are sometimes described by the conductivity of the medium, so that the calculation can be returned to the form of Equation (2-11). This can be done by using the concept of effective conductivity σ_{eff}, calculated by

$$\sigma_{eff} = \omega\varepsilon_0\varepsilon_r'' = \omega\varepsilon_0\varepsilon_{rd}'' + \sigma \tag{2-15}$$

The use of effective conductivity can be somewhat confusing, because it can lead one to falsely think that only the conductive losses of a medium are noteworthy. Yet another way of expressing the losses is to use the term loss tangent, defined as

$$\tan\delta = \frac{\varepsilon_r''}{\varepsilon_r'} = \frac{\sigma_{eff}}{\omega\varepsilon_0\varepsilon_r'}. \tag{2-16}$$

In the discussion above, only losses incurred by electric fields have been covered, but the effect of magnetic fields is dual. Thus the relative permeability μ_r is also a complex number, with the imaginary part representing the magnetic losses [5].

The damping of fields in different media is characterized by the skin depth δ_S, calculated by ($\sigma >> \omega\varepsilon$)

$$\delta_S = \sqrt{\frac{2}{\omega\mu\sigma_{eff}}}. \tag{2-17}$$

Skin depth is the distance over which the propagating field is damped into $1/e$ (≈ 37%) part of the original field.

2.2.3 Media boundaries

An interface of two different media requires an incident traveling wave to fulfill certain conditions. The conditions are derived from Maxwell's equations and for the electric field at the boundary of media 1 and 2 they read

$$\mathbf{E}_{1t} = \mathbf{E}_{2t} \tag{2-18}$$

$$\varepsilon_1\mathbf{E}_{1n} = \varepsilon_2\mathbf{E}_{2n}, \tag{2-19}$$

where the subindices t and n mark the tangential and normal components. Thus the tangential component penetrates the boundary intact, while the normal component depends on the material properties. The conditions for the magnetic field are dual, which means that if the interface is between two non-magnetic media, i.e. the typical case, it has no impact on the magnetic field.

2.2.4 Antenna radiation

The analysis of antennas begins from the Maxwell's equations (2-9) and (2-10). In addition to the electric current density **J**, the concept of magnetic current density $\mathbf{J}_m$ has been created. This artificial term is useful in calculations and when added, with minus

sign, to the right side of Equation (2-9) it makes the two equations (2-9) and (2-10) symmetric. The calculation of electric and magnetic fields created by the two types of current sources located in free space can be considered as the basic antenna problem [2].

For a group of current elements $\mathbf{J}(\mathbf{r}')$ located in volume elements dV' the electric field can be calculated by

$$\mathbf{E}(\mathbf{r}) = -j\omega\mu \int_V \overline{\overline{G}}(\mathbf{r}-\mathbf{r}')\cdot \mathbf{J}(\mathbf{r}')dV', \tag{2-20}$$

where $\overline{\overline{G}}(\mathbf{r}–\mathbf{r}')$ is called Green's dyadic. Note that the source vector point $\mathbf{r}'$ is distinguished from the field vector point $\mathbf{r}$. Green's dyadic represents the field at $\mathbf{r}$ caused by the unit point source at $\mathbf{r}'$ and it can be expressed using scalar Green's function $G(\mathbf{r}–\mathbf{r}')$ as

$$\overline{\overline{G}}(\mathbf{r}-\mathbf{r}') = \left(\overline{\overline{I}} + \frac{1}{k^2}\nabla\nabla\right) G(\mathbf{r}-\mathbf{r}'), \tag{2-21}$$

where $\overline{\overline{I}}$ is the unit dyadic and k the wave number. Next, the scalar Green's function is calculated by

$$G(\mathbf{r}-\mathbf{r}') = \frac{e^{-jk|\mathbf{r}-\mathbf{r}'|}}{4\pi|\mathbf{r}-\mathbf{r}'|}, \text{ where } |\mathbf{r}-\mathbf{r}'| = \sqrt{(\mathbf{r}-\mathbf{r}')\cdot(\mathbf{r}-\mathbf{r}')}. \tag{2-22}$$

The case with magnetic current sources is again dual. Then the calculation of magnetic fields can be done with Equation (2-20) by replacing the electric current density $\mathbf{J}$ with magnetic current density $\mathbf{J}_\mathrm{m}$ and permeability μ with permittivity ε. Additionally, in both cases the magnetic field can be solved from the electric field, and vice versa, from Equations (2-9) and (2-10), respectively.

The structure of antennas can be very complicated and the first challenge in the analytical calculation of the radiated fields is to find the expression for the current densities. However, if the equivalent current source for the structures can be found, the problem returns to the calculation of fields created by currents in free space, as in Equation (2-20). Nevertheless, in many cases the currents cannot be expressed with reasonable complexity and the designer is forced to use approximations and numerical simulations.

The space surrounding an antenna can be divided into three field regions based on the distance from the antenna and thus the properties of the radiated fields. The regions are

illustrated in Figure 2-3. Next to the antenna is the near-field region, which can be divided in lossless media into reactive and radiating regions [3]. The region closest to the antenna is the reactive near-field region, where the reactive part of the field is dominating. A commonly used distance for the outer boundary of the reactive near-field R_1 can be seen in Figure 2-3, where d is the longest dimension of the antenna [4].

When solving the radiation of an antenna, from Equations (2-21) and (2-22) it can be seen that the fields have components that depend on the distance R from the antenna as $1/R$, $1/R^2$ and $1/R^3$. The reactive components belong to the latter two groups and within the radiating near-field region ("Fresnel region") they become negligible. In this region the radiation pattern depends on the distance. The outer boundary of the Fresnel region, which at the same time is the boundary between near-field and far-field regions, is denoted in Figure 2-3 as R_2.

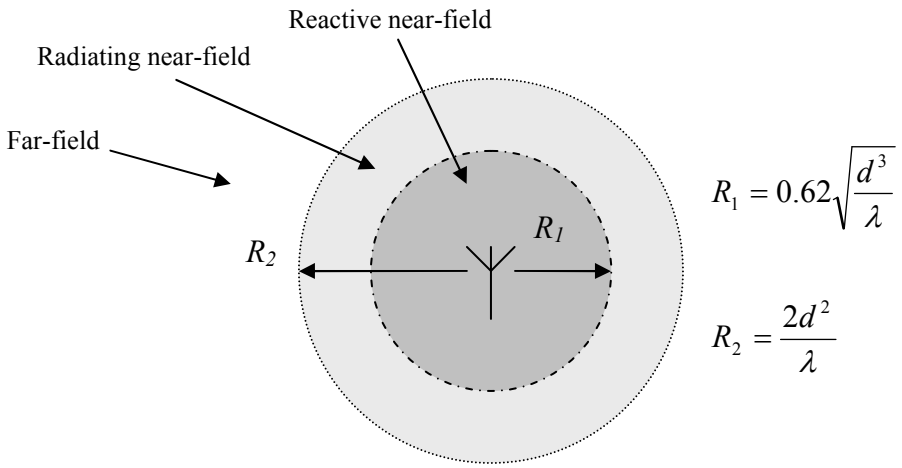

Figure 2-3. Antenna field regions.

In the far-field region ("Fraunhofer region") the radiation characteristics of the antenna do not depend on the distance, only the field strength decays as $1/R$. The boundary of near-field and far-field regions given above means that in the far-field the distance difference to the center and to the edge of the antenna is less than $\lambda/16$, and so the phase error is sufficiently small. Then the antenna is essentially seen as a point source and the traveling wave can be considered as a plane wave.

Approximations for the region boundaries are important generally in measurements, because normally only the far-field properties of antennas are of interest. Also, it is important in measurements to place the transmitting and receiving antennas far enough

from one another due to the possible errors caused by near-field coupling [8]. The different regions are also interesting in terms of user effect on handset antenna performance.

In the far-field the ratio of the electric and magnetic field amplitudes is defined by the wave impedance η of the material as

$$\eta = \frac{E}{H} = \sqrt{\frac{j\omega\mu}{\sigma + j\omega\varepsilon}}, \tag{2-23}$$

where E and H are the scalar values of the electric and magnetic field. However, in the near-field either electric of magnetic field can be dominant depending on the source. Figure 2-4 depicts two elementary radiators. An electrically small wire antenna, such as in Figure 2-4(a), has a large impedance and thus the electric field is dominant. On the other hand, an electrically small loop antenna, as in Figure 2-4(b), produces a dominant magnetic field [9].

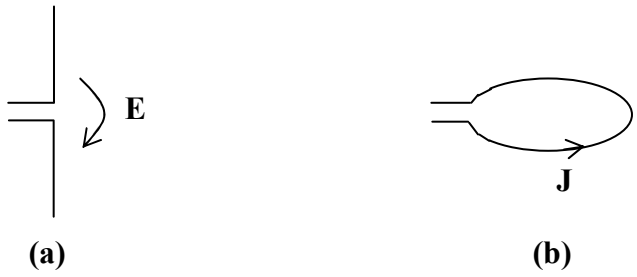

Figure 2-4. Elementary radiators: (a) small wire antenna, (b) small loop antenna.

2.3 Antenna properties

In order to be able to discuss the performance of antennas, a few basic properties need to be established first. This section provides short introductions to some of the most significant of them, with emphasis on the parameters important to handset antennas. Generally speaking antennas are reciprocal. Thus the properties described below apply both in transmission and reception. An exception to this is if the antenna itself has components that are not reciprocal or the medium surrounding the antenna is anisotropic. The electrical characteristics of antennas introduced in this section are divided into three groups. The division is used to make the reading easier, and the groups have strong interdependence.

The first group, which includes e.g. radiation pattern and directivity, describes the spatial characteristics of the radiated field. They require that the coordinate system in use is defined properly. Usually the spherical coordinate system, seen in Figure 2-5, is preferred [10]. In the figure θ denotes the elevation angle and φ the azimuth angle.

Antennas are always used as a part of a larger electronic system. Therefore the circuit parameters, which form the second group, are of great interest to the designer. Unfortunately no antenna is able to radiate all of the available power to the surroundings, but several coefficients, such as matching efficiency and radiation efficiency, have to be taken into account.

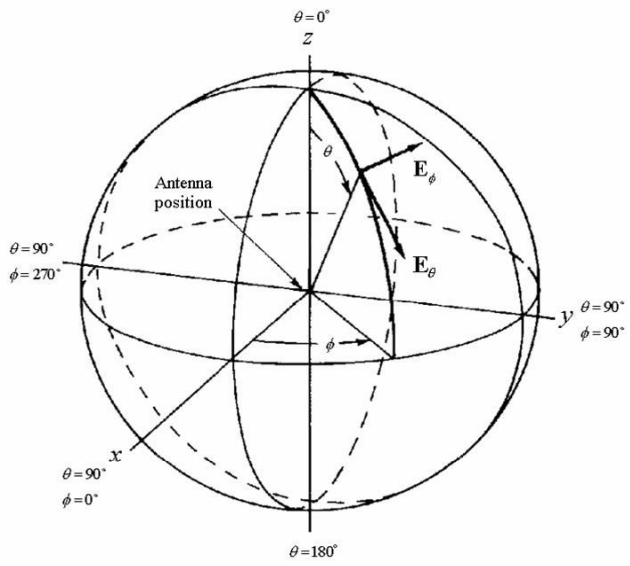

Figure 2-5. Standard spherical coordinate system [10].

The third group consists of parameters particularly interesting in handset antenna design, such as total radiated power (TRP) and total isotropic sensitivity (TIS). These terms are often used when discussing the active performance of a handset and they can be seen in industrial antenna requirements and specifications.

Besides the electrical properties, there are also other interesting parameters concerning antennas, such as size, weight and cost. Also, the SAR value produced by a handset can be regarded as an antenna-specific property.

2.3.1 Radiation parameters

The radiation pattern describes the spatial distribution of the electromagnetic far-field generated by the antenna. The quantity in question varies and it can be e.g. the power density, field strength or polarization of the radiated field. The pattern can be expressed

in a graphical form or in a mathematical equation as a function of angle (θ,φ). The graphical representation is often given as a simpler two-dimensional plane cut, where either θ or φ is kept constant.

Directivity D represents the antenna's ability to focus the radiated power into one direction. It is defined as the ratio of the power density from the antenna to the average power density. It is a function of angle, but in practice it is often given only to the direction of the pattern maximum. The directivity at the maximum is calculated with the help of the normalized power density function $P_n(\theta,\varphi)$, where the power at the maximum is set at unity. The equation for directivity is

$$D = \frac{4\pi}{\iint_{4\pi} P_n(\theta,\varphi)d\Omega}, \tag{2-24}$$

where $d\Omega$ is the solid angle element [3].

Gain G of an antenna is perhaps even more commonly used to measure the non-uniformity of the antenna's radiation pattern. It takes into account the power losses of the antenna. Gain is defined as the ratio of the power density to the power density in a scenario where all of the power accepted by the antenna would be radiated isotropically. Gain is defined as

$$G = \eta_r D, \tag{2-25}$$

where η_r is the radiation efficiency, introduced below. Directivity, and thus also gain, are often given only as the maximum in the direction of the main lobe, but they can also be expressed as a function of angle, $D(\theta,\varphi)$ and $G(\theta,\varphi)$, by multiplying D and G, respectively, by $P_n(\theta,\varphi)$.

Some antennas, e.g. link antennas, are designed to have high directivity. Handset antennas, on the other hand, in principle need to have an omnidirectional pattern, because the orientation of the device in relation to the base station is not fixed.

The polarization of an antenna describes the vector characteristics of the generated field. In reverse, due to reciprocality, the antenna polarization can be defined as the polarization of the incident wave which maximizes the reception. Polarization is also a function of the direction angle. The polarization of a wave describes the route that the tip of the field vector at a given point travels during a cycle. This route is perpendicular to the direction of propagation and there are three types of routes, i.e. polarizations that

can be distinguished. The three types of polarizations, and the conditions leading to them, are illustrated in Figure 2-6. It can be seen that the linear and circular polarizations are in fact merely special cases of the elliptical polarization.

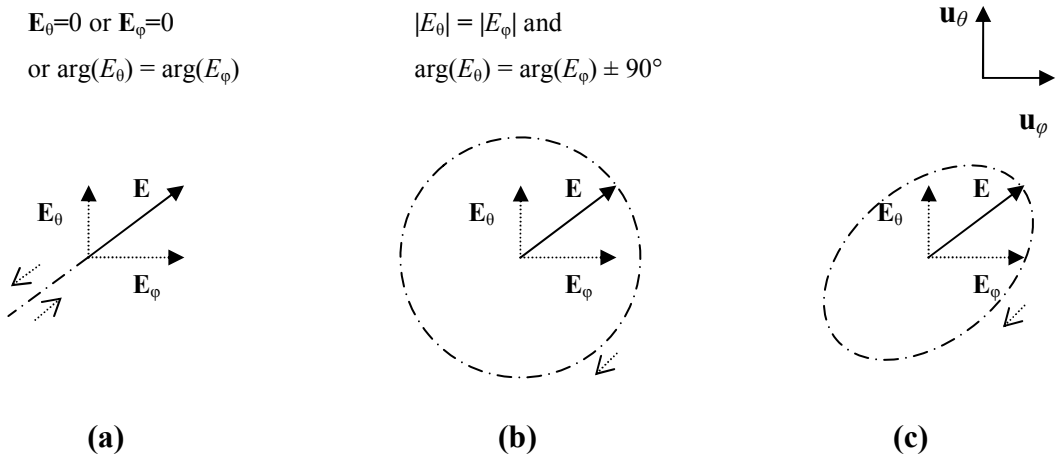

Figure 2-6. Wave polarizations: (a) linear polarization, (b) circular polarization, (c) elliptical polarization.

Usually the antenna radiation is designed to have a certain operating polarization, called co-polarization. However, in practice there exists also an orthogonal component, called cross polarization. If the polarization of the incident wave is not the same as that of the antenna, only a portion of the power is received by the antenna. This polarization matching is measured with polarization efficiency η_p.

2.3.2 Circuit parameters

An antenna can be considered as a circuit element with complex input impedance Z_a. The antenna impedance is of course frequency-dependent. It is also important to know that the input impedance is affected by the objects surrounding it. Thus the designer has to take into account the operating environment of the antenna. For example the input impedance, as well as other antenna properties, of a handset antenna can be greatly influenced by the head and hand of the user. The input impedance is written as

$$Z_a = R_a + jX_a. \tag{2-26}$$

The real part R_a, input resistance, splits further into radiation losses R_r and material losses R_l. R_r represents the power transferred into the air and is thus ideally dominant. R_l is caused by the conductive and dielectric losses inside the antenna. These two terms lead into the definition of radiation efficiency η_r as

$$\eta_r = \frac{R_r}{R_r + R_l}. \tag{2-27}$$

The imaginary part X_a of the input impedance, input reactance, is formed by the reactive near-fields of the antenna, where a part of the energy is stored, reminiscent of an inductor or a capacitor. If the power flux around an antenna could be seen, one could perceive that some of the energy moves back and forth out of the antenna, while only a portion continues propagating away [2].

One of the most challenging tasks in antenna design is the matching of the antenna impedance to the impedance of the feeding transmission line. The matching can be measured with the reflection coefficient at the junction of the antenna and the transmission line. The reflection coefficient seen from the line's direction is calculated by

$$\Gamma = \frac{Z_a - Z_0}{Z_a + Z_0}, \tag{2-28}$$

where Z_0 is the impedance of the feed line. A common value for Z_0 is 50 Ω. The portion of the available power entering the antenna is represented by the reflection efficiency η_{refl}, which is calculated by

$$\eta_{refl} = 1 - |\Gamma|^2. \tag{2-29}$$

Another way of expressing the level of matching often found in literature is through return loss L_{ret}, calculated in decibels by

$$L_{ret} = 20\log|\Gamma|, \tag{2-30}$$

which compares the incident power to the reflected power.

The bandwidth (BW) of an antenna represents the frequency range within which one of its characteristics, e.g. gain, side lobe level or input impedance, conforms to a defined acceptable level. Generally with small antennas the input impedance is the factor in question. There is no universal definition for bandwidth and the matching requirement varies between applications. For example, for handset antennas the bandwidth can be the frequency range over which the voltage standing wave ratio (VSWR) is less than 2 or 3 (e.g. [11]). These requirements lead to

$$VSWR = \frac{1+|\Gamma|}{1-|\Gamma|} < 2{,}3 \Rightarrow |\Gamma| < \frac{1}{3}, \frac{1}{2}. \tag{2-31}$$

The corresponding return losses are -9.5 dB and -6 dB, respectively.

The bandwidth can also be described with relative bandwidth B_r, which is calculated by

$$B_r = \frac{BW}{f_0}, \tag{2-32}$$

where f_0 is the center operating frequency.

2.3.3 Handset antenna parameters

The fundamental antenna parameters are valid also for handset antennas. However, in industrial antenna specifications the design targets are often defined with other parameters that can be derived from the concepts discussed above. The list of handset antenna parameters compiled here is not complete, but it includes some of the more prevalent concepts. The parameters introduced are effective isotropically radiated power (EIRP), total radiated power (TRP), total isotropic sensitivity (TIS) and mean effective gain (MEG) [12], [13].

EIRP compares the radiated power of an antenna to a reference level, which is the notional radiated power of a matched lossless isotropic antenna fed by the same amount of available power P_A. EIRP is a function of angle, although it often refers only to the value at the pattern maximum. EIRP can be calculated by

$$EIRP(\theta,\varphi) = \eta_{refl} P_A G(\theta,\varphi). \tag{2-33}$$

A term similar to EIRP is the effective radiated power (ERP). ERP uses the power radiated by a dipole as the reference level instead of an isotropic radiator, which means that in decibels ERP is always 2.15 units lower than EIRP.

TRP is a significant term in the active measurements of handsets due to the difficulty of direct measurements of matching and radiation efficiencies. TRP is normally measured by sampling the field at predetermined locations on a sphere around the device under test (DUT) and then integrating the field over the sphere. Using the circuit parameters introduced in the previous section TRP can be calculated by

$$TRP = \eta_{refl}\eta_r P_A. \tag{2-34}$$

Note that this particular definition of TRP does not take into consideration the losses presented by the possible user. TRP can also be calculated with the help of EIRP as

$$TRP = \frac{1}{4\pi} \int_0^{2\pi} \int_0^{\pi} EIRP(\theta, \varphi) \sin\theta d\theta d\varphi . \tag{2-35}$$

TIS is another measure of the antenna performance often found in handset specifications. Assume an ideal environment, where the incident power to the examined antenna arrives uniformly from every direction and in both orthogonal polarizations. Next assume that the incident power is decreased until the receiver reaches its sensitivity threshold, e.g. the bit error rate (BER) grows to a critical level. If the DUT is now replaced with an ideal isotropic antenna, the received power level is the TIS of the DUT. The equation for TIS reads

$$TIS = \frac{P_S}{\eta_{refl}\eta_r}, \tag{2-36}$$

where P_S is an application-specific parameter that stands for the conducted sensitivity threshold of the receiver.

MEG is a parameter describing the ability of the antenna to receive power in a multipath propagation environment. One way to calculate it is

$$MEG = \frac{P_{rec}}{P_V + P_H}, \tag{2-37}$$

where P_{rec} is the received power and P_V and P_H the incident powers at vertical and horizontal polarizations. MEG is measured by moving the antenna in its operational environment and comparing the received power to that of a reference dipole.

2.4 Field simulation

The equations in Section 2.2 in principle provide the necessary means for the solving of electromagnetic fields. However, in the more complex cases the analytical calculation of the fields becomes virtually impossible. Consequently several computational calculation methods have been developed. These methods require heavy computing, but with today's processing capabilities they have become commonplace tools.

At least as far as popularity goes, three numerical methods for the purposes of antenna design stand out: finite-difference time-domain (FDTD) [14], method of moments

(MoM) [15] and finite element method (FEM) [16]. Each of these methods naturally has its pros and cons making the argumentation over which method to employ complicated, simply due to the difficulty of finding decent comparisons and the fact that the order of superiority varies strongly depending on the structures and parameters under scrutiny.

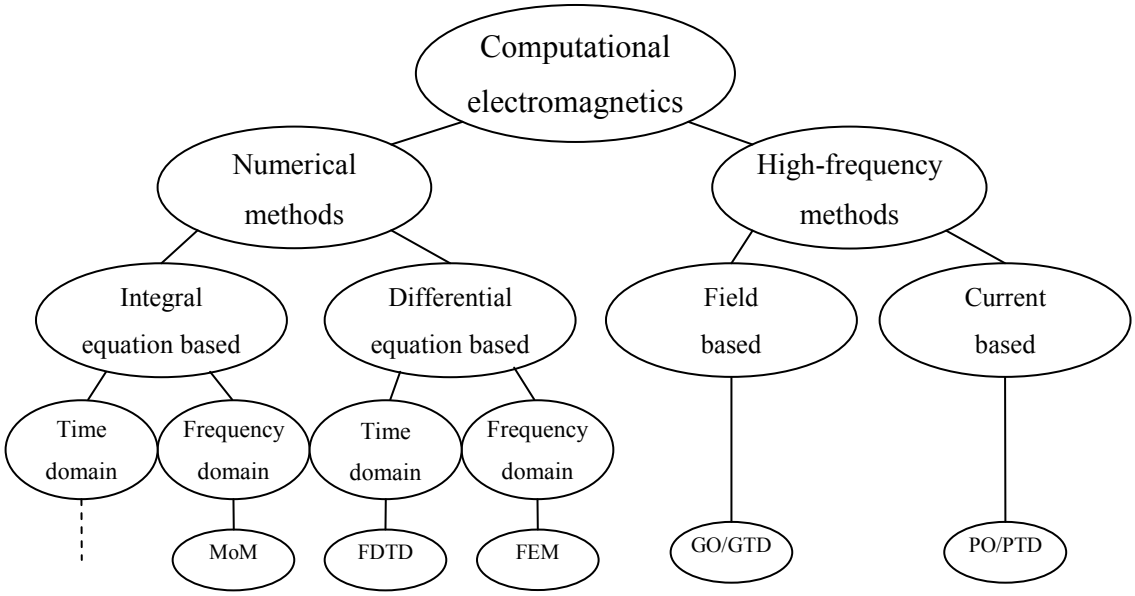

Figure 2-7. Categories of simulation methods.

This section first gives an introduction to FDTD and then describes briefly the other methods mentioned above as well as a few optics-related methods that can be used in computational electromagnetics. It is beneficial to have some insight on these methods in the selection and setup of the simulation for a given task. One possible division of the methods, taken from [1], is shown in Figure 2-7.

2.4.1 Finite-difference time-domain method

Finite-difference time-domain (FDTD) method is a popular computational technique for the simulation of electromagnetic fields and the interaction of fields and different materials. There are several commercial and open-source FDTD software programs available. FDTD is also the method used in the simulations of this thesis.

FDTD is based on the discretization of Maxwell's curl equations (2-5) and (2-6). Examining Equation (2-5) it can be seen that the time derivative of the E-field depends on the change of the H-field across space. This means that the value of the E-field can be computed if we know its previous value and the space-derivative of the H-field, which in turn is time-stepped similarly. Thus the electric and magnetic fields can be

calculated in a leapfrog manner, if the initial field plus boundary and source conditions are known [1], [14].

The idea of FDTD is to divide the space into a Cartesian coordinate grid of voxels and then allocate the components of the electric and magnetic fields to specified locations on each voxel. The scheme is known as Yee lattice and the distribution of the components is illustrated in Figure 2-8, where every H-field component is surrounded by E-field components and vice versa [17]. Now there is a clear connection to Equations (2-5) and (2-6) and also Figure 2-1.

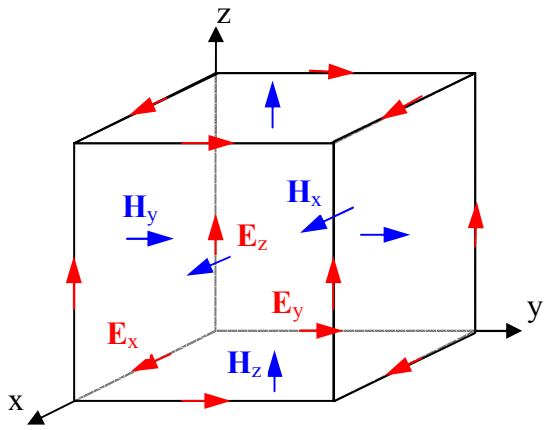

Figure 2-8. Yee lattice.

Let us now consider a one-dimensional example of a plane wave that is constant over the *xz*-plane. If the electric field is parallel to *z*-axis (E_z) and the magnetic field parallel to *x*-axis (H_x), Equation (2-5) simplifies to [1]

$$\frac{\partial E_z}{\partial y} = -\mu \frac{\partial H_x}{\partial t}. \tag{2-38}$$

Next the *y*- and *t*-axes are divided into discrete steps Δy and Δt, so that $y = m\Delta y$ and $t = n\Delta t$, where *m* and *n* are integers. Now the H-field at $y = (m + ½)\Delta y$ and $t = n\Delta t$ is approximated as

$$\begin{aligned} \frac{\partial H_x}{\partial t}\left[\left(m+\tfrac{1}{2}\right)\Delta y, n\Delta t\right] &= \frac{H_x\left[\left(m+\tfrac{1}{2}\right)\Delta y, \left(n+\tfrac{1}{2}\right)\Delta t\right] - H_x\left[\left(m+\tfrac{1}{2}\right)\Delta y, \left(n-\tfrac{1}{2}\right)\Delta t\right]}{\Delta t} \\ &= -\frac{1}{\mu}\frac{E_z\left[(m+1)\Delta y, n\Delta t\right] - E_z\left[m\Delta y, n\Delta t\right]}{\Delta y}, \end{aligned} \tag{2-39}$$

which can be easily modified to solve the H-field at the latest moment in time $t = (n + ½)\Delta t$. A similar approach is valid for the E-field. The above example sums the idea of FDTD, i.e. the fields are calculated using merely the earlier values of the fields.

Courant-Friedrich-Levy criterion sets the limit for the maximum time step in order to keep the finite-difference scheme stable [1], [17]. The criterion reads

$$\Delta t \leq \frac{1}{c\sqrt{\frac{1}{(\Delta x)^2}+\frac{1}{(\Delta y)^2}+\frac{1}{(\Delta z)^2}}}, \tag{2-40}$$

where Δx, Δy, and Δz are the grid steps. One can see that for a fine grid the maximum time step becomes smaller, which results in a longer calculation time, because usually shortening the total scanned time period is not possible.

Since FDTD simulation calculates the fields at all points throughout the computational domain the space must be truncated in order to keep the amount of data finite. The reflections from the boundaries introduce a possible source of error and several mathematical absorbing boundary conditions (ABC) have been developed to simulate an unbounded domain. Also, a popular implementation is to use an absorbing material called perfectly matched layer (PML). It is also possible to truncate the computational domain simply with perfectly conducting or perfectly magnetic planes, which set the tangential components of the E-field or H-field, respectively, to zero [17].

The basic principle of FDTD is intuitive and easy to implement. The modeling of structures consisting of different materials is fairly simple. As a time-domain method FDTD is suitable for wideband simulations. Another advantage is that FDTD produces field values over time, which enables the animated display of the fields. These animations offer an insight into the functioning of the model. In addition, the simulation of far-field characteristics is possible with a near-field to far-field transformation.

The weakness of FDTD relates to its fundamental principle of gridding the computational domain, which makes the modeling of detailed and rounded shapes difficult. With such structures the grid must be made finer, which extends the time needed for the calculations.

2.4.2 Other methods

Method of moments (MoM) divides the surface of the body under scrutiny into pieces with specific currents. These currents are approximated with a system of simultaneous linear algebraic equations. Once the currents are known, the radiation can be calculated with straightforward equations, such as Equation (2-20) [1], [15]. MoM is efficient in

simple models with high surface to volume ratio, but with complex volumes the matrices used in the calculations become heavy. In addition, the frequency-domain nature makes the method slow in wideband simulations. A method closely related to MoM is the boundary element method (BEM).

Finite element method (FEM) is another method gaining popularity in its application to antenna problems [4] [16]. With FEM the calculation space is divided into a finite number of surface or volume elements (usually triangles or tetrahedra) and the field values at element edges are computed using local partial differential forms of Maxwell's equations. FEM is a versatile method able to handle complex structures. FEM can be more accurate, but more difficult to implement when compared to FDTD.

Geometrical optics (GO) is a classic method, which treats waves as rays describing the propagation of energy. GO is able to simulate direct propagation, reflection and refraction of the rays for example in the propagation channel of radio communications systems. Geometrical theory of diffraction (GTD) is an extension of GO developed to overcome some of the limitations of GO by introducing models for diffraction. Both GO and GTD are fairly simple high-frequency methods and especially GTD is capable of solving problems involving complicated structures [1], [4].

Physical optics (PO) and its extension, physical theory of diffraction (PTD), are current-based calculation methods. The idea of PO is to calculate the scattered fields of induced surface currents. PTD is based on PO and it refines the surface-field approximations of PO to take into account scattering at body edges. These methods are somewhat more general than GO and GTD, but they are also best used in high-frequency problems [1], [13].

3 Specific absorption rate

3.1 Introduction

In the modern society we are constantly exposed to electromagnetic fields from sources such as power lines, electronic devices and mobile phones. The exposure to the fields is regulated with limits based on the best knowledge research has produced so far. The heating of tissue and the stimulation of nerves are well-known examples of effects caused by strong fields. Researchers have also presented theories about the biological effects of low-intensity fields, when the effects mentioned above do not occur. The research evidence of these low-intensity effects is however inconclusive and further research is necessary [18], [19].

The purpose of this chapter is to introduce the concept of specific absorption rate (SAR), which is the most important dosimetric quantity of exposure at radio frequencies. The chapter includes short introductions to dosimetry and the research on the health effects of radio waves. Standards and measurement techniques regarding SAR as well as the authorities controlling them are also presented here. Often the same standards are used for a larger scale of electromagnetic fields, but the scope of this chapter is mainly limited to frequencies relevant to mobile handsets.

SAR describes the absorption of power into lossy medium as a result of electric fields and currents present in the tissue. The loss mechanisms are described in Section 2.2.2. Local SAR is defined as the loss power dP_l absorbed into an infinitesimal mass dm, resulting in the following equation:

$$SAR = \frac{dP_l}{dm} = \frac{\sigma_{eff} E_{rms}^2}{\rho} = \frac{J_{rms}^2}{\rho \sigma_{eff}}, \tag{3-1}$$

where E_{rms} and J_{rms} are the root-mean-square values of the electric field strength and current density, respectively, σ_{eff} is the effective conductivity and ρ the density of the tissue see Equation (2-15). The unit of SAR is thus W/kg. At radio frequencies the power absorbed in tissue transforms into heat. This leads to another definition of SAR as

$$SAR = c_p \frac{\Delta T}{\Delta t}, \tag{3-2}$$

where c_p is the specific heat capacity of the tissue and ΔT the temperature change over a time period Δt.

A distinction must be made between the momentary SAR and the SAR in the regulative norms, where it is measured averaged over a certain mass of tissue and a period of time. The averaging mass is commonly 1 or 10 g, and the time 6 or 30 minutes.

3.2 Dosimetry

The human body is a relatively good conductor compared to the surrounding air and can act like a receiving antenna. Dosimetry studies how external fields acting upon the body couple into internal fields affecting tissue and cells (e.g. [20], [21]). The generated internal fields depend not only on the strength and the frequency of the external fields, but also on the shape, size and electrical characteristics of the body and the orientation of the body in relation to the external fields.

The SAR distribution within the body is typically highly inhomogeneous. The analytical calculation of the internal fields is possible only with simplified geometries, which yet provide us with valuable knowledge on the coupling mechanisms. The analytical calculations can be complemented with numerical methods, which are also in practice the only way to investigate more realistic exposure situations. In dosimetric measurements it is customary to use body phantoms containing homogeneous liquid that emulates the characteristics of tissue.

Tissues are made up of water and different salts and organic compounds and they can be considered as a mixture of insulators and conductors. The water content is focal in defining the electrical characteristics of tissues, because the salt content of tissue fluids is almost constant. Muscles and organs, which contain water, are better conductors than fat or bones. The major part of human body is composed of muscle tissue and other tissues similar to it. Therefore the average characteristics of the body are largely dictated by muscle tissue. For example the skin depth of the body is close to that of muscle tissue, as seen in Figure 3-1 [19]. The electrical characteristics are also frequency-dependent, due to the several dispersion mechanisms affecting biological tissues. Typically the relative permittivity decreases and conductivity increases as a function of frequency. Typical dielectric values for different tissues are shown in Table

3-1. The values are taken from an extensive database of the Italian National Research Council [22].

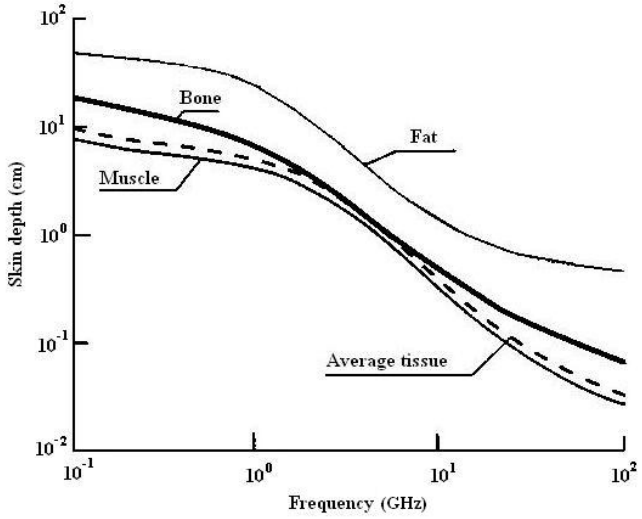

Figure 3-1. Skin depth in different tissues [19].

Table 3-1. Typical properties of tissues [22].

Tissue	Density (ρ) [kg/m^3]	Conductivity (σ_{eff}) [S/m]			Relative permittivity (ε_r')		
		900 MHz	1800 MHz	1900 MHz	900 MHz	1800 MHz	1900 MHz
Muscle	1040	0.94	1.34	1.40	55.0	53.5	53.4
Skin (dry)	1010	0.87	1.18	1.22	41.4	38.9	38.7
Blood	1060	1.54	2.04	2.11	61.4	59.4	59.2
Grey brain matter	1040	0.94	1.39	1.45	52.7	50.1	49.9
White brain matter	1040	0.59	0.91	0.96	38.9	37.0	36.9
Fat	920	0.05	0.08	0.08	5.5	5.3	5.3
Marrow bone	1810	0.04	0.07	0.07	5.5	5.4	5.4
Cortical bone	1810	0.14	0.28	0.29	12.4	11.8	11.7

The region from 30 MHz to 3000 MHz is called the resonance region, because at those frequencies the half-wavelength is close the dimensions of the human body. Different parts of the body have their own resonance frequencies. The human head, for example, has a resonance at about 400 MHz [5].

Figure 3-2 depicts the whole-body SAR produced by a plane wave with a power density of 10 W/m^2 calculated using a block model of an average human being [5], [23]. The E-field is parallel to the longitudinal axis of the body. Thus in this situation the coupling of the fields into the body is maximal.

A few observations can be made from the figure. At frequencies from 10 MHz upwards SAR is proportional approximately to the square of the frequency before reaching a maximum around 70 MHz. After that SAR starts to decrease inversely proportional to frequency and becomes fairly constant by 1000 MHz. If the body is grounded the mirror image causes the resonant frequency, i.e. where maximum SAR occurs, to be approximately half of that of an ungrounded body. On the other hand, the resonant frequency of a child is higher due to the smaller dimensions of the child's body [24].

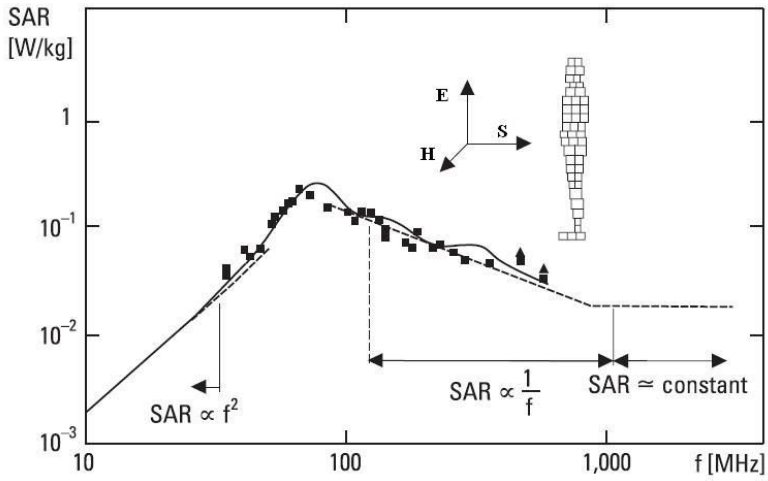

Figure 3-2. Whole-body SAR in 10 W/m2 plane wave conditions calculated using a block model of an average human body [5], [23].

The orientation of the body in relation to the incident field is essential for the amount of absorption. The polarization of the field can be either E-, H- or k-polarization, depending on whether the E-field, H-field or the propagation vector is parallel to the longest dimension of the body. SAR in the case of E-polarization was already depicted in Figure 3-2. H-polarization produces a generally lower SAR without the resonance peak, but at higher frequencies the absorption is close to E-polarization. Similarly to E-polarization, k-polarization generates a resonance peak in SAR, but it is clearly of lower strength.

At high frequencies the skin depth of radiation diminishes, causing the currents to funnel near to the surface of the body. At the resonance region the higher current

densities and especially the resonances described above can create local SAR hotspots deep inside the body. In plane wave conditions the local SAR at these hotspots can be up to 20 – 30 times higher than the whole-body SAR. However, above 1 GHz, the significance of the hotspots diminishes due to the strong attenuation of the fields in tissues. High values of SAR near the surface of the skin are biologically not as dangerous, because the peripheral circulation and thermal conduction to the surrounding air cool down the skin effectively.

The dosimetric principles related to the usage of handsets are further discussed in the following Chapter 4.

3.3 Biological and health effects of radio frequency fields

The biophysical mechanisms behind tissue heating and nerve stimulation by strong electromagnetic fields are known well and the present normative exposure limits are based on them. Radio frequency radiation is non-ionizing and therefore cannot directly cause DNA damages. The most important effect of radio waves is the heating present in lossy media. The harmful thermal effects, such as cataracts, are unchallengeable, but the non-thermal effects caused by weak fields have remained debatable. The possibility of adverse non-thermal effects has been under heavy biological and epidemiological research, but no conclusive evidence, one way or the other, has been found [18], [19]. It is worth pointing out that all biological effects do not necessarily lead to health effects.

The biological and health effects of radio frequency electromagnetic fields are investigated by epidemiological, human, animal and cell studies. An overwhelming amount of research results is already available. The amount of data would be too massive for an individual person to explore, but fortunately there are organizations that review and summarize the studies. These organizations include the World Health Organization (WHO) [25], the International Committee for Non-Ionizing Radiation Protection (ICNIRP) [26] and the Finnish Radiation and Nuclear Safety Authority (Säteilyturvakeskus, STUK) [18], [19]. The publications by STUK were used as the main sources for this section.

3.3.1 Thermal effects

Energy absorption from electromagnetic fields activates the body's thermoregulation with the purpose of keeping the temperature as close as possible to the normal 37°C and

preventing any damage to cells and tissues. Thermal energy is dissipated from the body by sweating and increased peripheral circulation. The consequences of excessive heating in the body vary from temporary disturbances in cell functions to permanent destruction of tissues. The translation of SAR values into heating is not straightforward. In addition to the characteristics of the exposing fields, one has to take into account a group of thermophysiological and ambient variables, e.g. the specific heat capacity of the tissues, the cooling by the blood circulation and the temperature of the surroundings. Therefore it has been suggested that limiting the temperature increase would be biologically more justifiable at radio frequencies instead of the current normative SAR limits.

Excessive whole-body heating happens only in rare conditions and for the general public more relevant is to approximate the local energy absorption. The local temperature rise can be estimated with the Pennes bio-heat equation. For brain tissue, when the temperature rise is less than 3°C the equation simplifies to

$$\Delta T = \frac{SAR\tau}{c_P}\left(1 - e^{-t/\tau}\right), \tag{3-3}$$

where τ is the thermal time constant, which typically is 2.5 – 6 minutes. Equation (3-3) applies when the cooling by the blood convection is at least as effective as the cooling by the thermal conduction. Figure 3-3 [18] depicts the heating of brain tissue in two cases as calculated by the simplified exponential model. Within six minutes the temperature increase reaches 90% of its maximum. More accurate approximations utilize numerical simulations, for example FDTD simulations can be combined with numerical modeling of the Pennes bio-heat equation.

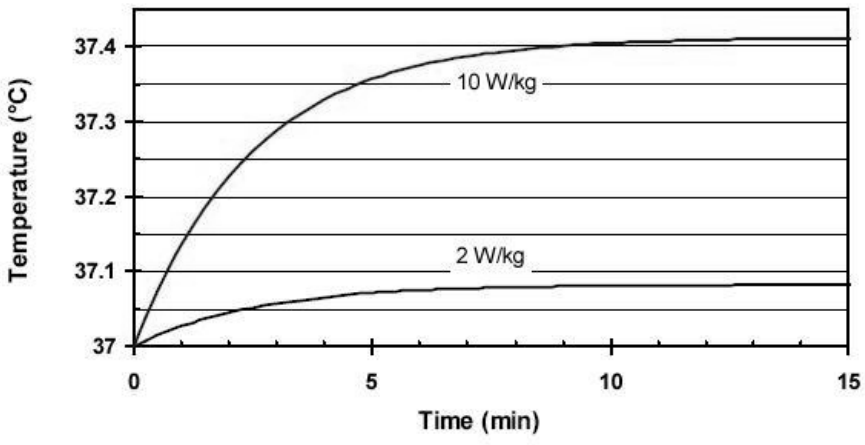

Figure 3-3. Calculated rise in brain temperature [18].

At low exposure levels the temperature increase is directly proportional to SAR. A rise of 3°C would require a local SAR of approximately 50 W/kg. At higher temperatures the heating becomes non-linear as the thermal convection strengthens. However, areas with less efficient cooling by the circulation, e.g. the lens of the eye, are more susceptible. Thus the lens may experience a temperature increase of 1°C at SAR level of 10 W/kg.

At cell level the heating does damage by disturbing the functioning of proteins. Cells begin to die when the temperature rises more than 5°C, but the tissues can endure momentary increases of tens of degrees. Most susceptible are brain and testicular cells.

An essential question is what the critical temperature increase for tissues and the whole body is. Table 3-2 lists the exposure conditions for some adverse effects. Some of the effects relate to the whole-body temperature increase, while some are of local nature. In terms of SAR values the limit for hazardous thermal load is considered to be the whole-body SAR of 4 W/kg.

Table 3-2. Temperature thresholds for adverse biological effects.

Effect	Object	Temperature threshold	Duration of exposure
Heat stroke	Human	> 42 °C	1 – 2 h
Damage to the central nervous system	Human, animal	42 – 44 °C	1 – 2 h
Skin burn	Human	55 – 60 °C	3 – 10 s
Pain sensation	Human	45 °C	3 – 10 s
Behavioural changes	Rat (whole-body)	1 °C increase	40 – 60 min
Cataracts	Rabbit (lens)	≥ 41 °C	≥ 30 min

The comparison of biological responses to continuous-wave and pulsed signals is still incomplete. However, it is clear that the interaction of pulsed signals and tissues depends not only on the pulse itself, but also on the size, shape and surroundings of the absorbing tissue. There are documented biological effects related to the rapid increase of temperature. One of these mechanisms is the auditory response to fast pulsed signals.

3.3.2 Mobile handsets

The concern over mobile phone safety is understandable, given the ubiquity of the devices. Mobile handsets are also operated close to the head and body, which means

that normally 10 – 90 % of the transmit power is absorbed into the user. Aside from the handset antenna design issues, which are discussed in Chapter 4, the factors affecting the absorption level are distance from the radiator, the anatomy and orientation of the user's hand and head plus the electrical characteristics of the tissues.

A significant portion of the power emitted by a mobile handset is absorbed into the user's head. As a result the outer layers of the brain and the skin next to the phone may experience a slight temperature increase. At its peak the increase is 0.3°C for the brain and a little more for the skin, while the natural variation of the brain temperature is about 1°C. The increase is too small to have any significant effect, but in theory the radiation may disturb normal cell and brain functions. When pressed against the head, handsets can warm the adjacent skin, but it normally is due to the mechanical heat transfer from the handset.

As of 2005, the cancer hazards relating to the use of mobile phones had been researched in 14 epidemiological studies, which all have yielded negative results in terms of increased risk of brain tumor. However, there is a further need for long-term epidemiological research because of the relatively short period handsets have been in use. During the time of this writing, the results from an extensive international research called INTERPHONE were eagerly awaited.

The proximity of the user to the handset means that the exposure happens in the near-field. Thus simple propagation or plane wave models cannot be used and the exposure must be measured either with SAR or the E-field strength. There is a table of SAR values of example mobile phone models in Appendix 1. The table contains test measurement results carried out by STUK as well as values reported by the phone manufacturers. The complete list of the test measurements by STUK can be found in [27]. The results are for the most part reasonably consistent and fall within the normal uncertainty margin of 30 %.

Bearing in mind the high penetration of mobile handsets in today's society the appliance of precautionary principle is in place to minimize the risks. This precautionary attitude has been adopted by authorities, including STUK [28], especially regarding children. The exposure can easily be lowered by using means to maximize the distance from the radiating part of the handset to the user, e.g. with a hands-free kit, and by trying to keep the connection to the base station as obstacle-free as possible.

3.4 Regulation of exposure

3.4.1 Safety standards

The known and potential health effects of electromagnetic fields create the need to govern the acknowledged risks. As a consequence several national and international safety norms have been created to limit the hazards. These norms can be found either in legislation or as standards and recommendations and they cover the whole spectrum from static fields to 300 GHz. Even though some of the norms are technically only advisory, they may still hold great authority, especially those set by the leading expert organizations. There are usually different limits for the occupational exposure and for the exposure of the general public. In addition, the conditions are divided into uncontrolled and controlled environments. Here we concentrate on the exposure limits for the general public in uncontrolled conditions. The most important standards regarding the mobile handsets are those limiting the exposure of the user and those harmonizing the measurement procedures.

The path that transforms the research results into practical actions in end-product design has many steps. The norms that form these steps are presented next, with emphasis on the radio frequency range. Table 3-3 lists the organizations mentioned in this section.

The research output concerning electromagnetic exposure is gathered and turned into general guidelines for limiting the exposure. The guidelines are made in cooperation with WHO. EU employs ICNIRP guidelines [29], while IEEE guidelines [30] are used in North America. These guidelines are also used internationally as models.

Table 3-3. International expert and standardization organizations.

Organization	Abbreviation
International Committee for Non-Ionizing Radiation Protection	ICNIRP
Institute of Electrical and Electronics Engineers	IEEE
International Electrotechnical Commission	IEC
European Committee for Electrotechnical Standardization	CENELEC
American National Standards Institute	ANSI
Federal Communications Commission	FCC
World Health Organization	WHO

The ICNIRP guidelines contain two kinds of values: basic restrictions and reference levels. The basic restrictions are given in variables that are as close as possible to the biological effects. The quantities in question are current density (< 10 MHz), SAR (100 kHz – 10 GHz) and power density (> 10 GHz). The trouble with the basic restrictions is that measurements inside the body are difficult, if not impossible, to conduct. The purpose of the reference values is to transform the basic restrictions into upper limits of quantities that are measurable outside the body, e.g. E-field and power density. The reference values are set low enough to ensure that in no circumstances are the basic restrictions exceeded. The limits for occupational exposure are fivefold compared to the exposure of the general public.

At 10 MHz – 10 GHz the objective of the basic restrictions is to prevent excessive heating of the body. The requirement is to limit the local temperature increase caused by radio frequency radiation to less than 1°C. For the whole-body exposure the threshold for health hazards is considered to be SAR value of 4 W/kg. The SAR limits set for the general public should provide a safety margin with a ratio of 25 – 50 compared to known adverse exposure levels. SAR is defined as time-averaged. In ICNIRP guidelines the averaging time is 6 minutes, which is chosen based on the thermal time constants of human tissues.

The exposure limits allow a higher value for local SAR compared to the whole-body SAR, because the normal thermoregulatory functions of the body even out the temperature increase at local hotspots. Usually in the design of mobile handsets limiting the local SAR values is a more relevant task, because the user is exposed to the near-field of the handset and the SAR distribution caused by a near-field is always superficial [19].

The ICNIRP guidelines also define how to handle broadband and pulsed signals. Broadband signals consisting of components in the range of 10 MHz – 10 GHz should conform to

$$\sum_{i=10MHz}^{10GHz} \frac{SAR_i}{SAR_L} \leq 1, \tag{3-3}$$

where SAR_i is the SAR caused by exposure at frequency i and SAR_L is the respective SAR limit. At other frequency ranges the same condition is used, but with the quantities relevant for those ranges. Pulsed signals can be described with the term specific

absorption (SA), which is SAR multiplied by time. ICNIRP limits the maximum SA caused by a single pulse at 0.3 – 10 GHz to 2 mJ/kg for the general public.

The guidelines introduced above are used as a basis for legislative actions. The maximum allowed exposure, including SAR values, has been set by various regulatory bodies, including The Council of the European Union [31] and FCC in USA [32]. After the exposure limits are set, there needs to be standards that determine how the manufacturers can make sure their products are compliant with the respective laws. Such standard for mobiles phones in Europe is the CENELEC standard EN 50360 [33], which is a harmonized product standard under the Radio & Telecommunication Terminal Equipment (R&TTE) Directive [34].

Until recently, the standards for SAR measurement methodologies were not harmonized internationally, as different standards were created by CENELEC in Europe [35] and IEEE in USA [36]. However, in 2005 IEC published a new standard for SAR measurements (IEC 62209-1 [37]), which has already been adopted by CENELEC (EN 62209-1) and which will also be the basis for the next standard in USA. Overall the recent trend has been towards the harmonization of the different standards and limitations around the world.

3.4.2 SAR limits

The energy absorbed by the users of mobile handsets is controlled by limiting the resulting SAR values. The European and American standards concerning SAR are summarized in Table 3-4. The limits of Table 3-4 are for the general public. The US limits have been slightly stricter, but recently IEEE changed its recommendations [30], seen in the parentheses, to be consistent with the guidelines of ICNIRP [29]. A difference between the ICNIRP guidelines [29] and the IEEE standard [30] is that the former considers pinnae as part of the head while the latter classifies them as extremities. This is worth noticing since the spatial peak SAR often occurs in the pinnae.

In SAR testing of mobile terminals the exposure is assumed constant over the duration of the averaging time. Thus the time-averaging requirement does not apply [38].

The values of Table 3-4 offer a reference level for the SAR aspect of antenna design. The SAR targets set by the manufacturers or their customers for the design of handsets

may, however, be significantly lower, although the consumers rarely choose phone models based on their SAR levels.

Table 3-4. SAR standards and limits for the general public. The limits for occupational exposure are fivefold.

	Europe	USA
Limits	Council Recommendation 1999/519/EC [31] (EN 50360 [33])	FCC/OET Bulletin 65 [32] (IEEE/ANSI C95.1 [30])
Measurement method	EN 62209-1 (IEC 62209-1 [37])	IEEE 1528 [36]
Whole-body SAR [W/kg]	0.08	0.08 (0.08)
Spatial peak SAR, head and trunk [W/kg]	2	1.6 (2)
Spatial peak SAR, extremities [W/kg]	4	4 (4)
Averaging time [min]	6	30 (30)
Averaging mass [g]	10	1 (10)

3.4.3 SAR measurements of mobile handsets

Different standards are followed around the world regarding the SAR testing of wireless devices [35], [36], [37]; although in recent years there has been progress towards unification. The most recent IEC standard [37] was not available for this work, but fortunately the different standards have considerable common ground. The standards include specifications for the measurement system, the measurement protocol, the uncertainty assessment and the measurement reporting. Even though calorimetric SAR measurements are in theory possible based on Equation (3-2), SAR assessment is almost invariably done by measuring the E-field.

The standard SAR measurement system comprises of the phantom, the measurement equipment, the scanning system and the mobile phone holder. In brief, SAR testing is performed using an automatically positioned miniature probe, which measures the E-field distribution in a phantom model representing the human head exposed to the fields produced by a mobile phone. The E-field values are then converted to SAR values, from which the mass averaged SAR value is calculated. An example of a SAR testing system is depicted in Figure 3-4 [39].

Figure 3-4. SAR measurement equipment [39].

The standards include instructions for the calibration procedure of the measurement equipment, and requirements for the sensitivity, linearity and isotropy of the probe. The accuracy of the system is tested before every compliance measurement occasion with a simplified performance check that utilizes dipole sources as reference of exposure. The simplified performance check is a straightforward test of repeatability in order to detect possible errors over short time periods. In addition, a system validation must be conducted at least annually using standard phones with known SAR values.

The geometry is a dominant factor for exposure. Consequently a Specific Anthropomorphic Mannequin (SAM) model simulating the human head has been developed based on the size and shape of the 90 percentile large adult male reported in 1989 [40]. The large head constitutes a worst case scenario, since dosimetric studies suggest that larger heads couple more energy. The SAM shell is filled with liquid possessing dielectric properties similar to those of head tissues. A heterogeneous head structure would be more realistic, yet more difficult to implement. Thus a homogeneous liquid is used enabling the free movement of the measuring probe inside the phantom. The phantom can be either an upright or a sagittally-bisected horizontal model. The latter is used in the system of Figure 3-4. Table 3-5 shows the target dielectric properties of the tissue-simulant liquid. These properties can be achieved with example recipes offered in the standards. The standards also define reference points on the phantom for the calibration of the scanning system and the reproducible positioning of the device under test (DUT).

Table 3-5. Target dielectric properties of head tissue-equivalent material [35], [36].

Frequency [MHz]	Relative permittivity (ε_r')		Conductivity (σ_{eff}) [S/m]	
	CENELEC	IEEE	CENELEC	IEEE
300	45	45.3	0.85	0.87
450	44	43.5	0.88	0.87
900	42	41.5	0.99	0.97
1450	41	40.5	1.20	1.20
1800 – 2000	40	40.0	1.38	1.40
2450	39	39.2	1.84	1.80
3000	39	38.5	2.40	2.40

The measuring probe must be small enough not to have any resonances over the relevant frequency range and not to significantly disturb the field distribution inside the phantom. The E-field values are measured with orthogonal dipole elements including integral diode detectors. The DC output of the diodes is then read by a remote amplifier. The dipoles are located at the very tip of the probe to allow the field to be assessed as close as possible to the phantom shield. The standards recommend the probe diameter to be less than 8 mm, but even smaller probes are needed to reduce the uncertainties due to field gradients.

The automatic positioning system holding the probe must be able to scan throughout the whole volume of the phantom. The accuracy of the probe tip position needs to be better than ± 0.2 mm. Accurate positioning of the probe is important for the evaluation of the three-dimensional SAR distribution, and also because multiple SAR values are combined and interpolated to get the mass-averaged SAR.

The holder used in the positioning of the DUT must be made of low-loss and low-permittivity materials. Nevertheless, the standards still require a substitution test to verify that the holder does not affect the readings. The positioning is critical, because exposure in the near-field of an antenna varies significantly due to even small changes in the setup. In addition, the position of the SAM in relation to the DUT affects the performance of the antenna, and thus SAR.

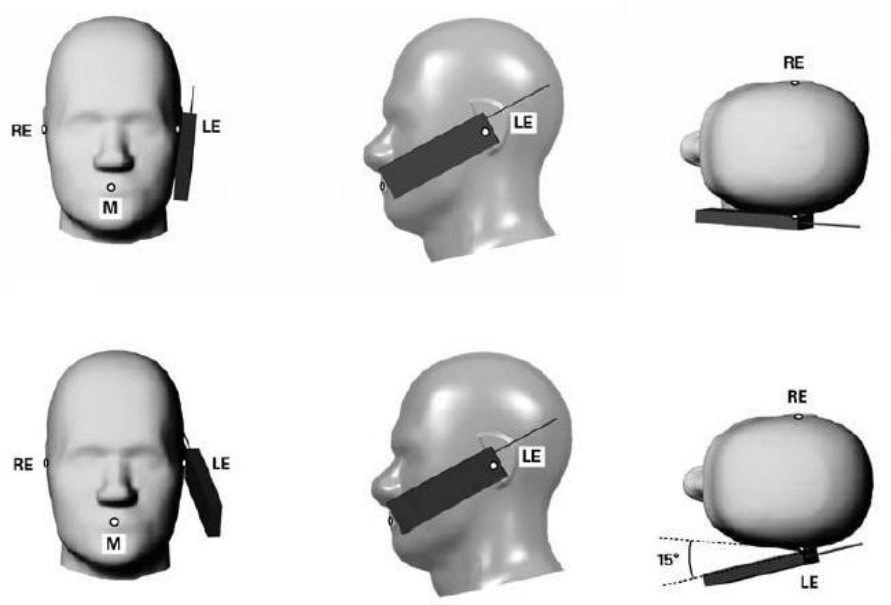

Figure 3-5. The two SAR test positions on the left side of the phantom. The reference points for the right ear (RE), left ear (LE), and mouth (M) are indicated [36].

The measurement procedure begins with preparatory actions. The dielectric properties of the SAM liquid are measured, a simplified performance check is conducted and the DUT is prepared and positioned for testing. The battery must be fully charged and the DUT set to transmit at its highest power level. The tests are conducted in the "cheek" and "tilted" positions on both sides of the phantom. The positions are illustrated in Figure 3-5 [36]. A notable fact is that the test configurations do not employ a phantom hand for a more realistic use case of the DUT. The exclusion of the hand is consistent with the worst case scenario approach, as the hand commonly reduces the generated SAR in the head. The hand and its position would also be difficult to standardize, making the repeatability questionable.

The test is first performed at the center frequency of each operating band. Then the configuration resulting in the maximum SAR is used to test the low-end and high-end frequencies of every transmitting band. Multiband devices must be measured in each transmitting band with the corresponding maximum power level.

The measurement procedure typically begins with an area scan, where a coarse measurement grid is used to find the approximate locations of the local SAR maxima. The volumes around the maxima are then scanned more thoroughly with a typical grid spacing of 5 mm. The SAR value at a test point for every measurement configuration is

recorded at the beginning and at the end of the procedure to ensure a sufficiently small amount of drift.

The software part of the measurement system has several important functions. It must define the scanning grid and control the positioning apparatus. In the post-processing phase the mass-averaged SAR is calculated from the local SAR values utilizing appropriate interpolation and extrapolation methods. The mass-averaging volume has the shape of a cube. The standards use a density of 1000 kg/m^3, which gives a cube edge length of 2.15 cm for a mass of 10 g. Extrapolation is needed to define local SAR values near the phantom shell, where the maximum SAR normally is located. The cubic volumes are moved in the vicinity of the local SAR maximum to find the maximal mass-averaged SAR.

The importance of the uncertainty assessment of the results is emphasized in the standards and detailed instructions for the evaluation of different components contributing to the uncertainty are given. The total uncertainty of SAR values shall not exceed 30 %.

Finally, the results along with the uncertainty assessment shall be reported. In addition, all the information regarding the measurement setup must be recorded.

4 Handset antenna design

4.1 Introduction

The development of modern wireless communications devices has put significant pressure on the antenna performance, as the size of the device has decreased in parallel to the increase in the number of communications systems supported by a single terminal. This challenge has been the inspiration for scores of studies.

In practice the synthesis of an antenna is done through analysis, since there are no universal mathematical models to create antenna structures based on the target properties [2]. The desired antenna performance is pursued by trying different antenna types and changing their parameters. This emphasizes the role of experience and source literature, not forgetting the importance of the knowledge of the fundamental theory.

Due to the reciprocal nature of antennas, and assuming an isotropic medium, the transmitting and receiving characteristics of an antenna are identical. This is a helpful aspect in the design and measurement process of antennas. However, the requirements of a transmitting antenna are often different from those of a receiving antenna.

In addition to the electrical requirements, the design of a handset antenna has to take into account the resulting exposure of the user. Compliancy with the SAR limits is one challenge more to the antenna designer, but it also bears a reward. Namely, the reduction of the power absorbed by the user is desirable in terms of increasing the total radiation efficiency of the handset. Research on the matter has produced known principles that can be utilized to reduce the SAR. However, it must be said that these principles only generate trends to the SAR levels and do not guarantee any absolute SAR values.

This chapter starts with a short recap of the utilized technology and the requirements placed for modern handsets and their antennas. Next, the special characteristics and design challenges of small internal antennas are presented. Although the emphasis of this thesis is on SAR, the different antenna parameters are so interconnected, that they cannot be examined separately. Finally, the interaction of handset and its user is discussed.

4.2 Specifications

4.2.1 Technology

Table 4-1 presents the frequency ranges of some of the most widely used wireless communications systems. Of these systems E-GSM 900 and GSM 1800 are used in most of the world, including Europe and Asia, and GSM 850 and GSM 1900 in the Americas. UMTS 2100, which is a newer system deployed in Europe and Asia, belongs to the third generation (3G) of wireless systems.

Table 4-1. Wireless communications system bands.

System	Frequency [MHz]	Relative bandwidth (B_r) [%]
GSM 850	824 – 894	8.1
E-GSM 900	880 – 960	8.7
GSM 1800	1710 – 1880	9.5
GSM 1900	1850 – 1990	7.3
UMTS 2100	1920 – 2170	12.2

In addition to the systems of Table 4-1 there can be a number of other supplemental systems integrated in a single modern handset, e.g. Bluetooth (BT) and Wireless Local Area Network (WLAN), to name a couple. These systems, however, normally operate at a lower power level and do not require the handset to be held near the head of the user. Thus they are of less importance in the SAR considerations.

A variable greatly affecting the resulting SAR values of handsets is naturally the applied transmitting power level. Table 4-2 [19] summarizes the transmit frequencies and maximum powers of the mobile communication systems already presented in Table 4-1. GSM systems divide transmissions into eight time slots. During a call each phone is allocated one of the slots, during which it may transmit. Therefore the average power is one eighth of the peak burst power. The more recent UMTS system has a continuous, albeit varying, signal.

The transmit power of mobile terminals in GSM and UMTS systems is adjusted automatically depending on the quality of the connection to the base station. The exposure is then highest when the base station is far away or the connection is weak due

to some other reason. The radiation in newer systems is not more powerful, although their data transfer rate is far superior.

Table 4-2. Maximum transmit powers in mobile communication systems [19].

System	Uplink frequency [MHz]	Peak power [W]	Mean (rms) power [W]
GSM 850	824 – 849	2	0.25
E-GSM 900	880 – 915	2	0.25
GSM 1800	1710 – 1785	1	0.125
GSM 1900	1850 – 1910	1	0.125
UMTS 2100	1920 – 1980	< 1, typically 0.25	0.125

4.2.2 Requirements

The requirements set for the handset antenna are dictated by five parameters: resonance frequency or frequencies, bandwidth, radiation efficiency, SAR and size. As said earlier in Section 2.3.3, the antenna specifications may communicate the requirements with different parameters, such as TRP and TIS, but the design problem always reverts back to the five fundamental parameters above.

The resonant frequency of a handset antenna essentially determines the possible operating frequency of the handset. As a single handset needs to operate in several systems and thus frequency bands, typically one or several multiresonant antennas are used.

The bandwidth is normally defined as the frequency range, over which the matching is better than a given threshold. With handsets the typical threshold for the reflection coefficient is -6 dB, Equation (2-30), which means that more than 75 % of the power proceeds to the antenna. The difficulty is to achieve the required matching over all of the operating bands. Perfect matching is possible only in a finite number of frequencies and it is more beneficial to accept less than perfect, but still good enough, matching to obtain a wider operational band.

The average radiation efficiencies of real mobile terminals in free space are typically 30 – 80 % [42], [43], which is a rather large variation. The power is lost e.g. in the plastics, battery and display of the device. In a talk position the efficiency is further decreased significantly.

The SAR requirements were discussed in Chapter 3. The most important normative limits for the antenna designer are 2 W/kg (10 g averaging) in Europe and 1.6 W/kg (1 g averaging) in the USA.

A crucial factor for the obtainable level of antenna performance is the available volume. The more space there is for the antenna structure, the better the performance can be. A typical planar handset antenna volume is a few cubic centimeters. Unfortunately the diminishing overall size of modern handsets and the increasing number of supported systems, and hence increasing number of antennas, means that the antennas must be squeezed into an ever-reducing space.

The operation principle of handsets requires the antenna to have an omnidirectional radiation pattern. However, directivity is a far-field parameter and it should not be confused with the SAR characteristics of a handset, since the user exposure is produced by the near-fields.

Due to the inconsistent orientation of the handset with respect to the base station and the cross-polarizing nature of the signal path, especially in an urban environment, the polarization is of little importance to the handset antenna design.

4.3 Small internal antennas

The development of mobile handsets has seen a dramatic reduction in the handset size and an increase in the level of integration. Consequently the size of antennas has also decreased. Small antennas in general have many virtues, e.g. low profile, light weight, low cost and ease of integration. As a drawback reduced antenna size results in poorer overall performance and the designer has to find a compromise between size, efficiency and bandwidth. Small antennas are known to have low directivity and poor radiation efficiency [4], [41]. Fortunately in the case of mobile handsets low directivity is a desirable characteristic. Note that the small antennas discussed here refer specifically to electrically small antennas, i.e. compared to wavelength.

Especially in recent years electrically small internal antennas have passed the more traditional external whip and helix antennas as the most popular choice for handsets. Internal antennas are protected by the casing and are thus mechanically more durable and convenient to handle. In addition, they offer more flexibility for industrial design.

The types of internal antennas used in handsets include planar, helix, dielectric resonator and chip antennas [13].

As the reactance of small antennas is relatively large, the input impedance varies rapidly as a function of frequency. Thus small antennas are essentially resonators with narrow bandwidths. Therefore it is worthwhile to present the basics of resonator theory next. The antenna structure is not always resonant in itself, so a matching circuitry may be necessary to achieve resonance.

This section also includes discussion about the possible ways to design an antenna that fulfills all the requirements. The radiation of handsets is always a combination of the contributions of the antenna itself and the chassis it is mounted on. In fact, the chassis often is the main contributor. This issue is therefore also discussed in this section. In addition, a type of small planar antenna, called planar inverted-F antenna (PIFA) is introduced. This type of antenna was utilized in the research part of this thesis work.

4.3.1 Small antenna as a resonator

A resonator is a structure that has a natural resonating frequency [5]. An electric resonance occurs, when the capacitive and inductive components of a circuit cancel each other and the circuit is seen as purely resistive. The capacitance C and inductance L of the resonator define the resonance frequency as

$$f_r = \frac{1}{2\pi\sqrt{LC}}. \tag{4-1}$$

The quality factor Q of a resonator compares the energy stored in the resonator W to the loss power P_l. In other words it compares the reactive part of the impedance to the resistive part. The quality factor is defined as

$$Q = \frac{2\pi f_r W}{P_l}. \tag{4-2}$$

Another way of calculating the quality factor is

$$Q = \frac{f_r}{2\Delta f_{3dB}}, \tag{4-3}$$

where $2\Delta f_{3dB}$ is the half-power bandwidth of the resonator. This expression is derived for example in [5]. One can see that narrow bandwidth results in high Q.

Figure 4-1 depicts an example of an antenna as a parallel resonator. The different conductances, g_r, g_c, and g_d, are normalized to the conductance of the generator and represent radiation losses, conductive losses and dielectric losses, respectively. Similarly, b is the normalized input susceptance of the antenna.

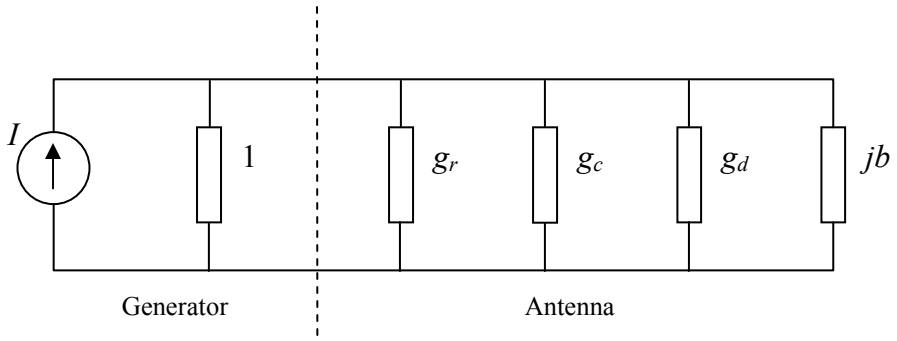

Figure 4-1. Resonator model for an antenna.

The total quality factor Q_l, also called loaded quality factor, is divided into unloaded quality factor Q_0, representing the internal losses of the antenna, and external quality factor Q_e, which describes the losses caused by external connections to the antenna. Q_0 is further divided into Q_r, Q_c and Q_d, the subindices referring to the different loss types of the antenna according to Figure 4-1. The connection between these is [44]

$$\frac{1}{Q_0} = \frac{1}{Q_r} + \frac{1}{Q_c} + \frac{1}{Q_d}, \tag{4-4}$$

because the quality factors are inversely proportional to the respective power losses, as seen in Equation (4-2). Furthermore, radiation efficiency can now be expressed as

$$\eta_r = \frac{Q_0}{Q_r} = \frac{Q_r^{-1}}{Q_r^{-1} + Q_c^{-1} + Q_d^{-1}}. \tag{4-5}$$

An interesting observation can be made from Equation (4-4). By increasing the conductive and dielectric losses, thus lowering the respective quality factors, it is possible to lower the unloaded quality factor, which results in larger bandwidth. However, this naturally lowers also the radiation efficiency, according to Equation (4-5), so in total usually no performance advantage is obtained.

The antenna size ultimately sets the limit for the minimum radiation quality factor Q_r and thereby for the maximum bandwidth of a small antenna. For example, for a small antenna acting as a purely electric or magnetic radiator the fundamental lower limit of Q_r is [4]

$$Q_r = \frac{1+2(kr)^2}{(kr)^3\left[1+(kr)^2\right]} \approx \frac{1}{(kr_a)^3}, \tag{4-6}$$

where k is the wave number ($k = 2\pi/\lambda$) and r_a denotes the radius of the smallest possible sphere enclosing the antenna. The approximation applies, when $kr_a << 1$. Although Equation (4-6) only represents the theoretical limit for Q_r, small antennas in practice behave qualitatively the same way. According to Equation (4-6), the bandwidth is approximately proportional to the volume in wavelengths (V_a/λ^3). As a conclusion, the best antenna performance, i.e. high efficiency and large bandwidth, is achieved with an antenna that has not been object to intensive miniaturization and a structure that makes use of the available space as efficiently as possible.

The relative bandwidth B_r is inversely proportional to the unloaded quality factor Q_0 of a resonator. With a set criterion for the maximum allowed VSWR, the relative bandwidth can be calculated from

$$B_r = \frac{1}{Q_0}\sqrt{\frac{\left(VSWR/g - 1\right)(VSWR - g)}{VSWR}}, \tag{4-7}$$

where g is the normalized total conductance ($g = g_r + g_c + g_d$, see Figure 4-1) of the resonator. It should be noted, however, that maximum bandwidth is not achieved with critical coupling ($g = 1$), but with slight overcoupling ($g < 1$), also called optimal overcoupling.

4.3.2 Design considerations

A basic task in handset antenna development is the matching. A multiresonant antenna is needed to cover the frequencies of all the utilized systems. The traditional design principle is to create an antenna element shape that can be naturally excited with several frequencies. The multiresonant feature can be created by utilizing either separate resonant paths or several resonances of a single path [45]. A multiresonant antenna can also be realized with the addition of high-Q matching resonators or parasitic elements.

For an adequate performance level, typically the required length of the antenna is $\lambda/4$. For 900 MHz a quarter wavelength is 8.3 cm, which is too much to be straightforwardly fit inside a handset casing among all the other parts. Hence miniaturization methods are needed. A simple means is to use meandering and slots to increase the length of the

resonant path. Another way is to alter the resonant frequency by loading the antenna dielectrically or reactively, thereby increasing the electrical length of the antenna. However, the miniaturization also always means sacrificing some other aspect of the performance.

As the number of radio systems supported by the handsets increases, while the volume reserved for the antenna often decreases, there needs to be enhancement in the antenna's bandwidth-to-volume ratio (BVR). As discussed in Section 4.3.1, some of the size-related fundamental limits for antenna performance have already been solved. Furthermore, in Section 4.3.1 it was explained, that by reducing the efficiency, e.g. with lossy materials or attenuators, the bandwidth can be increased. This is an example of the trade-offs between different antenna qualities the designer has to deal with.

One method to control the bandwidth is the optimization of the combination of the antenna and the handset chassis, which is discussed in the following section. In fact, without the contribution of the radiation from the chassis it would not be even possible to reach today's bandwidth requirements with the modern antenna sizes.

Additional techniques utilized to increase the bandwidth include the use of multiresonant antenna structures or matching circuits. If tuned close to one another, multiple resonances can be used to increase the bandwidth of a single band. The disadvantage of increasing bandwidth with multiple resonances is the more complex design.

The BVR of an antenna can also be enhanced by mechanical or electrical frequency tuning [41]. These methods, although being very useful and important for the antenna performance enhancement, have received less attention than the traditional introduction of novel antenna element shapes. Frequency tuning is possible in devices that operate only in a part of the system bandwidth at a time. A simple tuning principle involves the altering of the antenna geometry and hence its effective length. Electrical tuning is typically accomplished with switches or varactors and by loading the antenna with alternative additional reactances or controllable matching circuits. The benefits of frequency tuning can, however, be overshadowed by the increased cost, power loss and distortion of the signal.

4.3.3 Effect of chassis

In a handset the metal chassis acts as a part of the radiating system. In fact, studies have shown that the handset antenna element itself often produces only a minor part of the radiated power at the lower operating frequencies. Below 1 GHz the contribution of the antenna can be only about 10 %. As the frequency increases, the share of the antenna increases and at 1800 MHz the contributions of the antenna and the chassis are roughly equal [41], [42].

As the role of the metal chassis of a handset is more substantial than that of a mere ground plane, the mechanical characteristics of the chassis are known to have a crucial effect on the antenna performance. Thus also the chassis dimensions have to be considered when attempting to optimize the bandwidth, efficiency and SAR of the handset. Unfortunately the mechanical aspects of the whole terminal are never alone for the antenna designer to decide. In the following the effect of chassis dimensions on the bandwidth, efficiency and SAR is discussed.

The metal chassis consists of ground conductors in the printed wiring board (PWB) and other metal parts, including the components and interference shields which are connected to the ground conductors. Radio frequencies essentially see the chassis as a solid metal plate having dimensions close to those of the PWB [41]. The typical longitudinal shape and convenient length of the chassis of handsets results in their ability to support resonances of their own, acting like a thick dipole. Like in the case of the antenna, the resonant frequency of the chassis depends on its effective length, which can be increased with slots and meandering.

The antenna development can either utilize the radiation from chassis or try to minimize the excitation of the chassis currents. However, the volume available for the antenna is normally insufficient for the required performance level to be achieved with an isolated antenna, especially for the low-frequency systems. When the antenna is used to excite radiating currents on the chassis, it is possible to obtain much larger operating bandwidths. However, it must be taken into account, that in a combined system of antenna and chassis, a strong interrelationship between bandwidth, efficiency and SAR values can be seen. As a general rule of thumb stronger coupling to the chassis wavemodes results in a wider bandwidth, simultaneously with a decrease in the radiation efficiency and an increase in the local SAR values [41].

In an antenna-chassis setup the antenna resonances are excited by the feed, and the antenna in turn excites the chassis resonances. The performance of the handset is then determined by the interaction of the dominant resonant modes of both the antenna and the chassis. An analysis method for the combination of the antenna and chassis of a mobile handset is presented in [41], [42]. This method considers the antenna and the chassis as a system of coupled radiating resonators, which both support their own fairly independent wavemodes. These wavemodes are characterized by their respective resonant frequencies and quality factors, which can be independently adjusted to reach the desired performance of the antenna-chassis combination.

The stronger the coupling between the antenna and the chassis, the bigger the part of the radiation that comes from the chassis, and the stronger the chassis dimensions affect the radiation characteristics. The chassis can be excited either through magnetic or electric fields. The level of coupling depends on the size and shape of both the antenna and the chassis and the location and orientation of the antenna in relation to the chassis.

When considering the chassis dimensions, the strongest coupling occurs when the antenna and chassis resonant frequencies are near each other. At chassis resonances the bandwidth and SAR reach their maxima and the radiation efficiency its minimum. The first resonance and a bandwidth maximum can be found at a chassis length of around 0.4λ. Another maximum is found when the chassis length is approximately equal to the wavelength. Naturally the same rules apply for the chassis width. In [42], both a reduction in the radiation efficiency and an increase in the SAR values were found at a chassis length of about 0.36λ, which is very close to the length that gives the maximum bandwidth. Similar results have been reported in other studies, as well, but the behaviour of SAR values related to the chassis length also depends on the distance to the user's head.

The location and orientation of the antenna on the chassis also affect the strength of the coupling from the antenna to the chassis. A chassis with a length of $\lambda/2$ has its E-field maxima at the open ends. Thus shorted patch antennas, including PIFAs, which couple capacitively, have the largest bandwidth when placed at the end of the chassis. Also, for maximal coupling, the fields of the antenna and the chassis should be in parallel. If a shorted patch antenna is placed partly outside of the edge of the chassis and also bent downwards, the bandwidth increases, as it strengthens the coupling. Most efficiently this is done by placing the open end of the patch outside the chassis. On the other hand,

extending the antenna outside the chassis reduces the efficiency and increases the SAR values, which also happens for example already when the antenna width approaches that of the chassis. In addition, the location of the shorting of a patch antenna can be used to influence the level of coupling to the chassis, and thus the bandwidth. For an increase in the bandwidth the shorting should be placed at the short edge of the chassis and, if possible, the patch would be best positioned along either one of the longer edges of the chassis instead of between them.

A wideband study [43], [46] concluded that the effect of the chassis is significant at the first and second order resonances of the chassis and that at higher frequencies the antenna element is dominating. The role of the chassis is illustrated in Figure 4-2 [46], where the current distributions on the chassis at the three first chassis resonances are drawn. In the figure brighter colors signify stronger currents. In the first two resonances the dipole-like current distribution is clear and dominating, while in the last one the currents associated with the antenna, located at the top, have gained ground. Also, strong currents at the edges can be observed. In conclusion, to obtain a reduction in SAR values redesigning the antenna element alone is not sufficient, but it is as important, if not more important, to control the distribution of the chassis currents.

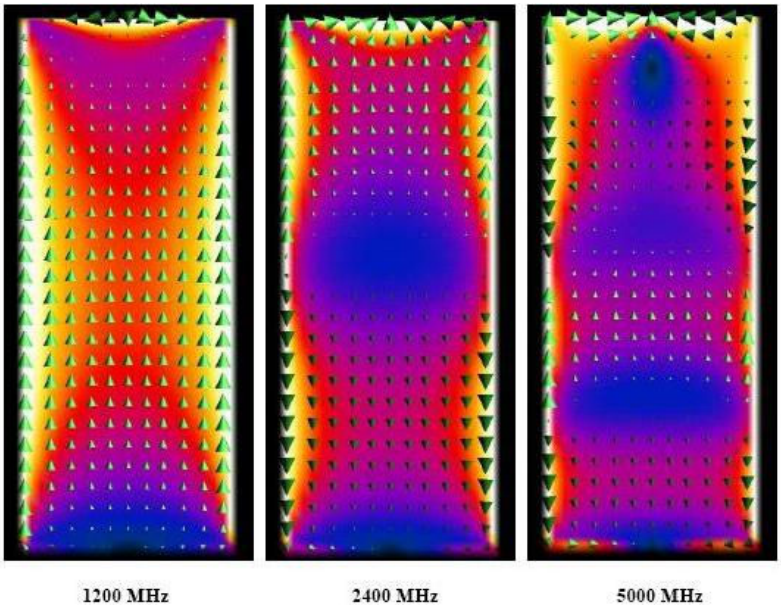

Figure 4-2. Current distribution on the chassis at the three first resonances [46].

The major role of the chassis gives reason to suggest that the antenna can be used merely as a non-resonant coupling element exciting the resonances of the chassis. Recently very promising designs utilizing this idea have been reported [43]. The

matching of the coupling element based antenna is realized with separate matching circuitry. Therefore the coupling element can be optimized individually to obtain the strongest possible coupling to the chassis wavemodes.

The optimized coupling elements seem to offer a competitive bandwidth with structures occupying incredibly small volumes, e.g. 0.7 cm^3 in [43]. The disadvantage of coupling element based antennas is increased SAR and decreased efficiency in talk position. Nevertheless, the benefits from the increased BVR exceed the drawbacks on the SAR and efficiency levels.

4.3.4 Planar inverted-F antenna

Next we shall take a glimpse at a particular planar antenna type relevant in this thesis. The antenna is called planar inverted-F antenna (PIFA) [45]. Due to its compact size, low production cost and suitability for multiband operation different configurations of PIFAs have attracted much attention. Another advantage of PIFA is the shielding effect of the ground plane, which results in reduced backward radiation and lower SAR values. Shorted planar antennas are typically self-resonant and no additional resonance or matching circuitries are needed, since the resonance tuning and impedance matching are built-in features of PIFAs. A basic PIFA setup is illustrated in Figure 4-3. The configuration consists of a shorted patch element on top of a ground plane with air substrate.

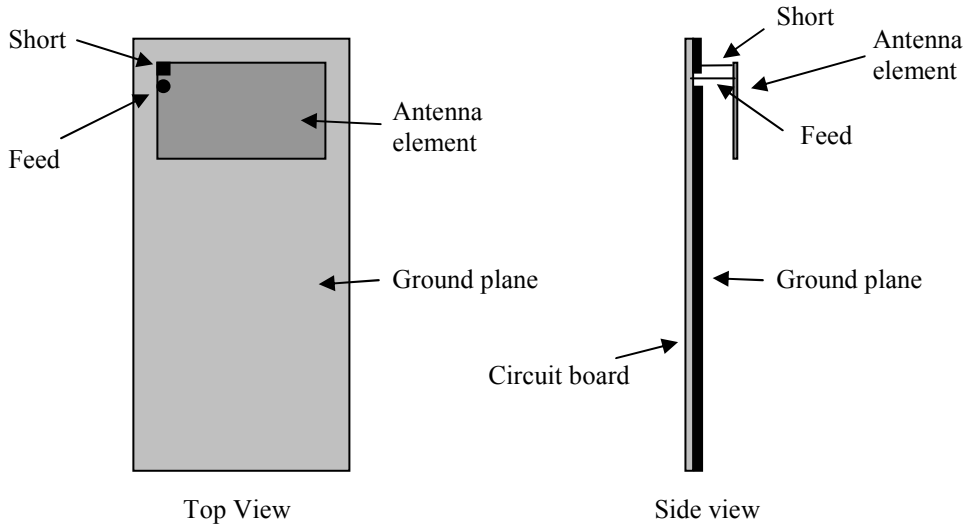

Figure 4-3. Basic handset PIFA configuration.

A typical design process involves the modification of the antenna element to reach the desired resonant frequencies. For obtaining multiband operation two design concepts

are utilized [45]. One can either use different resonant paths to generate separate resonant modes or one can use several resonant frequencies of a single path. An example depicting the former concept can be seen in Figure 4-4(a), where two different resonant paths are created by a U-shaped slot. The meandered patch in Figure 4-4(b) represents the latter concept.

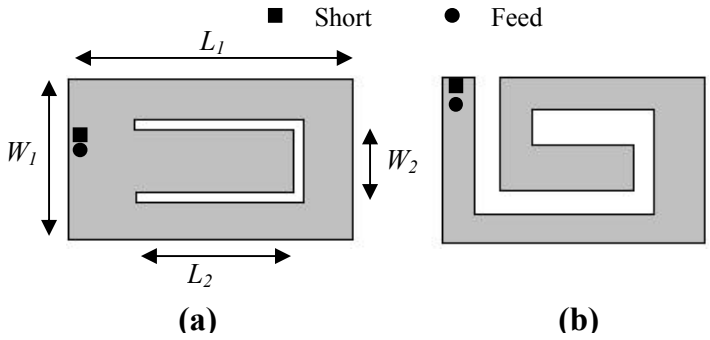

Figure 4-4. Examples of multiband PIFAs: (a) patch with U-shaped slot, (b) meandered patch.

Formulas for the tuning of simple patches can be found in literature, e.g. [45], [47]. As an example using the notation of Figure 4-4(a) the two resonance frequencies f_{r1} and f_{r2} of the patch in question can be approximated from

$$f_{r1} = \frac{c}{4(L_1 + W_1)}, f_{r2} = \frac{c}{4(L_2 + W_2)}. \quad (4\text{-}8)$$

Once the necessary resonances have been excited, the antenna must be matched to the feed. The matching is done by optimizing the location of the feed and then possibly slightly altering also some dimensions of the antenna element.

In practical internal antenna design cases the inside of the cover is crowded with other components and the use of simple antenna elements is rarely possible due to the limited and often irregular space available. Introducing separate patches or parasitic shorted patches and folding the patch are among the techniques used for fitting the PIFA inside the cover and reaching the optimal resonances and bandwidths. The coupling between different patch elements is adjusted by the distance between them.

In addition, according to the principles of Section 4.3.3, the radiation from the chassis must be utilized to achieve the required bandwidths. This is done by shaping and placing the antenna so that the coupling between the antenna and the chassis is as strong as possible. However, self-resonant antennas, including PIFAs, are not efficient in terms of coupling to the chassis [43]. The task of shaping and locating the antenna for optimal

coupling is hindered e.g. by the need to create the necessary resonances in the antenna. Consequently only a part of the volume occupied by the antenna contributes to the coupling.

4.4 Handset and user

4.4.1 Effect of user

The user affects the operation of a handset antenna in two ways: by changing the radiation characteristics of the antenna and by absorbing a portion of the radiated power. Regarding the radiated power, the total efficiency of a handset, in fact, often is largely determined by the user absorption, which can be 1.5 – 10 dB [42]. The power is absorbed not only to the head of the user, but also to the hand and the rest of the body.

The power flow from the transmitter of a handset via the antenna to the surrounding space is illustrated in Figure 4-5. The efficiency coefficients derived from the circuit parameters of the antenna, as presented in Section 2.3.2, are joined by the coefficient describing the power that is absorbed by the user. This term, labeled here as user absorption coefficient η_u, is defined as

$$\eta_u = 1 - \frac{TRP}{P_r}. \tag{4-9}$$

The total antenna efficiency η_{tot} can then be presented as

$$\eta_{tot} = \frac{TRP}{P_A} = \eta_{refl}\eta_r\left(1-\eta_u\right). \tag{4-10}$$

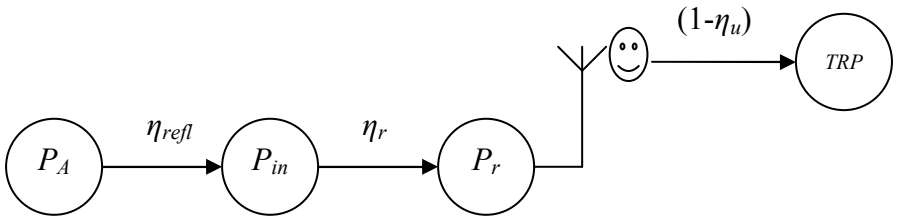

Figure 4-5. Power flow chart of a transmitting handset antenna. The terms included are power available at the feed line (P_A), reflection efficiency (η_{refl}), power accepted by the antenna (P_{in}), radiation efficiency (η_r), radiated power (P_r), user absorption coefficient (η_u) and total radiated power (TRP).

In addition to the minimization of the biological effects on the user, the reduction of user absorption enhances the total efficiency of the handset. The antenna design naturally has a large influence on the level of absorption, but there are also other factors,

beyond the designer's control, radically affecting the absorption. These factors include the use position of the terminal and the varying position of the hand. When researching the user effect, the differences in the simulation and measurement setups also create strong variations in the results.

The contribution of the chassis to the radiation complicates the determination of whether the user is in the near-field of a handset antenna as the far-field boundary is calculated using the longest dimension of the antenna (Figure 2-3). The distance to the far-field boundary is depicted in Figure 4-6 as a function of antenna length. If the radiation originated only from the antenna element, it would be possible for the user to be in the far-field in certain use positions. However, due to the radiation from the chassis, the user is in the near-field of the antenna.

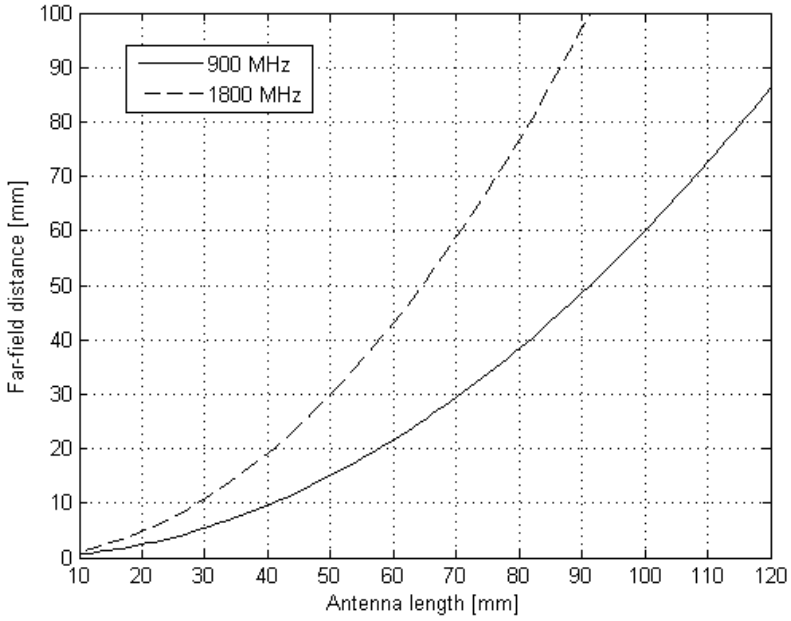

Figure 4-6. Distance to the far-field boundary, calculated with the equation in Figure 2-3.

Positioned in the near-field of the antenna, the user can be considered as a part of the radiating system affecting the fundamental radiation parameters. Intuitively, placing lossy dielectric tissue close to the antenna lowers its resonant frequency, as the electrical length of the antenna is increased. The effect of dielectric material on resonators is also described by perturbation theory, presented e.g. in [42]. A dielectric load also decreases the unloaded quality factor Q_0 of a resonating antenna, thus increasing the bandwidth. The magnitude of the user effect is difficult to predict and it depends on the relative permittivity of the material and the distribution of the fields –

the higher the permittivity and the bigger part of the antenna fields inside the dielectric the bigger the effect is. Contrary to the common conception, in a recent study [46] it was shown that in the vicinity of dielectric material the resonance frequency of a handset antenna can in some cases increase.

As explained earlier in Section 4.3.3, the currents on the handset chassis cause a large part of the radiated power. The general principles regarding the role of the chassis have been found to mainly apply both in the talk position and in free space [43], [46]. Chassis resonances produce a bandwidth maximum simultaneously with an increase in SAR and a decrease in efficiency. However, the role of the chassis is significant only at the two or three low-order resonances.

When placed beside a user's head, the radiation efficiency of a handset antenna increases rapidly with increasing frequency. The reason for this is the decreasing contribution of the chassis [43], [46]. At higher frequencies, when the radiation is dominated by the antenna, the radiation efficiency stays more constant.

The distance between the handset and the lossy material strongly affects the induced SAR values and the radiation efficiency, the former decreasing and the latter increasing with increased distance. At a chassis resonance the change is less abrupt. When close to the head, the chassis resonance can even cause the SAR values to increase with increasing distance [41].

Also the hand of the user absorbs some of the power radiated by a handset. Thus including a hand in the evaluation setup decreases the SAR values in the user's head. A hand also reduces the radiation efficiency, especially if it covers the parts of the chassis that contribute the most to the radiation. However, the antenna parameters have similar dependence on the chassis dimensions with and without the hand. Most commonly handset antennas are placed on the backside of the chassis and in a location where the user is less likely to hold his hand. These principles are used to minimize the effect of the user.

4.4.2 Dosimetric rules

The research on the energy absorption mechanisms from the near-fields of an antenna to adjacent biological tissue has produced somewhat contradictory results. The goal of such research is to gain understanding on the near-field functioning of antennas and the resulting peak SAR values and their locations.

In [48] it was concluded that the main power dissipation mechanism is brought forth by the magnetic fields and the SAR maximum in human tissue can be found next to the location of maximum antenna current. The electric fields were seen of less importance.

For a long time the conclusions of [48] were considered to be the best explanation for the absorption mechanism, but new diverging theories have also emerged. The results of [42] showed, that the location of peak SAR is not related to the maximum antenna current, but electric fields after all define the location. Examining the E-field boundary conditions, Equations (2-18) and (2-19), reveals, that while the component parallel to the surface of the tissue penetrates the boundary unattenuated, the perpendicular component is strongly attenuated at the boundary. This is the case especially with high-permittivity tissues, within which the peak SAR is found at the location of significant parallel electric field components. In case of a dipole antenna such a location can be found near the center point of the dipole. With low-permittivity tissues, on the other hand, the perpendicular component is not attenuated as strongly at the boundary, and the peak SAR is located next to the total electric field maximum.

At this point a short review of tissue parameters from Table 3-1 and Table 3-5 reveals that muscle, skin and brain tissues have high permittivities and conductivities, while bone and fat tissues have low permittivity and conductivity. The head tissue-equivalent liquid used in SAR measurements and simulations has a relatively high permittivity and conductivity.

Furthermore, the results of [46] showed that at low frequencies the location of peak SAR values follow the current maxima of the chassis. When the frequency is increased the growing role of the antenna moves the peak SAR location close to the antenna.

4.4.3 Controlling SAR

Finding ways to reduce the power absorbed in the head of the handset user is always desirable. Besides minimizing the possibility for any health effects, directing the power away from the head increases the total radiation efficiency. The mass-averaged SAR levels can fundamentally be lowered in two ways: by reducing the total power absorbed into the user or by making the power absorption distribution as even as possible. Next a brief summary of the principles learned so far to control SAR is presented.

As learned earlier in this thesis, the SAR levels can be decreased by sacrificing other performance parameters of the antenna, e.g. simply by lowering the transmit power of

the handset. Also, optimizing the chassis dimensions in terms of the trade-off between SAR and bandwidth is possible. However, using meandering and slots for the tuning of the chassis often results in higher current concentrations, which in turn are sources for high SAR levels. The knowledge that strong currents cause the highest SAR levels is significant and it prods to limit the current densities on the handset chassis. An interesting issue is the antenna location, which is known to have an influence on the strength of coupling to the chassis wavemodes as well as the SAR levels and bandwidth.

A remarkable part of the electromagnetic fields from a handset will inevitably be directed towards the user. However, the coupling into the user also depends on the polarization of the incident fields, as highlighted by Equations (2-18) and (2-19). Therefore, if the polarization of the electric fields towards the user was mainly tangential to the surface of the head, a smaller portion of the power would actually be absorbed into the head.

The next chapter deals with a known method for reducing SAR values in the head of the handset user. In the method a shorted parasitic radiator, sometimes called a SAR shield, is mounted on the chassis opposite to the antenna.

5 Parasitic radiator

5.1 Introduction

In [49] a method utilizing a parasitic radiator attached to the front – or user's head – side of the handset chassis was introduced. The parasitic radiator was a plate parallel to the PWB shorted in its upper corners. The configuration was studied with simulations and measurements. At 900 MHz the parasitic radiator was found to significantly reduce the coupling between the PWB and the head phantom placed beside the handset. The best results, approximately 6 dB reduction in SAR and 1 dB increase in efficiency, were obtained with the parasitic radiator having a length of 40 – 45 mm. The study also concluded that the method had no effect at 1800 MHz. The working principle of the parasitic radiator was said to be the cancellation of a part of the near-field near the head. The minimum SAR was achieved with a resonating length of the parasitic radiator. At this length the currents on the parasitic radiator are at their maximum and of opposite phase to the currents on the PWB, resulting in the cancellation. In addition, the distance between the parasitic radiator and the PWB and the width of the shorting strips were said to affect the resonance frequency.

The method was investigated further in another study [46], which partly confirmed the previous results, but also brought new information. The study showed, that even though the parasitic radiator causes an increase in the total electric field towards the head, it reduces the component parallel to the surface of the head, especially close to the vertical center point of the chassis. Thus the SAR in the head is decreased. When the antenna was placed beside a SAM head model, the simulations at 900 MHz showed a 46 % reduction in SAR with the plate having a length of 45 mm. However, the cost of the SAR reduction was a significant reduction in bandwidth, as well. The minimum bandwidth potential also occurred at the plate length of 45 mm. A reduction in SAR was also seen at 1800 MHz with a 10 mm long plate. However, the studies of [46] also showed that other factors, e.g. the distance between the lossy tissue and the handset, strongly affect the behaviour of SAR.

The research reported in this chapter tackled the challenge of implementing the method in a handset platform project. The idea was to create the parasitic radiator around the

phone display, as was suggested in [49]. The goal was to be able to reduce the resulting SAR at least at 900 MHz, but possibly at other frequency bands as well. Although [49] concluded the method had no effect at 1800 MHz, [46] showed the parasitic radiator could perhaps be used to somewhat control – and most importantly reduce – SAR also at the higher frequencies. An ideal parasitic radiator would then be a single multiresonant structure, which would reduce SAR in all of the transmitting bands of a 3G handset. The research was based on simulations with a commercial software that utilizes the FDTD method, SEMCAD X by SPEAG AG [39].

The simulations were carried out at three different frequencies, 900 MHz, 1800 MHz and 1950 MHz, corresponding to the transmitting frequencies of the GSM 900, GSM 1800 and UMTS2100 systems, respectively. The functioning of the method was tested by gradually shaping and locating the parasitic radiator so that it could be fit inside the casing of the handset under development. Although most of the simulations were conducted with a simplified phone model, the boundary conditions for the dimensioning of the parasitic radiator were chosen based on the handset platform. In addition, the tuning of the parasitic radiator to a given resonance frequency was investigated.

As a lateral investigation, also the differences regarding SAR levels between a simplified handset model and a more complex model were looked into. A practical handset contains several metallic and dielectric components which should be considered in the design process of the antenna. It was also of interest, whether both the simplified model and the more complex model would follow the principles discussed in Chapter 4 regarding the SAR generation at different frequencies.

Lastly a set of measurements was done to verify some of the results from the simulations. The measurements were performed with MapSAR2 by IndexSAR [50], which is a SAR assessment system intended for research and development purposes. MapSAR2 is a simplified version of the standard-compliant SAR measurements systems.

5.2 Simulations

5.2.1 Models

When creating the models for the simulations, the idea was to keep an industrial point of view. Thus the user was modeled with the SAM head model containing

homogeneous tissue-simulant liquid similarly to the SAR measurement standards. The electrical properties of the liquid were according to the CENELEC standard [35], as seen in Table 3-5. The liquid was covered with a thin low-permittivity (ε_r = 3.7) shell. The phone was positioned in the standard "cheek" position on the left side of the head. The models used in this thesis did not include a hand. This practice is consistent with the current SAR measurement standards.

In the simulations the handset was modeled in two ways, either as a simple model consisting only of the PWB and the PIFA, or a more complex model with additional parts of the phone included. In the simple model the PWB and the antenna structure were set as perfectly conducting materials. The more complex model is from this point on labeled full model, although the model actually was not all-inclusive due to two reasons. Firstly, at the time of the research the handset was still under development; secondly, to limit the simulation time, some of the smaller parts were left out. Thus, as additional parts the full model included a casing, a battery connected to the ground plane in one of its corners, two grounded component shields and two grounded cameras in the upper part of the phone near the antenna, a non-grounded speaker under the antenna and a three-layer display, which metal parts were also grounded. The casing and the glass top of the display were set as lossless dielectric materials and the rest of the parts were set as perfectly conducting materials.

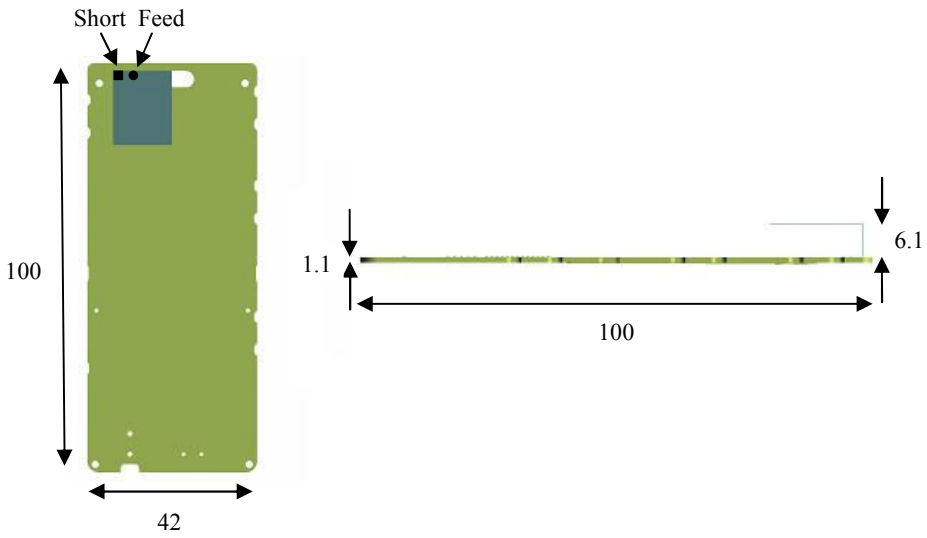

Figure 5-1. Dimensions of the simple phone model in millimeters.

The simple model along with the dimensions of the PWB and the antenna height can be seen in Figure 5-1. The full model beside the head phantom is depicted in Figure 5-2. The distance between the PWB and the surface of the head at the closest point was

4.4 mm. When the simple model was used, the location of the PWB was the same as with the full model, and a small gap could be found between the phone and the SAM.

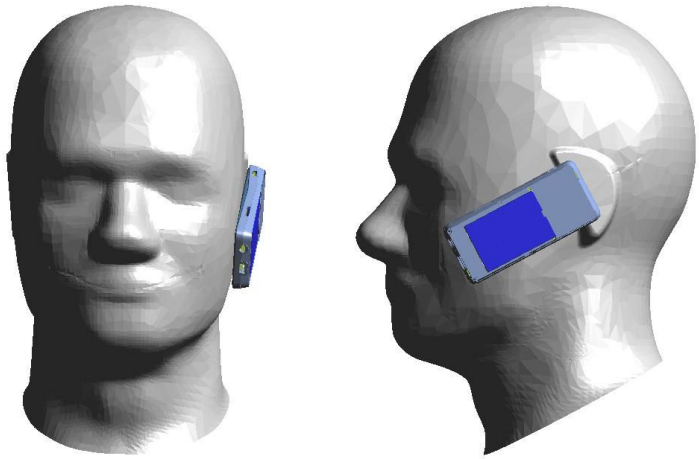

Figure 5-2. Full model beside the SAM.

Different antennas were created for the different frequencies to keep them as simple as possible. The used antenna type was PIFA. A rectangular patch similar to the one seen in Figure 5-1, but with different dimensions for each frequency, was used in the 1800 MHz and 1950 MHz simulations. For 900 MHz a meandered patch was designed. The location of the shorting and the feed was kept constant. The matching of the antennas was not paid much attention to, since the results were normalized to the same total radiated power. However, two different antennas were created for 900 MHz, because when the simple phone model was used, the antenna matched for use with the more complex model radiated only a few percent of the source power. Consequently the results proved to be too inaccurate after the normalization.

As different antennas were used for each frequency, comparisons between the results at different frequencies are not perfectly accurate. However, the different antennas were designed to be as simple and general as possible. Besides, in real cases the dimensions of the resonance paths of the PIFA are also different for each frequency. Thus, comparisons between different frequencies based on the results of this thesis can be considered to have a satisfying level of reliability.

The effect of the handset parts and the SAM on the resonance frequency of the antenna is depicted in Figure 5-3 and Figure 5-4. The figures present example snapshots taken of the reflection coefficient during the process of creating the antennas for the 900 MHz

simulations, Figure 5-3, and the 1800 and 1950 MHz simulations, Figure 5-4. The matching curves show that the addition of the phone parts to the simple model deteriorates the matching and lowers the resonance frequency. The inclusion of the head, however, has only a minor influence on the resonance frequency. In the higher frequency case in Figure 5-4, adding the head beside the simple model notably increases the resonant frequency. This kind of effect was mentioned earlier in Chapter 4, as similar results were reported in [46]. Another conclusion from the figures is that the head influences the full model clearly less than the simple model.

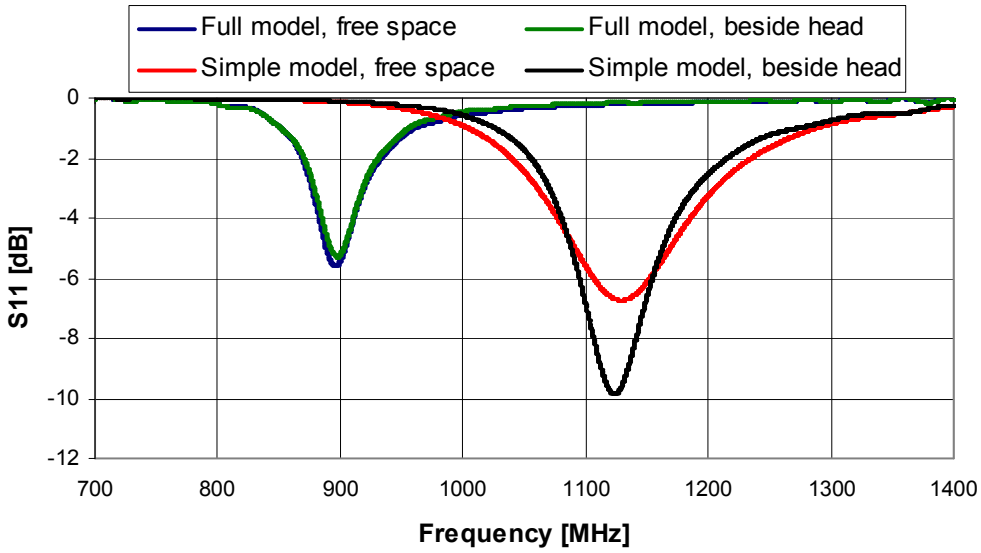

Figure 5-3. Reflection coefficient of a draft meandered PIFA which was then tuned for the 900 MHz simulations.

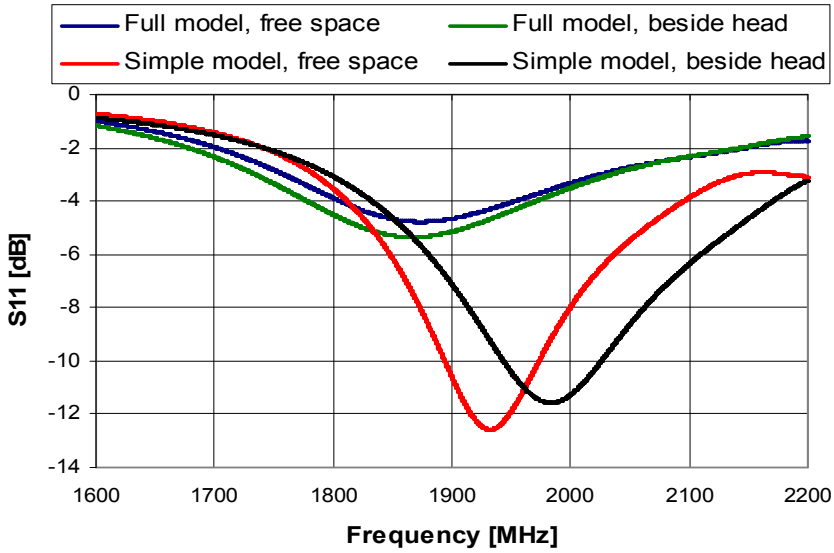

Figure 5-4. Reflection coefficient of a draft rectangular PIFA which was then tuned separately for the 1800 MHz and the 1950 MHz simulations.

Two types of parasitic radiators, plate and loop, as seen in Figure 5-5, were created for the simulations. In addition, two locations were used. The upper location was aligned with the upper edge of the PWB and the lowered location was 7 mm lower. The parasitic radiator was connected to the ground plane in its upper corners with 1.3 mm wide shorting strips, which was also the width of the loop strip. The length of the parasitic radiator l was varied between 53 mm and 3 mm and the height from the PWB h between 3.1 mm and 2.4 mm.

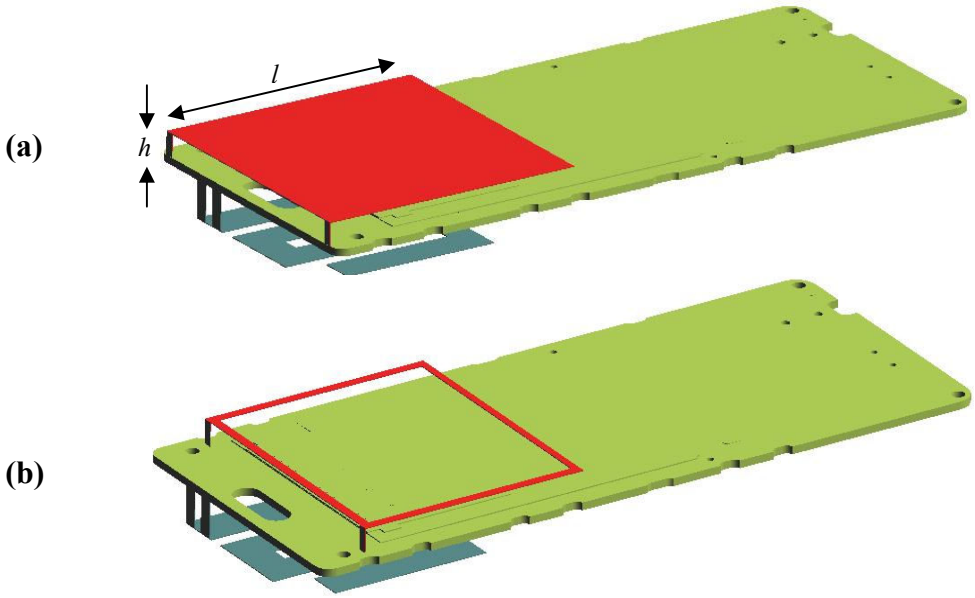

Figure 5-5. The setups for the parasitic radiator with the simple phone model: (a) The plate-like parasitic radiator in the upper location, (b) The loop-like parasitic radiator in the lowered location.

The lowered location, the maximum length of 53 mm, and the height range from 2.4 mm to 3.1 mm coincide with the location and dimensions of a gap inside the casing of the handset and around the display. The target was to be able to find a SAR-reducing dimensioning for the parasitic radiator that would fit inside this available space.

5.2.2 Reference results

Next we shall take a look at results from simulations without any parasitic radiator. These results are used as reference when evaluating the functioning of the parasitic radiator, but they also offer interesting information regarding the differences between the simple and the full model. The reference results can be seen in Table 5-1. The table contains SAR values averaged over 10 g of tissue mass and the percentage of the radiated power, which is absorbed in the head. The SAR levels are normalized for 0.25 W of radiated power at 900 MHz and for 0.125 W at 1800 and 1950 MHz. This

normalization applies through all the studies in this thesis, and it corresponds to the transmitting powers of the different systems, as seen in Table 4-2.

Table 5-1. Reference values without the parasitic radiator for 10 g SAR and the total losses in the head.

Model	900 MHz		1800 MHz		1950 MHz	
	SAR (10 g) [W/kg]	Total losses (%)	SAR (10 g) [W/kg]	Total losses (%)	SAR (10 g) [W/kg]	Total losses (%)
Simple	1.46/1.75	59.6/71.8	0.47	42.0	0.60	42.7
Full	1.77	71.1	0.77	44.3	0.88	45.3

In Table 5-1, two SAR values are provided for the simple model at 900 MHz. As mentioned earlier, two different antennas were used at 900 MHz due to the large transition in matching between the simple and the full model. The lower SAR value is for the antenna that was otherwise used with the full model and the higher value is for the antenna that was used in simulations with the simple model.

One can see that the SAR levels and the portion of the absorbed power at 900 MHz are clearly higher than at the higher frequencies. Removing the contribution of the dissimilar transmitting powers changes the situation partly. Without the normalization, the full model SAR values are quite close to each other, despite the much higher total loss at 900 MHz. It means that the absorption at 900 MHz is more evenly distributed in the head. The same difference can be seen between the simple and the full model, but only at 1800 and 1950 MHz, where the total losses increase only slightly with the full model, but the SAR level increases approximately 50 %. At 900 MHz comparisons between the SAR levels of the simple model and the full model are more difficult to make, since the results obtained using the full-model antenna with the simple model were unreliable. However, the results obtained with different antennas for the simple and the full model suggest that the model type has only a minor effect at 900 MHz.

The SAR generation with both handset models can be viewed in the following figures, in which the distribution of local SAR, i.e. non-averaged, inside the SAM on a plane parallel to the PWB is plotted. The chosen plane is about 10 mm beneath the point on the SAM surface closest to the phone, but there is a variation of a few millimeters in the plane location due to the different voxelization in the simulations. In the figures the scale is proportioned to the maximum local SAR of each case. This approach was

chosen to ease the examination of the distributions. The comparison of absolute SAR levels between the cases can be done by looking at Table 5-1, since the mass-averaged SAR follows the level of the local SAR in these cases quite accurately. In addition, a green dot is added to the figures to identify the location of the maximum local SAR. This point, however, is not on the plotted plane, but closer to the surface of the SAM.

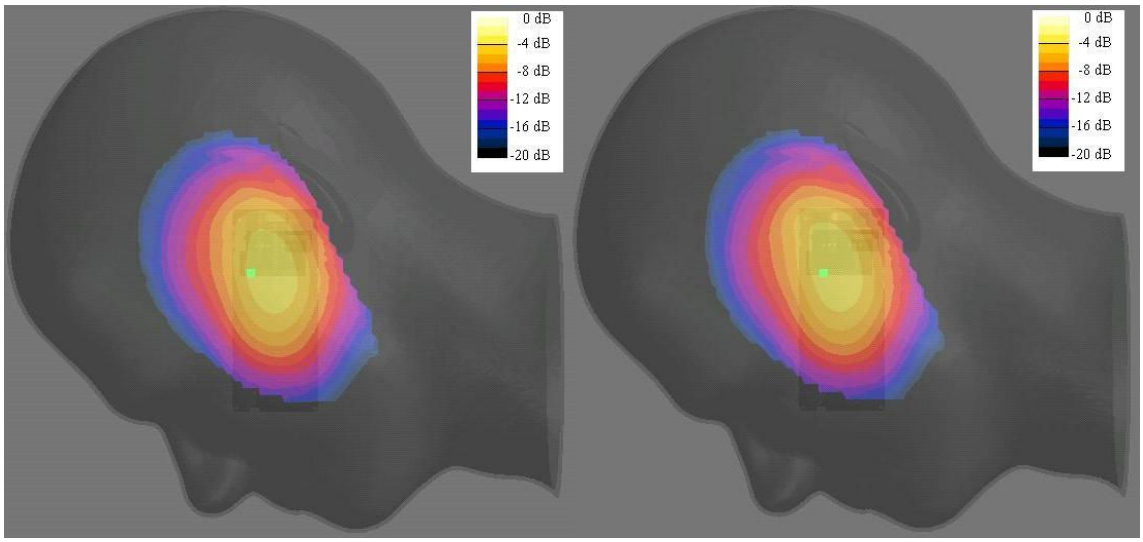

(a) **(b)**

Figure 5-6. Simple model SAR distribution at 900 MHz: (a) Simple model antenna, (b) Full model antenna.

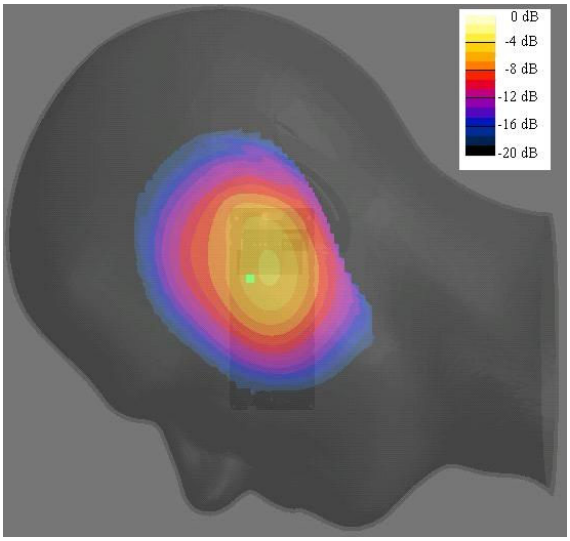

Figure 5-7. Full model SAR distribution at 900 MHz.

Figure 5-6 depicts the SAR distribution of the simple model using both the simple model antenna and the antenna that was otherwise used with the full model. One can see that the distributions are nearly identical, again suggesting, that comparisons between full model and the simple model can be made at 900 MHz, although different antennas

were used for the models. Figure 5-7 shows the SAR distribution of the full model at 900 MHz. These figures confirm that the SAR distribution is similar with both phone models.

The SAR distributions at 1800 and 1950 MHz are illustrated in Figure 5-8 and Figure 5-9.

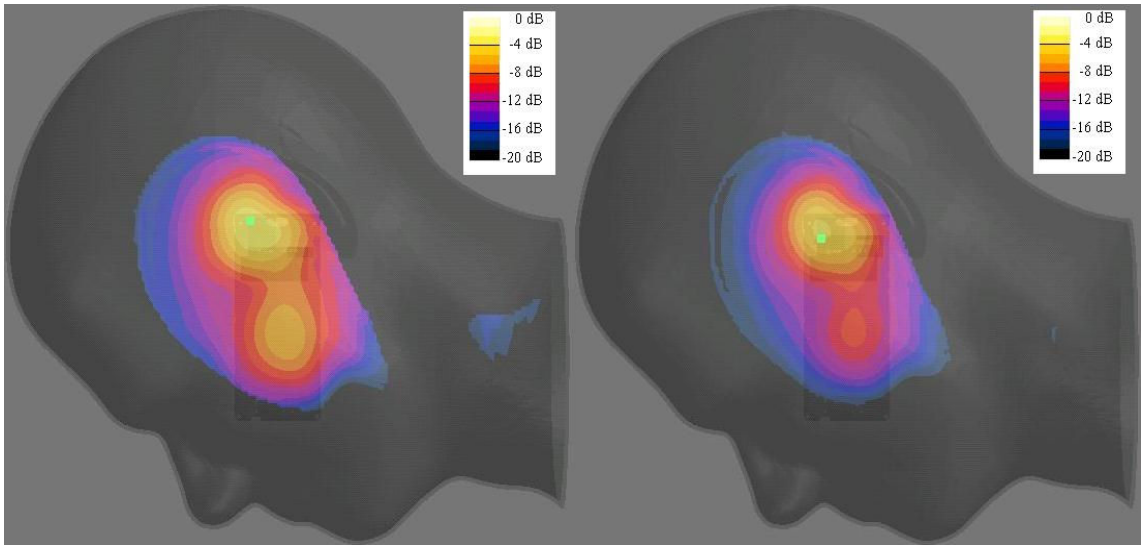

(a) **(b)**

Figure 5-8. SAR distribution at 1800 MHz: (a) Simple model, (b) Full model.

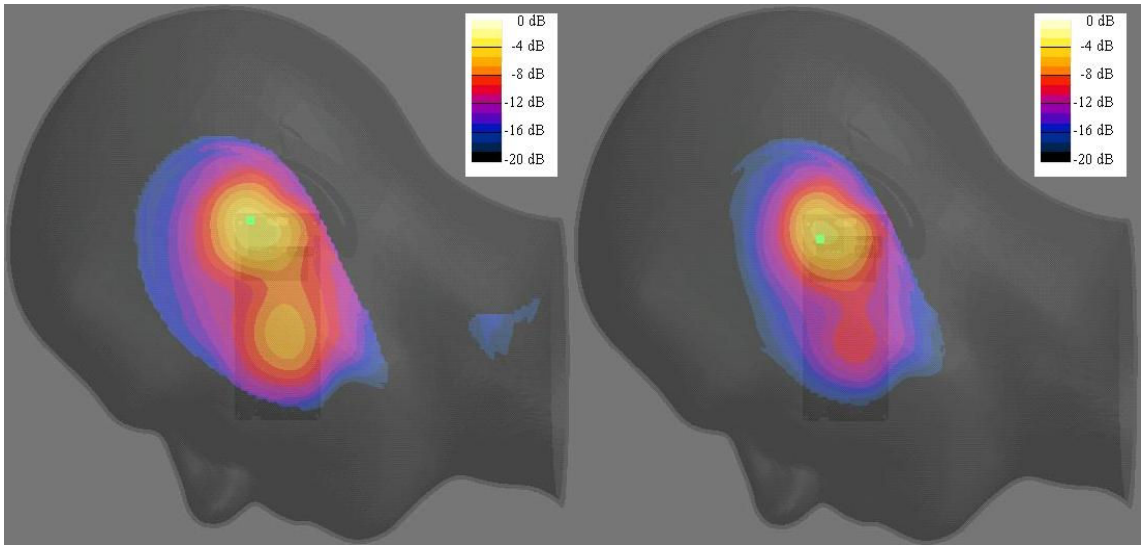

(a) **(b)**

Figure 5-9. SAR distribution at 1950 MHz: (a) Simple model, (b) Full model.

At both of the higher frequencies two local maxima can be seen, one at the top of the PWB close to the antenna and another near the vertical centre point of the PWB. The maximum close to the antenna is stronger, a rule that is further boosted by the full

model. This observation also confirms the conclusion made from the results of Table 5-1, that the full model concentrates the SAR more strongly to one hotspot at 1800 and 1950 MHz. In addition, the full model moves the maximum SAR point slightly downwards, i.e. away, from the feed of the antenna.

Let's now consider how the SAR distributions agree with the principles presented in Chapter 4, where it was learned, that with high-permittivity materials the SAR inside the material relates to the current distribution on the PWB. The current distributions, as seen in Figure 4-2, show a single maximum close to the vertical centre of the PWB at the first chassis resonance, and two maxima at the second resonance. In Figure 5-6 and Figure 5-7 a single maximum can be seen and in Figure 5-8 and Figure 5-9 two maxima. Thus in total the SAR distributions follow the principles discussed in Chapter 4 quite well.

5.2.3 Parasitic radiator – results

The following presents the results from the different investigations on the parasitic radiator. The radiator was examined regarding its location, length, height and shape at the three frequencies. The simulations can be divided into two parts. First, attempts were made to fit the parasitic radiator inside the casing of the full model. Thereafter simulations with the simple model were conducted to study the tuning of the parasitic radiator.

The results are presented as curves showing maximum SAR in the head averaged over 10 g of tissue as a function of the length of the parasitic radiator. The SAR value at zero length represents the reference value, from Table 5-1. When considering the results, it is best to observe trends in the SAR levels rather than absolute magnitudes or variations.

In [46] and [49] the parasitic radiator was located at the top edge of the PWB, on the opposite side to the antenna. This was also the starting point for the studies here. The first results in Figure 5-10 and Figure 5-11 show how the SAR behaves at the upper and the lowered location. For the lowered location the radiator was moved 7 mm from the top edge of the PWB. These simulations were run with the simple phone model and plate-like parasitic radiator.

At 900 MHz in the upper location the result is expected, as it is similar to the results of [46] and [49]. The SAR minimum is obtained when the length of the parasitic radiator is around 45 mm, but also all the other lengths reduce SAR compared to the reference case

without any parasitic radiator. At best the SAR reduction is a whopping 38 %. Then, in the lowered location, we observe a deterioration in the SAR reduction capabilities of the method. The curve is still similar, but the best reduction is only 14 %. When the radiator is shorter than 25 mm, there is even a slight increase in SAR.

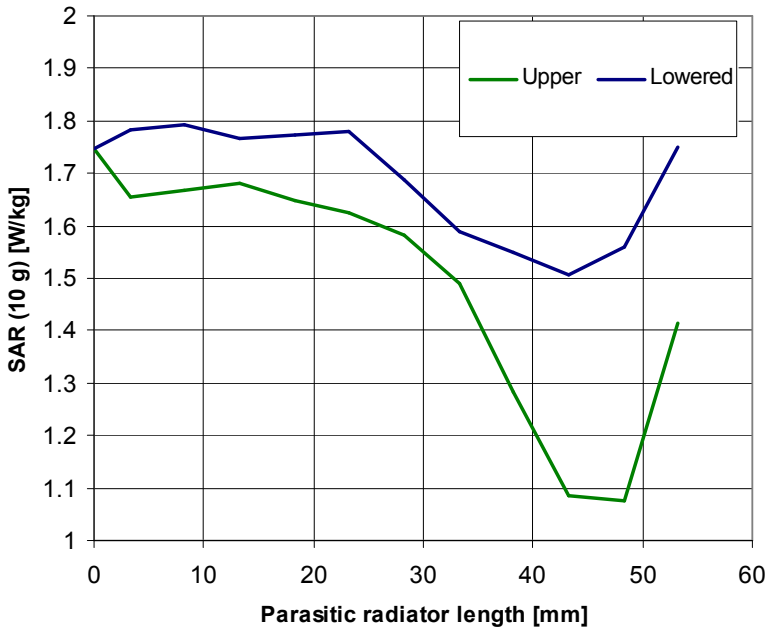

Figure 5-10. The effect of the location of the parasitic radiator at 900 MHz. Simple model, plate, h = 3.1 mm.

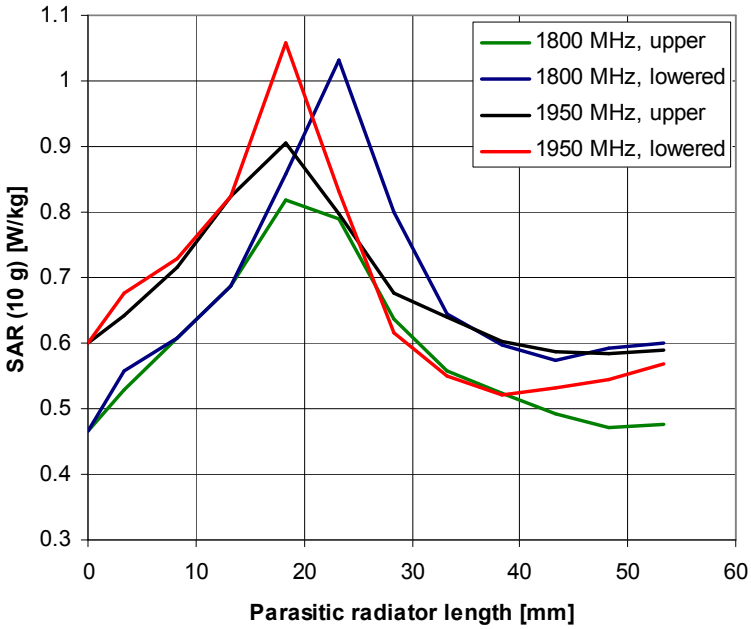

Figure 5-11. The effect of the location of the parasitic radiator at 1800 and 1950 MHz. Simple model, plate, h = 3.1 mm.

At 1800 and 1950 MHz the results show a dramatic peak in SAR at around a length of 20 mm. At 1950 MHz the peak is expectedly at a little shorter parasitic radiator length. Disappointingly the reduction in SAR at short radiator lengths, which was reported in [46], is not found. When comparing the two locations, the lowered case seems to have more variation in SAR. While in the upper location the SAR values settle close to the reference value with parasitic radiator lengths above 30 mm, in the lowered location a clear increase at 1800 MHz and a decrease at 1950 MHz can be seen. For example with radiator length of 43 mm the SAR increase at 1800 MHz is 23 % and the SAR decrease at 1950 MHz 11 %.

As a whole the upper location results in lower SAR, supporting the concept of using the parasitic radiator as a SAR shield. The location of the resonance at 1800 and 1950 MHz is logical when compared to the 900 MHz case. However, it is peculiar that the resonance at the 900 MHz curve gives a SAR notch, while at the higher frequencies SAR peaks can be observed. The radiator lengths that give clear reduction in SAR at 900 MHz do not cause significant changes in SAR at the higher frequencies, when considering the upper location. The lowered location, however, is more complicated.

To analyze the effect of the parasitic radiator two example cases were chosen from the results in Figure 5-10 and Figure 5-11. One of the examples is the case giving the maximum SAR reduction in the upper location at 900 MHz and the other is the case resulting in maximum SAR increase in the upper location at 1950 MHz. The SAR levels and total losses of these cases are compared against the reference levels in Table 5-2 and the SAR distributions of the cases are depicted in Figure 5-12.

Table 5-2. SAR levels and total losses of two example parasitic radiator cases compared to the reference levels without any parasitic radiators.

Frequency [MHz]	Example case			Reference case	
	Parasitic radiator length [mm]	SAR (10 g) [W/kg]	Total losses (%)	SAR (10 g) [W/kg]	Total losses (%)
900	48	1.08	61.6	1.75	71.8
1950	18	0.91	41.3	0.60	42.7

The best case regarding SAR at 900 MHz occurs when the parasitic radiator length is 48 mm. Then the mass-averaged SAR drops 38 % compared to the reference value. However, the total absorbed power reduces less, which means that the usage of the

parasitic radiator in this case results in a more even SAR distribution. This conclusion is supported, although not very evidently, by Figure 5-12(a), which can be compared to the SAR distributions in Figure 5-6.

The other example, parasitic radiator having a length of 18 mm at 1950 MHz, is interesting. Although the SAR increases by over 50 %, the total losses slightly decrease. Looking at Figure 5-12(b) reveals that this is due to the increased concentration of absorption into the upper maximum.

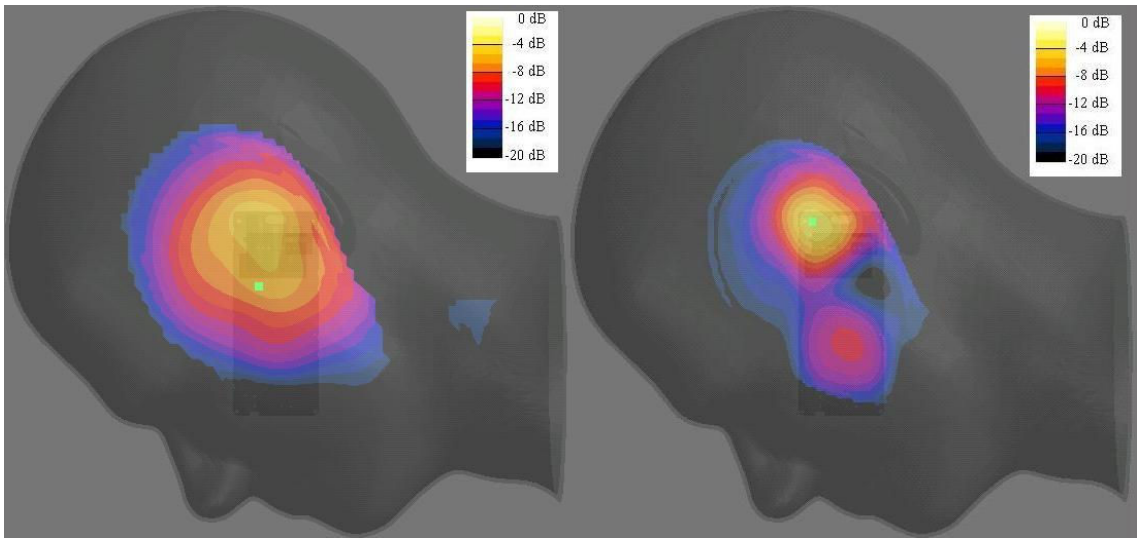

(a) **(b)**

Figure 5-12. SAR distributions of the two example cases: (a) l = 48 mm, h = 3.1 mm, upper location, 900 MHz, (b) l = 18 mm, h = 3.1 mm, upper location, 1950 MHz.

The next step was to see how the SAR would behave when changing the height of the parasitic radiator. This was done using the simple model with the plate-like radiator in the lowered location. The examinations were at this point done using only two different heights, the original 3.1 mm and a lower 2.4 mm height. This compact range of possible height is derived from the dimensions of the gap between the display and the casing. The results from the height test are presented in Figure 5-13 and Figure 5-14.

At 900 MHz it can be observed that the reduction in SAR is further decreased with the smaller height. However, the limited range of parasitic radiator lengths makes it impossible to see at which length the curve of the lower height would start to rise again. This issue was dealt with later, when studying the tuning of the parasitic radiator.

At 1800 and 1950 MHz the lower height generally yields smaller variation in SAR, with both the peak being lower and the SAR with parasitic radiator lengths above 30 mm

settling closer to the reference value. As was already seen above, when considering the two locations, with lengths above 30 mm the SAR is increased at 1800 MHz and decreased at 1950 MHz.

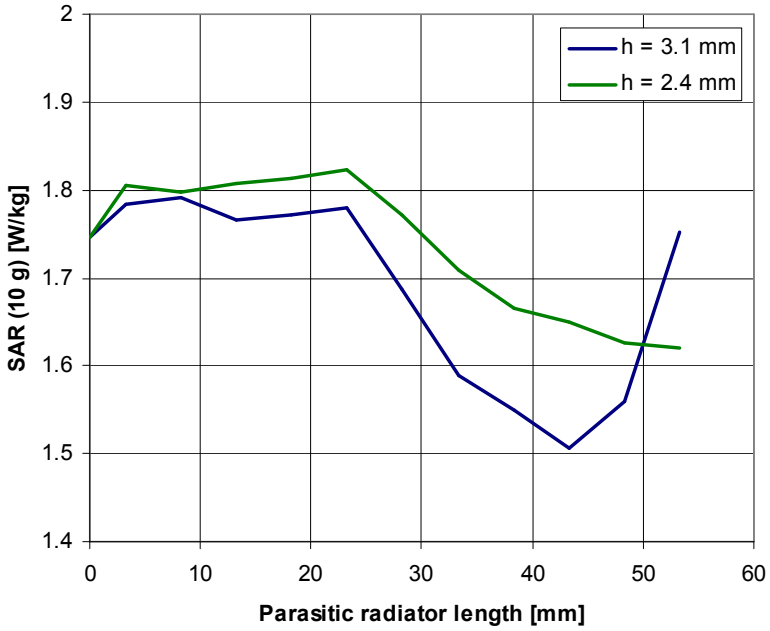

Figure 5-13. The effect of the height of the parasitic radiator at 900 MHz. Simple model, plate, lowered location.

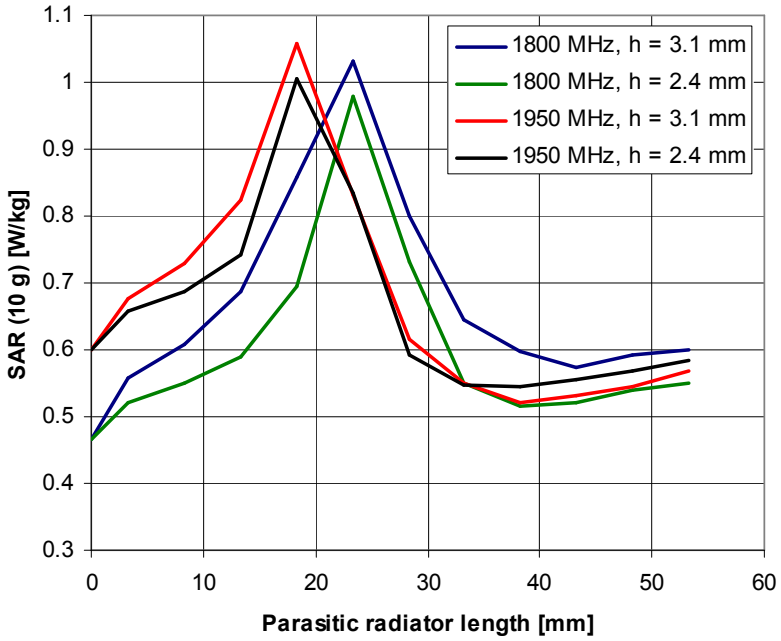

Figure 5-14. The effect of the height of the parasitic radiator at 1800 and 1950 MHz. Simple model, plate, lowered location.

Inevitable compromises have to be made when applying the parasitic radiator in a handset. For example, having a solid plate as the radiator is rather unrealistic. Therefore

the next practical step was to study if the parasitic radiator could be remodeled as a stripline loop having the same outer dimensions as the plate-like model used earlier. The effect of the type of the loop is depicted in Figure 5-15 and Figure 5-16. The simulations were first done in the lowered location with the simple phone model.

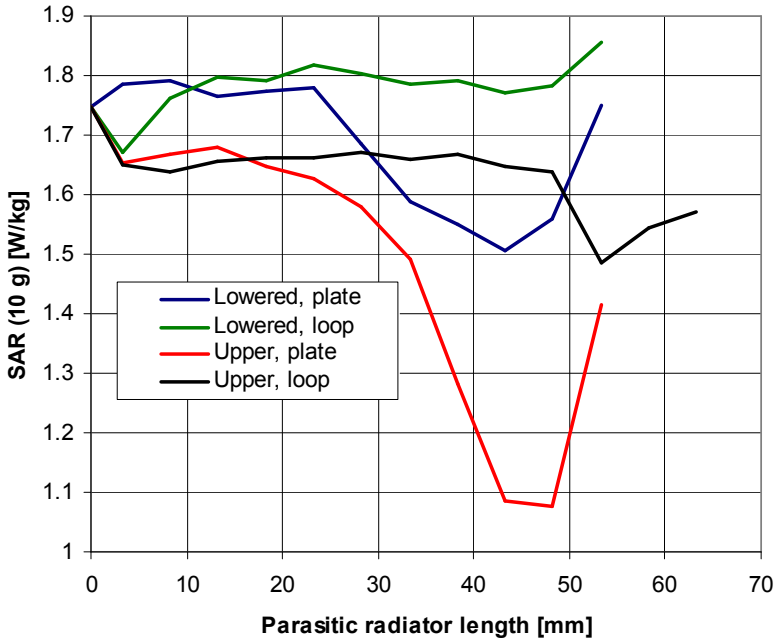

Figure 5-15. The effect of the type of the parasitic radiator at 900 MHz. Simple model, h = 3.1 mm.

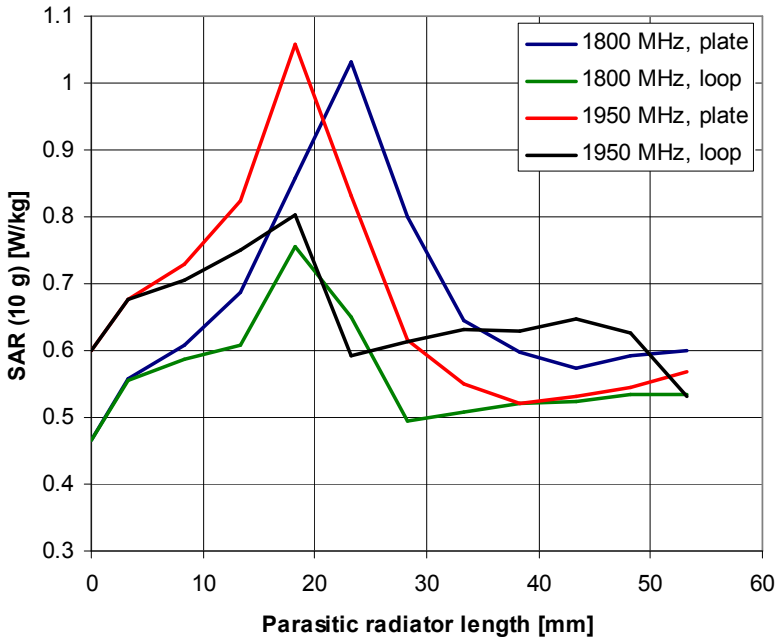

Figure 5-16. The effect of the type of the parasitic radiator at 1800 and 1950 MHz. Simple model, lowered location, h = 3.1 mm.

At 900 MHz the consequence of the remodeling was that the method effectively stopped from working in the lowered location. It is a little strange, since the same SAR peaks,

albeit muted, can be seen at 1800 MHz and 1950 MHz. After this observation the 900 MHz case was revalued in the upper location. There a dip can be seen at l = 53 mm. To get a better idea of the behaviour of SAR in this upper location the parasitic radiator length was extended beyond the normal 53 mm. In total the SAR reduction in the upper location with the loop-like radiator was equal to the reduction in the lowered location with the plate-like radiator.

At 1800 and 1950 MHz the trends in SAR are still visible, but generally the variation is clearly dampened when using the loop-like parasitic radiator.

Next the parasitic radiator was placed inside the full model. The loop-like radiator type was used and, being inside the casing, the loop was in the lowered location. In the full-model simulations the height was again reduced to 2.4 mm to be able to scan the normal range of parasitic radiator lengths without intersecting with the casing window. Comparisons between the two models can be viewed in Figure 5-17 and Figure 5-18.

A pleasant observation can be made from Figure 5-17. With the full model a dramatic notch in SAR is evident again, the maximum reduction in SAR being 30 %. Compared to the earlier cases the notch seems to be steeper, i.e. the "bandwidth" of the parasitic radiator is smaller. After observing the narrow nature of the resonance, the simple model case was again investigated with 2.5 mm steps in radiator length, but to no avail. Note that the SAR levels of the two cases in Figure 5-17 are not perfectly comparable, since two different antennas were used.

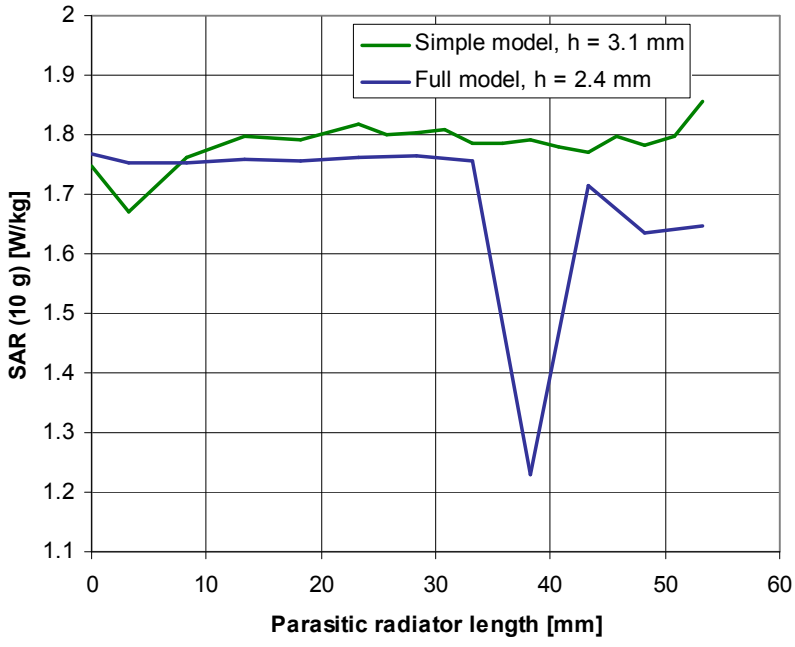

Figure 5-17. The effect of the type of the phone model at 900 MHz. Loop, lowered location.

At 1800 and 1950 MHz the full model gives higher SAR, as was already seen in the reference cases. The SAR peaks are further dampened, but interestingly enough, a reduction of about 5 % in SAR at 1950 MHz is now visible at very short parasitic radiator lengths.

As expected, the resonance in the full model occurs with a shorter parasitic radiator length than with the simple model. The shift is probably mainly caused by the dielectric load from the added phone parts.

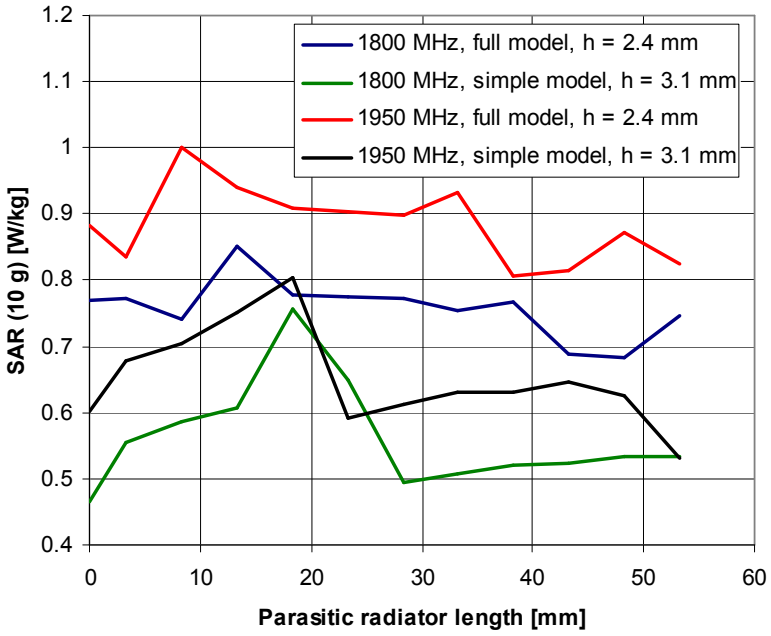

Figure 5-18. The effect of the type of the phone model at 1800 and 1950 MHz. Loop, lowered location.

Let us now review the case producing the notch in SAR at 900 MHz. The total losses at the resonance are reduced to 48.2 %, compared to 71.1 % in the reference case. The SAR distribution of the case is illustrated in Figure 5-19.

In the figure the plane is again taken approximately 10 mm inside the head and the colors are normalized to the maximum local SAR of this particular case. One can see that the relative SAR in the plane is clearly lower than in the previous cases, e.g. in Figure 5-7. Also, the local SAR maximum is stronger than in the reference case, but the location of it is moved from just inside the SAM liquid closer to the surface into the low-permittivity SAM shell. Combining this information gives reason to support the theory presented in the introduction to this chapter, that at the resonance of the parasitic radiator the total electric field between the phone and the SAM is increased, but a smaller part of the field is coupled inside the SAM liquid.

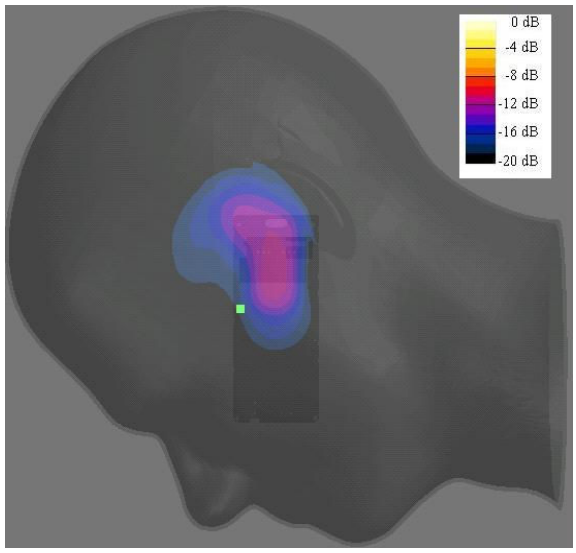

Figure 5-19. SAR distribution at 900 MHz, l = 38 mm, full model, loop, lowered location, *h* = 2.4 mm.

After gaining insight on how susceptible the method is to adjustments in the location, height and model of the parasitic radiator, the focus was redirected to the tuning of the radiator. The previous results showed, that the method indeed decreases SAR with certain radiator lengths. If tuning methods were known, the method could better meet the demands of the different phone models regarding the dimensioning of the parasitic radiator. In the following research the simple model was again used in the upper location and the earlier strict limitations on the radiator length were relaxed. This was done to get the most noticeable results. The research was limited to 900 MHz.

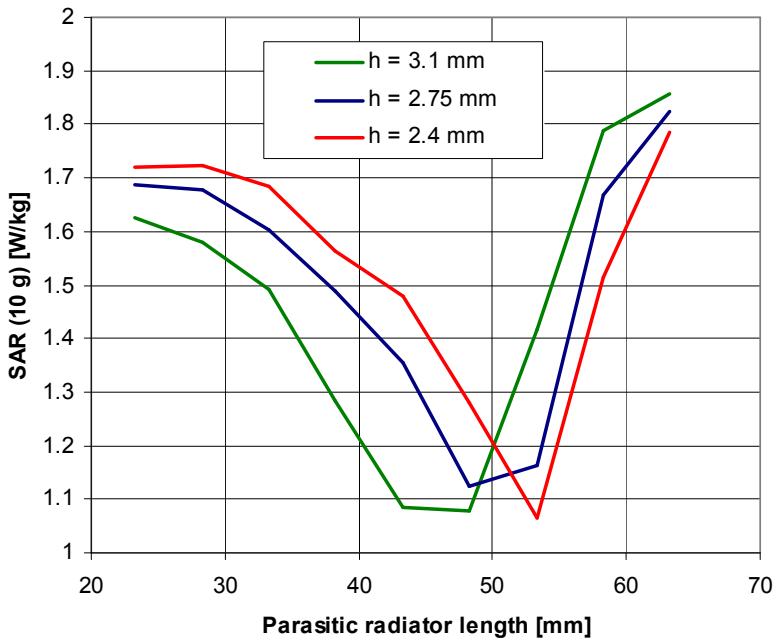

Figure 5-20. The effect of the height of the parasitic radiator at 900 MHz. Simple model, plate, upper location.

At first the influence of the height of the parasitic radiator was examined. Already earlier results, seen in Figure 5-13, hinted that the height might be a factor to be considered when determining the resonating length of the radiator. This proved to be true, as seen in Figure 5-20, where SAR values with parasitic radiator lengths around the resonance are shown for three different radiator heights. The evident perception is that increasing height moves the resonance to a lower frequency. It is a plausible conclusion, since the same rule also generally applies with antennas.

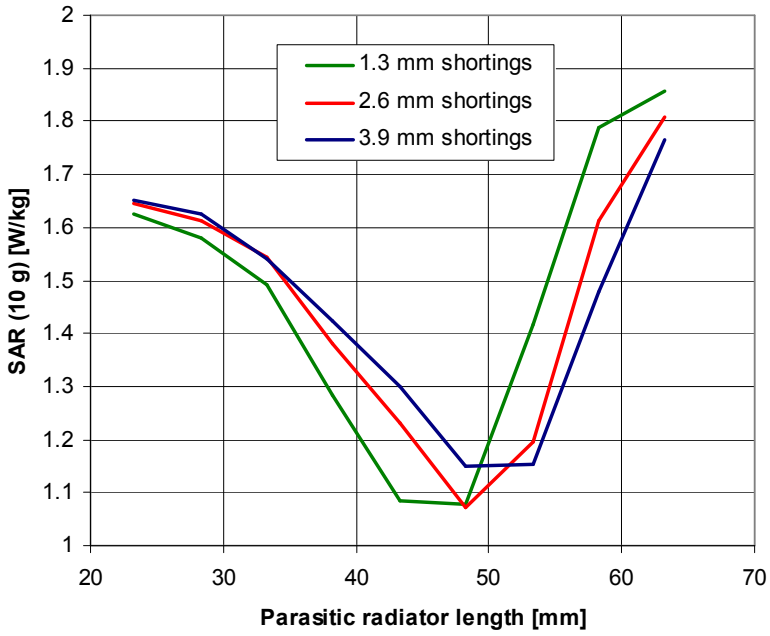

Figure 5-21. The effect of the shorting strip width at 900 MHz. Simple model, plate, h = 3.1 mm.

The second thing considered was the width of the two shorting strips in the upper corners of the parasitic radiator. From the original 1.3 mm width the shortings were widened to 2.6 mm and to 3.9 mm. The results are in Figure 5-21. One can see that the width has a significant effect, with wider shorting resulting in longer resonance length.

As a conclusion the tuning of the parasitic radiator can be realized by varying its height or the width of the shortings. Based on the results presented here the tuning does not significantly affect the amount of the reduction in SAR.

In the introduction of this chapter an idea was presented about combining the different parasitic radiator lengths giving minimum SAR for each frequency. Ideally this multiresonant structure, perhaps after a little fine-tuning, would then reduce SAR in all of the transmitting bands. However, disappointingly the simulation results did not show any significant and consistent reductions in SAR at 1800 and 1950 MHz. Small

reductions at these higher frequencies were seen at the same parasitic radiator lengths giving minimum SAR at 900 MHz. This naturally is a promising result.

Nevertheless, as a possible incentive for future work a dual-resonating structure was briefly examined with one dimensioning. The structure of the parasitic radiator can be seen in Figure 5-22, although full phone model was used when testing the idea. The length of the larger loop, 38 mm, was chosen based on the radiator length giving the notch in SAR at 900 MHz, visible in Figure 5-17. The SAR minima at 1800 and 1950 MHz were also obtained at parasitic radiator lengths close to 40 mm, as seen in Figure 5-18, but for the examination a larger difference between the lengths was desired. Therefore for the smaller loop the length giving the small reduction in SAR at 1950 MHz, 3 mm, was chosen instead. The structure was then evaluated at all the three frequencies.

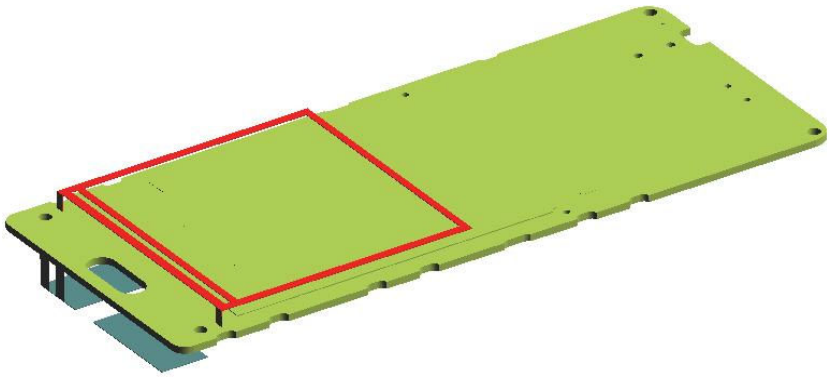

Figure 5-22. An illustration of the double-loop parasitic radiator.

At 900 MHz the reduction in SAR was even greater than with the single-loop parasitic radiator. The reduction increased from 30 % to 35 %. At 1950 MHz the reduction in SAR increases to 16 %, when it had been 5 % and 9 % at separate radiator lengths of 3 mm and 38 mm, respectively. At 1800 MHz no reduction in SAR is obtained, which was also the case with the single-loop parasitic radiators of the lengths at issue.

The reasons for the reduced SAR is not delved into within the scope of this work, but it presents a new interesting research problem. A parasitic radiator giving reductions in SAR, while being compact enough in shape and size to be utilized in a real handset, would certainly be worthwhile as a research subject.

5.3 Measurements

5.3.1 Setup

As a final part of this thesis a simple measurement campaign was done to verify the viability of the studied method in reality. The measurements were performed at 900 MHz. The MapSAR2 benchtop SAR measurement system, which was utilized in the measurements, is depicted in Figure 5-23. The system consists of a spherical bowl filled with tissue-simulant liquid, a measurement probe, a probe amplifier and a pen tablet. The system is operated by placing the DUT next to the bowl and then scanning the SAR values and distribution with the movable probe. The MapSAR2 system is not fully compliant for measuring mobile phone SAR values, but it can give a good idea for the designer about the SAR levels of the DUT.

The system has one considerable shortcoming compared to the standards. As the DUT must be placed tangentially to the spherical head phantom, the different points of the DUT are at a varying distance from the measuring probe. To get the maximum mass-averaged SAR, the position giving maximum local SAR is first sought manually without moving the probe. After that, the DUT is fixed into that position for the mass-averaging scanning.

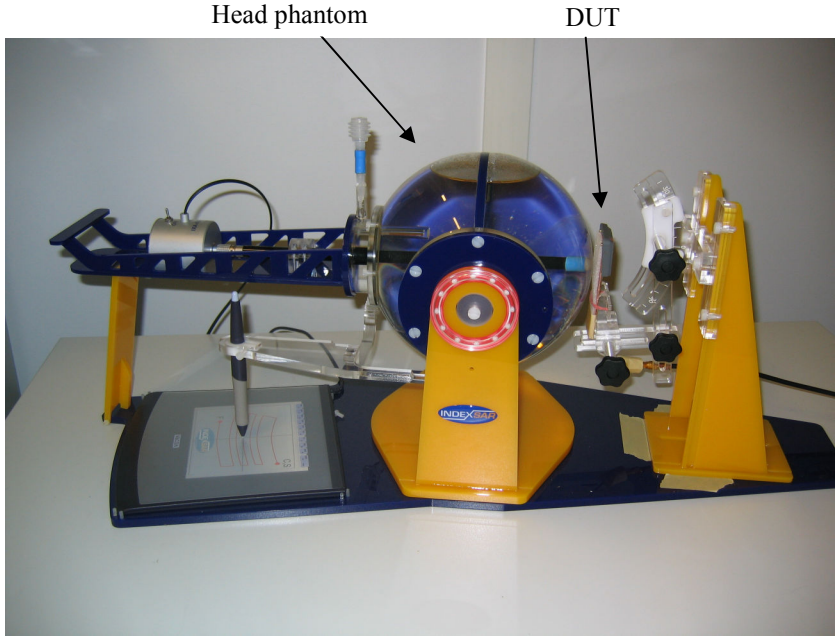

Figure 5-23. MapSAR2 measurement system [50].

Two photos of the prototype used in the measurements can be viewed in Figure 5-24. The size of the prototype PWB, 100 cm x 42 cm, was according to the model of the

handset development project, as in the simulations. A PIFA was designed for 900 MHz and placed on top of a piece of plastic frame, which was the biggest difference between the prototype model and the simple model in the simulations. The antenna emulated the shape of the antenna used in the 900 MHz simulations and it was made of conducting tape. The parasitic radiator, also of conducting tape, was placed on top of foam plastic in the lowered location 7 mm from the top edge of the PWB. The thickness of the foam plastic was approximately 3.5 mm. The connection of the parasitic radiator to the ground plane was realized making use of the two screws which held the frame under the antenna.

(a)

(b)

Figure 5-24. Prototype used in the measurements: (a) Front, including the parasitic radiator, (b) Back, including the antenna.

For the measurements two procedures were adopted. In the first procedure the position of the prototype in relation to the head phantom was kept constant regardless of the length of the parasitic radiator and thus the location of maximum SAR. The reasoning for this procedure was to keep the distance between the prototype and the head phantom constant more easily as variation in the distance could easily render the results worthless. The simulations also showed, that the location of maximum local SAR is quite constant, see Figure 5-6, Figure 5-7 and Figure 5-12(a). The position, which was fixed closest to the head phantom was 35 mm from the top edge and in the horizontal centre point of the PWB. A gap of approximately 1 mm was left between the parasitic radiator and the head phantom.

In the second procedure the position of the prototype was set by moving it manually around the probe and seeking for the maximum local SAR. The prototype was then fixed into this position. The search for the position yielding maximum SAR was repeated for every parasitic radiator length. The positioning for maximum SAR meant that no gap was left between the prototype and the head phantom in this case.

In both procedures the length of the parasitic radiator was reduced from 60 mm in 5 mm steps by cutting slices from its lower edge. The mass-averaged SAR was then examined as a function of the radiator length.

One factor of inaccuracy in the measurements was the changing impedance, hence matching, of the antenna due to the variation in the parasitic radiator length. Therefore before and after each measurement the reflection coefficient of the antenna was measured to be able to compensate for the differences in matching in the final calculated results.

5.3.2 Results

The results from the measurements are presented in Figure 5-25. For the plotting the results were first scaled to 0.25 W of available power from the signal generator and then compensated for the losses due to the finite reflection coefficient of the antenna. The SAR level without any parasitic radiator is again plotted at l = 0 mm.

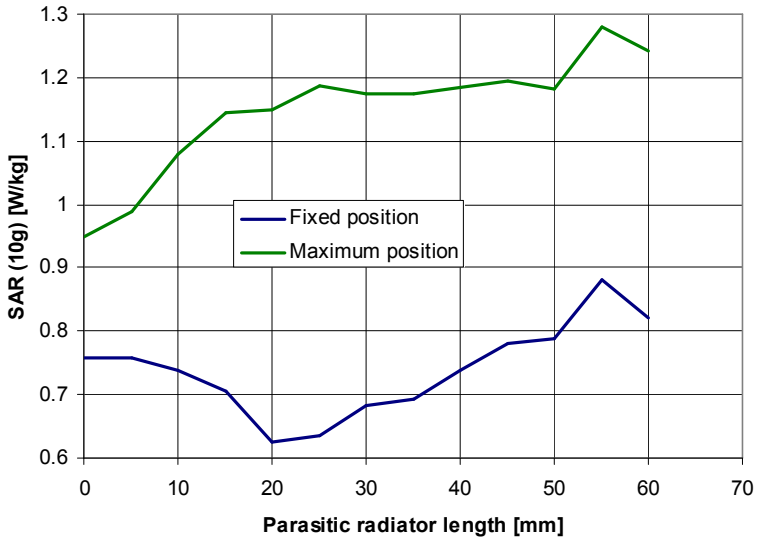

Figure 5-25. SAR measurement results with the two measurement procedures.

There are a couple of noteworthy matters common for both positions. First of all, the overall SAR level is lower compared to the 900 MHz simulations. The reason is

somewhat unknown, but most probably related to the prototype and the measurement setup. In the simulations the dielectric parts were modeled as lossless and the metal parts as perfectly conductive, but in the measurements a portion of the radiated power was inevitably lost in the different parts of the setup. The measurement system has been tested earlier with commercial phone models and the results have been similar to those reported by the manufacturers. As a positive observation, the result curves do not look random and distinctive trends are present.

Let us then first consider the results from the fixed position measurements. On a general level the curve looks as expected. A minimum in SAR can be seen when the parasitic radiator length is 20 mm, compared to the 43 mm in the simulations for the lowered location, see Figure 5-10. The magnitude of the reduction compared to the reference case is 17 %, which is in the same order as in the simulations. There are several possible causes for the shift in the length of the parasitic radiator, at which the SAR minimum occurs. Compared to the simulations the parasitic radiator was higher, which was earlier in this work shown to move the SAR minimum to a shorter length of the radiator, and the whole prototype was slightly closer to the head than in the simulations, which could affect the resonating parasitic radiator length. The dielectric load caused by the foam plastic may also have been a contributor to the differences between the simulations and the measurements. It is a little worrying, that the SAR minimum is obtained with the parasitic radiator length of 20 mm, since with that length the simulations showed a remarkable increase in SAR at the higher frequencies.

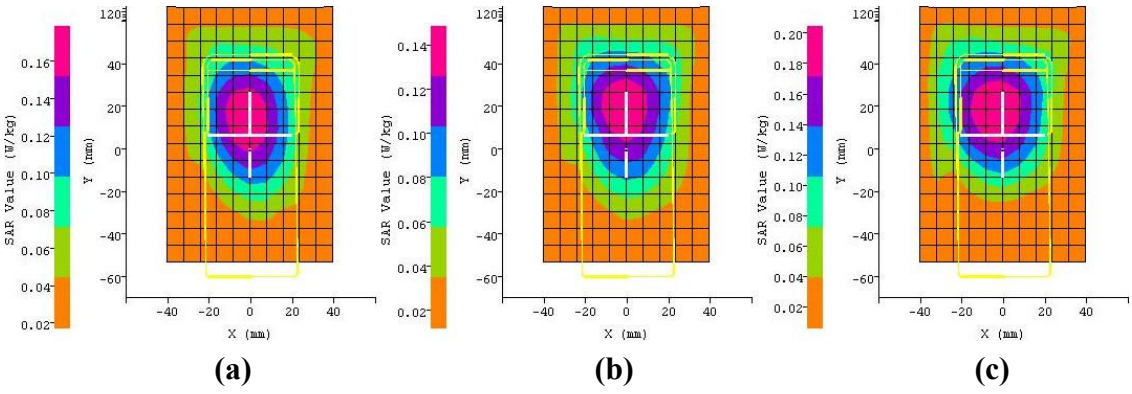

Figure 5-26. SAR distribution in the fixed position with three different parasitic radiator lengths: (a) l = 0 mm, (b) l = 20 mm, (c) l = 55 mm.

The SAR distribution from the scanning with the prototype in the fixed position can be seen in Figure 5-26. The prototype is outlined in the pictures with yellow lines and the

spot closest to the head phantom marked with a white cross. In all the cases the distributions are quite similar, which was expected based on the simulations.

The results obtained from the second measurement procedure were disappointing, since the lowest SAR was obtained without the parasitic radiator. In the procedure the point on the prototype yielding maximum local SAR was set closest to the head phantom. This point, however, was in all cases found to be in the close vicinity of the antenna feed and just above the upper edge of the parasitic radiator, as it were that the electric fields in that location could "leak" to the head and thus make the parasitic radiator useless.

The SAR distributions in the maximum SAR position can be seen in Figure 5-27. Compared to Figure 5-26 the distributions show a sharper SAR concentration, especially when the parasitic radiator was in use.

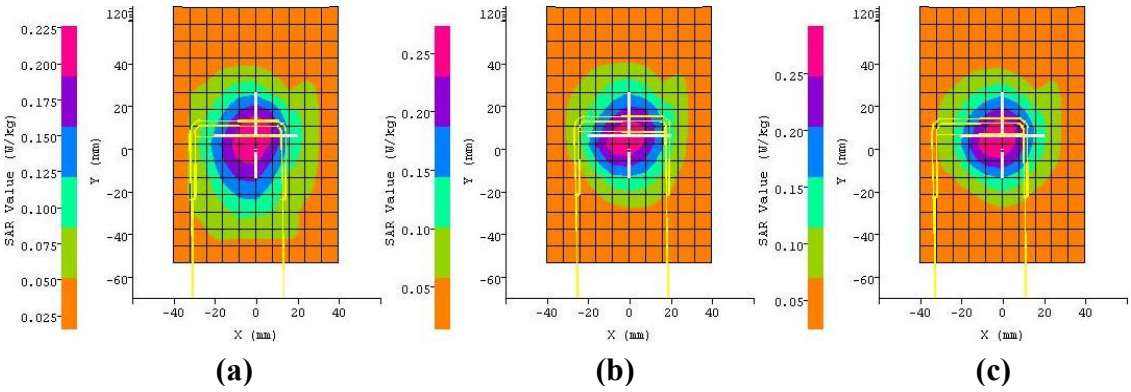

Figure 5-27. SAR distribution in the maximum position with three different parasitic radiator lengths: (a) l = 0 mm, (b) l = 20 mm, (c) l = 55 mm.

5.4 Research summary

Attaching a parasitic radiator with certain dimensions on the other side of the PWB opposite to the antenna is known to reduce power absorption in the user of a handset. This method was investigated by simulations and measurements and the results are presented in this chapter. The research was conducted to gain more insight on the specifics of the method, and thus to be able to apply and optimize it in the given handset project.

In the simulations two types of parasitic radiators were used in two different locations. The simulations were run at 900, 1800 and 1950 MHz. Most of the simulations were done with a simplified handset model, but also a more complex model was used to see if

the method could be applied in a more realistic case. The more complex, or full, model placed certain restrictions on the dimensioning of the parasitic radiator, which were taken into account in the simulations.

When creating the antennas for the simulations, it was seen that the addition of the parts used in the full model moved the antenna resonance to a lower frequency and also deteriorated the matching at the resonance compared to the simple model. The addition of the head beside the phone had a lesser effect, especially with the full model.

When the reference SAR levels for both of the handset models were investigated, it was observed that at 900 MHz the full model has only a small effect on the SAR compared to the simple model, but at the higher frequencies the full model concentrates the energy absorption more strongly to the area close to the antenna, thus increasing the mass-averaged SAR. Because of the increase the SAR levels at all the three frequencies were quite close to each other with the full model, while with the simple model the higher frequencies had had lower SAR.

First the utilization of the parasitic radiator was examined at a location opposite to the antenna. The behaviour of SAR as a function of the length of the radiator at 900 MHz was similar to the earlier studies [46], [49] and a strong reduction of about 30 % in SAR was seen at radiator lengths of about 45 mm. Unfortunately no such reductions in SAR were observed at 1800 and 1950 MHz. Instead, a towering increase of approximately 50 % in SAR around radiator lengths of 20 mm was present. Regarding the location of the parasitic radiator it was found that moving the radiator downwards on the PWB resulted in worse SAR performance, yet the reduction, only weaker, at 900 MHz was still obtained.

When the height of the parasitic radiator was varied inside the space limitations of the given handset, it was found that smaller distance to the PWB resulted in smaller SAR variation as a function of the length of the radiator.

Transforming the parasitic radiator from a plate to a loop further decreased the effect of the parasitic radiator to a point that it seemed to totally remove the ability of the radiator to reduce SAR at 900 MHz. Therefore the area of the parasitic radiator should be maximized for best possible performance. However, at 900 MHz the full model again generated the notch in SAR, but the notch was seen to be very narrow. When contemplating the cause for the SAR reduction, proof was found supporting the theory,

that a smaller part of the incident field is coupled into the head. At 1800 and 1950 MHz the variation in SAR was dampened with the full model, but a small reduction in SAR, as opposed to the simulations with the simple model, was observed at short radiator lengths, similarly to [46].

The following step in the simulations was to examine the tuning of the parasitic radiator. It was found that the tuning, indeed, is possible. The resonating length could be increased by decreasing the height of the radiator and by increasing the width of the shorting strips.

As final simulations, the possibility to utilize at double-loop parasitic radiator to further enhance the SAR performance was briefly touched upon. The results were inspiring and further work could prove to be very fruitful.

Lastly, two sets of measurements were conducted. The first set, where the prototype was kept in a fixed position in relation to the measurement system, produced promising results somewhat similar to the simulations. However, a worrying fact was that in the measurements the SAR minimum was obtained with a parasitic radiator length that in the simulations gave significant SAR increases at 1800 and 1950 MHz. The results of other set, however, were not as expected and no reduction in SAR could be reproduced.

In all the simulation cases the SAR values at 1800 and 1950 MHz were reasonably close to the reference value with the parasitic radiator lengths that gave minimum SAR at 900 MHz. Based on the results it can therefore be concluded, that adding a parasitic radiator to reduce SAR at 900 MHz has tolerable, if any, adverse effect on SAR levels at the other frequencies. In addition, the SAR levels at 900 MHz are generally known to be higher. Thus sacrificing SAR performance at 1800 and 1950 MHz to benefit the 900 MHz frequency area could still be worthwhile.

This research was performed for one handset position and at three single frequencies. As an idea for further research, the effect of the distance between the phone and the SAM could be examined and the study on the parasitic radiator extended to cover whole frequency bands. The narrow nature of the full-model SAR notch at 900 MHz casts a doubt over the functionality of the method over whole bands. Thus, means to widen the bandwidth of the parasitic radiator should be investigated. Also, the usage of the shorting strips regarding their location, number and shape could possibly be better

optimized. In addition, the effect of the different handset parts on the SAR generation could be studied after modeling the parts more accurately.

A lesson learned from the measurements is that a significant amount of time and effort should be put into the planning and construction of measurements involving SAR, as it is very susceptible to variation in the measurement conditions. It also means that simulation results should not be taken as the ultimate truth, since the simulations can never model the reality with absolute perfection.

6 Summary and conclusions

The motivation for this thesis work came into being from the need to be able answer to the challenge of an antenna design task of a modern 3rd generation handset. The goal of the thesis was to improve the SAR performance of the given handset by the application and optimization of a known specific method. A motivator for this and all research aiming to reduce SAR in a handset user is not only to minimize the possibility for any health effects, but also to improve the performance of the handset antenna in terms of increased radiation efficiency. Although at the moment the regulative SAR limits are sometimes met with ease, at least in the high-frequency bands, the future may very well bring stricter limits.

The beginning of this work consisted of literature study dealing with the basics of antennas and SAR and the special characteristics of handset antennas. Also, available reports discussing the specific method known to enable reductions in the level of electromagnetic exposure of handset users were studied. Research on this method was then conducted with the target of implementing it in the realistic handset case. Improvements in the understanding of the method were needed to be able to optimize it to the requirements of the given handset. In the following the lessons learned during this work are summarized and conclusions based on these lessons presented.

In the beginning of the literature study a general look at the subject of antennas was taken, along with the basic electromagnetic theory behind antennas and the mechanisms causing power absorption inside tissues. The power absorption inside media was learned to be caused by two loss mechanisms: ionic conductivity and polarization of dielectric materials. When reviewing the research on the possible health effects of radio frequency radiation it was learned, that the fear of adverse effects due to the usage of mobile handsets is not supported by scientific proof, but the interest in further research is still present. The industrial motivation for the limitation of the electromagnetic exposure of the user is created by the need for standard compliancy. As a final part of the literary work the special characteristics of handset antenna design were looked into. When dealing with handset antennas certain parameters are emphasized, for example due to the resonating nature of small antennas. The most important parameters,

including size, bandwidth, radiation efficiency and SAR were said to be strongly interrelated and improvements in one of the parameters often means sacrificing the performance measured in one or several of the other parameters. A peculiarity with handsets is the major role of the metal chassis in producing the radiation, which can, and also must, be utilized to achieve the required performance level.

After the literary work, research on a method known to produce reduction in SAR was conducted. The method is based on a parasitic radiator attached to the handset on the user's side of the PWB. The aim was to be able to use the method in a 3rd generation handset platform project the author was involved in during the making of this thesis. The method was mostly investigated with simulations, but a simple campaign of measurements was also performed. The challenge in implementing the method within the project was the tight boundary conditions regarding the dimensions of the parasitic radiator. As always in the design process of the handset, the antenna designer has to struggle to find the necessary means for an adequate antenna performance amidst the competing structural demands of the different parts of the phone.

The research with simulations gave valuable information about the method. Very promising SAR reductions were found at 900 MHz, while the usefulness of the method was seen to be strongly dependent on the location and type of the parasitic radiator. It was verified that the parasitic radiator works best when it is located close to the antenna and its area is maximized. At 1800 and 1950 MHz no incessant reductions were found. Instead, a considerable SAR peak was present at the higher frequencies with certain parasitic radiator lengths. However, those parasitic radiator lengths yielding the most favorable results at 900 MHz did not produce significant increases in SAR at 1800 and 1950 MHz. Therefore the method in total seems attractive for implementation in real handsets.

The tuning of the parasitic radiator was also proved to be possible by altering its height or the width of the shorting strips, with which the parasitic radiator is connected to the ground plane. The tuning is an important feature that enables the adaptation of the dimensions of the parasitic radiator to match the dimensional demands of each implementation.

Two types of phone models, a simplified model and a more complex model including some of the realistic phone parts, were used in the investigations. The models were

based on the handset platform under development. The usage of the more complex and realistic model created a new and interesting dimension to the knowledge on the SAR generation of handsets and on the functioning of the method involving the parasitic radiator. At 900 MHz the SAR behaviour was very similar with the two models, but with one significant exception. Namely, when the parasitic radiator was moved to a lowered location farther away from the antenna and its area was reduced, the more complex model still produced a strong reduction in SAR at a certain parasitic radiator length, but with the simple model this reduction could not be seen at all. At 1800 and 1950 MHz the SAR levels were generally clearly higher with the more complex model, but research on the parasitic radiator showed no dramatic differences between the two models at these frequencies.

The results of the small-scale measurement campaign investigating the usage of the parasitic radiator were dual. The first of the two measurement procedures yielded promising results partly similar to the simulations, but the other procedure produced no reductions in SAR. Although the output of the measurement campaign was not very extensive, it showed that it indeed is possible to obtain SAR reductions with the investigated method. The problem with the measurements of this thesis was the divergence of the measurement setup, in terms of the phone model and the SAR measurement system, from the setups in the simulations and the SAR measurement standards.

A specific challenge created by the usage of 3rd generation handsets is the extended range of frequencies. Also, a modern handset is very likely to be small in size, thus further tightening the boundary conditions regarding the dimensioning of the parasitic radiator. The results of this work prove that despite these challenges it is possible to utilize the method for lowering SAR in 3rd generation handsets.

From an industrial point of view, the investigated method offers a very potential option for keeping the SAR produced by a handset within the regulative limits. The amount of SAR reduction attained with the method is enticing, but since the successful realization and validation of the method requires precise prototype and measurement setups, the implementation probably would need a considerable amount of time and money. In an industrial project these resources are seldom ample. A notable fact is that standard-compliant measurement systems are few and far between, which further hinders the reliable verification of the functioning of the method. As another conclusion of the

research it can be said, that simulations with simple models are advantageous for discovering useful trends and methods to reduce SAR. However, tenacious engineering work is required for bringing these methods into reality, because even small changes in the evaluation setup under investigation can cause misleading variation in SAR. The principles found in simulations could also be brought closer to reality by a more thorough modeling of the studied handset and its different parts.

As a motivation for further research, it was shown briefly with simulations that a multiloop parasitic radiator could enhance the functioning of the method at multiple frequencies. The utilization of the parasitic radiator should also be investigated over whole frequency bands instead of single frequencies, and finding means for increasing the utilizable frequency band, i.e. the bandwidth of the parasitic radiator, would be valuable. The scientific understanding of the functioning of the parasitic radiator in the more realistic handset cases would be another major research subject, e.g. regarding the possible utilization of the display in the implementation of the method.

The purpose of this thesis work was to first gather information about handset antenna design, especially SAR-related issues, and then to examine means to apply the learned lessons and better the SAR performance of a real handset case. During the process many questions were answered, but several new ones were also uncovered. As a whole, an informative package on the issues from one point of view was gathered and useful research results gained on the specific SAR reduction method. The most significant output of this work includes proof supporting the earlier theory regarding the working principle of the method [46], and most importantly knowledge about the applicability and the optimization possibilities of the method for industrial implementation.

References

[1] W. L. Stutzman and G.A. Thiele, *Antenna theory and design*, 2nd edition, New York, USA, 1998, John Wiley & Sons, 648 p.

[2] I. Lindell and K. Nikoskinen, *Antenniteoria (Antenna theory, in Finnish)*, 3rd edition, Helsinki, Finland, 1995, Otatieto, 347 p.

[3] IEEE Std 145-1993, *IEEE Standard Definitions of Terms for Antennas*, IEEE, New York, USA, March 1993, 40 p.

[4] C. A. Balanis, *Antenna Theory: Analysis and Design*, 3rd Edition, Hoboken, USA, 2005, John Wiley & Sons, 1117 p.

[5] A. V. Räisänen and A. Lehto, *Radio engineering for wireless communication and sensor applications*, Boston, USA, 2003, Artech House, 396 p.

[6] A. Sihvola and I. Lindell, *Sähkömagneettinen kenttäteoria, 2. Dynaamiset kentät (Electromagnetic field theory, 2. Dynamic fields, in Finnish)*, 2nd edition, Helsinki, Finland, 1996, Otatieto, 200 p.

[7] R. A. Adams, *Calculus, a complete course*, 4th edition, Don Mills, Ontario, Canada, 1999, Addison-Wesley, pp. 929-935.

[8] A. Lehto and A. Räisänen, *Mikroaaltomittaustekniikka (Microwave measurements, in Finnish)*, 5th edition, Helsinki, Finland, 2001, Otatieto, 215 p.

[9] P. Vainikainen, S. Tretyakov and V. Sibakov, *S-26.3382 EMC design and testing*, Course material, Spring 2006, Radio Laboratory, Helsinki University of Technology.

[10] IEEE Std 149-1979. *IEEE standard test procedures for antennas,* 1979, Antenna Standards Committee of the IEEE Antennas and Propagation Group, New York, USA, August 1980, 135 p.

[11] Johanson Technology, www-page, available at http://www.johansontechnology.com, cited 15.06.2007.

[12] CTIA Certification, *Test Plan for Mobile Station Over the Air Performance*, Revision 2.1, CTIA, Washington, USA, April 2005, 142 p.

[13] A. Lehto, P. Vainikainen, T. Laitinen and C. Icheln, *S-26.3401 Antenna Techniques in Telecommunication*, Course material, Spring 2007, Radio Laboratory, Helsinki University of Technology.

[14] A. Taflove and S. C. Hagness, *Computational Electrodynamics: The Finite-Difference Time-Domain Method*, 3rd edition, Norwood, USA, 2005, Artech House, 1006 p.

[15] R. F. Harrington, *Field computation by moment methods*, New York, USA, 1968, The Macmillan Company, 229 p.

[16] J. L. Volakis, A. Chatterjee and L. C. Kempel, *Finite Element Method for Electromagnetics: Antennas, Microwave Circuits, and Scattering Applications,* New York, USA, 1998, IEEE Press, 368 p.

[17] Schmid & Partner Engineering AG, *SEMCAD-X Reference Manual*, March 2007, included with the software.

[18] K. Jokela, D. Leszczynski, W. Paile, S. Salomaa, L. Puranen and P. Hyysalo, *Radiation safety of mobile phones and base stations*, STUK-A161, Helsinki, Finland, 1999, Radiation and Nuclear Safety Authority of Finland, 76 p.

[19] H. Nyberg and K. Jokela (Editors), *Ionisoimaton säteily – Sähkömagneettiset kentät* (*Non-ionizing radiation – Electromagnetic fields, in Finnish*), Helsinki, Finland, 2006, Radiation and Nuclear Safety Authority of Finland, 555 p.

[20] C. H. Durney, et al., *Radiofrequency radiation dosimetry handbook*, 2nd edition, USAFSAM-TR-78-22, Brooks AFB, TX, USA, 1978, 141 p.

[21] The International EMF Dosimetry Handbook, www-page, available at http://www.emfdosimetry.org, cited 15.09.2007.

[22] Italian National Research Council, Institute for Applied Physics, Florence, Italy, *Dielectric Properties of Body Tissue in the frequency range 10 Hz – 100 GHz*, www-page, available at http://niremf.ifac.cnr.it/tissprop/, cited 15.09.2007.

[23] M. J. Hagmann, O. P. Gandhi and C. H. Durney, "Numerical Calculation of Electromagnetic Energy Deposition for a Realistic Model of Man", *IEEE Trans. on Microwave Theory and Techniques*, Vol. MTT-27, No. 9, September 1979, pp. 804–809.

[24] P. J. Dimbylow, "FDTD calculations of the whole-body averaged SAR in an anatomically realistic voxel model of the human body from 1 MHz to 1 GHz", *Physics in Medicine and Biology*, Vol. 42, No, 3, March 1997, pp. 479–490.

[25] World Health Organization, *Electromagnetic fields*, www-page, available at http://www.who.int/peh-emf/en/, cited 15.09.2007.

[26] International Commission on Non-Ionizing Radiation Protection, Publications – EMF, www-page, available at http://www.icnirp.de/pubEMF.htm, cited 15.09.2007.

[27] Radiation and Nuclear Safety Authority of Finland, *Measurements of mobile telephone radiation*, www-page, available at www.stuk.fi/sateilytietoa/ sateilevat_laitteet/laitteiden_valvonta/en_GB/matkapuhelimet/, cited 21.08.2007.

[28] Radiation and Nuclear Safety Authority of Finland, Mobile *Telephony and Health – A common approach for the Nordic competent authorities*, www-page, available at http://www.stuk.fi/sateilytietoa/sateilevat_laitteet/matkapuhelin/en_GB/index/, cited 23.08.2007.

[29] International Commission on Non-Ionizing Radiation Protection (ICNIRP), "Guidelines for limiting exposure to time-varying electric, magnetic, and electromagnetic fields (up to 300 GHz)," *Health Physics*, April 1998, Vol. 74, No. 4, pp. 494-522.

[30] IEEE Std. C95.1 - 2005, *IEEE Standard for Safety Levels with Respect to Human Exposure to Radio Frequency Electromagnetic Fields, 3 kHz to 300 GHz*, IEEE, New York, USA, April 2006, 248 p.

[31] The Council of the European Union, "Council Recommendation of 12 July 1999 on the limitation of exposure of the general public to electromagnetic fields (0 Hz to 300 GHz)", 1999/519/EC, *Official Journal of the European Communities*, L 199, 30 July 1999, pp. 59-70.

[32] Federal Communications Commission (FCC), Office of Engineering and Technology (OET), *Evaluating Compliance with the FCC Guidelines for Human Exposure to Radiofrequency Electromagnetic Fields, Additional Information for Evaluating Compliance of Mobile and Portable Devices with FCC Limits for Human Exposure to Radiofrequency Emissions*, Supplement C (Edition 01-01) to OET Bulletin 65 (Edition 97-01), June 2001, 57 p.

[33] European Std. EN 50360:2001, *Product Standard to Demonstrate the Compliance of Mobile Telephones with the Basic Restrictions Related to Human Exposure to Electromagnetic fields (300 MHz - 3 GHz)*, CENELEC, Brussels, Belgium, July 2001, 5 p.

[34] The European Parliament and The Council of the European Union, "Directive 1999/5/EC of The European Parliament and of The Council on radio equipment and telecommunications terminal equipment and the mutual recognition of their conformity", 1999/5/EC, *Official Journal of the European Communities*, L 91, 7 April 1999, pp. 10-28.

[35] European Std. EN 50361:2001, *Basic Standard for the Measurement of Specific Absorption Rate Related to Human Exposure to Electromagnetic fields from Mobile Phones (300 MHz - 3 GHz)*, CENELEC, Brussels, Belgium, July 2001, 51 p.

[36] IEEE Std. 1528-2003, *IEEE Recommended Practice for Determining the Peak Spatial- Average Specific Absorption Rate (SAR) in the Human Head from Wireless Communications Devices: Measurement Techniques*, IEEE, New York, USA, December 2003, 149 p.

[37] International Std. IEC 62209-1:2005 Ed. 1.0, *Human exposure to radio frequency fields from hand-held and body-mounted wireless communication devices – Human models, instrumentation and procedures – Part 1: Procedure to determine the specific absorption rate (SAR) for hand-held devices used in close proximity to the ear (frequency range of 300 MHz to 3 GHz),* IEC, Geneva, Switzerland, February 2005, 215 p.

[38] D. Seabury, ETS-Lindgren, *An Update On SAR Standards And The Basic Requirements For SAR Assessment*, April 2005, www-page, available at http://www.ets-lindgren.com/pdf/sar_lo.pdf, cited 30.09.2007.

[39] Schmid & Partner Engineering AG, www-page, available at http://www.speag.com/, cited 25.09.2007.

[40] C. C. Gordon, T. Churchill, C. E. Clauser, B. Bradtmiller, J.T. McConville, I. Tebbetts and R. A. Walker, *1988 Anthropometric Survey of U.S. Army Personnel: Methods and Summary Statistics*, Technical Report NATICK/TR-89/044, U.S. Army Natick Research, Development and Engineering Center, Natick, Massachusetts, USA, 1989, 335 p.

[41] J. Ollikainen, *Design and implementation techniques of wideband mobile communications antennas*, Doctoral dissertation, Helsinki University of Technology, Radio Laboratory publications, Espoo, Finland, 2004, 70 p.

[42] O. Kivekäs, *Design of high-efficiency antennas for mobile communications devices*, Doctoral dissertation, Helsinki University of Technology, Radio Laboratory publications, Espoo, Finland, 2005, 50 p.

[43] J. Villanen, *Miniaturization and evaluation methods of mobile terminal antenna structures*, Doctoral dissertation, Helsinki University of Technology, Radio Laboratory publications, Espoo, Finland, 2007, 69 p.

[44] A. Lehto and A. Räisänen, *RF- ja mikroaaltotekniikka (RF and microwave engineering, in Finnish)*, 7th edition, Helsinki, Finland, 2002, Otatieto, 267 p.

[45] K.-L. Wong, *Planar Antennas for Wireless Communications*, Hoboken, New Jersey, USA, 2003, John Wiley & Sons, 301 p.

[46] J. Poutanen, *Interaction between mobile terminal antenna and user*, Master's thesis, Helsinki University of Technology, Radio Laboratory, 2007, 100 p.

[47] T. Taga, "Analysis of planar inverted-F antennas and antenna design for portable radio equipment," Chapter 5 in *Analysis, Design, and Measurement of Small and Low-Profile Antennas*, K. Hirasawa and M. Haneishi (Editors), Boston, USA, 1992, Artech House, 270 p.

[48] N. Kuster and Q. Balzano, "Energy absorption mechanism by biological bodies in the near field of dipole antennas above 300 MHz," *IEEE Transactions on Vehicular Technology*, vol. 41, no. 1, February 1992, pp. 17-23.

[49] M. Sager, M. Forcucci and T. Kristensen, “A novel technique to increase the realized efficiency of a mobile phone antenna placed beside a head-phantom”, *IEEE Antennas and Propagation Symposium*, vol. 2, June 2003, pp 1013- 1016.

[50] IndexSAR, www-page, available at http://www.indexsar.com/, cited 12.01.2008.

Appendix 1 SAR values of mobile phone models

Phone model	STUK measurement [W/kg]	Value given by the manufacturer [W/kg]
LG C1100	1.00	1.12
LG KG110	1.12	0.728
LG L3100	1.23	0.30
Motorola T191	0.96	1.01
Motorola V150	0.56	0.67
Motorola V180	0.77	0.87
Nokia N70	1.01	0.95
Nokia N73	0.85	1.12
Nokia N-Gage QD	0.48	0.57
Samsung SGH-X680	0.80	0.59
Samsung SGH-X820	1.15	0.639
Samsung SGH-Z540	0.38	0.54
Siemens M55	0.80	0.64
Siemens MC60	0.60	0.67
Siemens ME45	1.12	0.98
SonyEricsson Z200	0.77	0.94
SonyEricsson Z300	0.90	0.75
SonyEricsson Z310i	0.43	0.70